Characteristics of VPE GaAs radiation detectors after proton irradiation

Craig Whitehill

Dept. of Electronics and Electrical Engineering
University of Glasgow
Supervisor: Prof I. Thayne

Experimental Particle Physics Group
Detector Development Laboratory
Dept. of Physics and Astronomy
University of Glasgow
Supervisor: Prof K. Smith

Thesis submitted for degree of Doctor of Philosophy

Contents

List of Figures

Abstract

It is known that macroscopic characteristics of semiconductor particle detectors degrade in high radiation environments such as those found in the ATLAS experiment on the LHC ring at CERN. In order to investigate the degradation mechanisms, measurements were carried out on semiconductor devices before and after proton irradiation.

Results are presented on measurements carried out on Schottky barrier particle detector devices fabricated on Vapour Phase Epitaxially (VPE) grown gallium arsenide (GaAs) substrates. These high purity substrates are thought to offer better quality of device compared to the commonly investigated Semi-Insulating Undoped (SI-U) GaAs material.

Detailed explainations of characterisation techniques used to investigate material electrical properties are given, followed by results of characterisation measurements, initially on unirradiated devices.

The measurements performed on these devices identified the presence of the EL2 defect with a characteristic energy of 0.73 eV and concentration in the order of 2×10^{14} cm^{-3}. This deep level defect is responsible for giving the VPE GaAs material the high resistivity required for good semiconductor detector operation. The effectiveness of a detector is characterised by its Charge Collection Efficiency, which in the VPE GaAs Schottky barrier detectors is found to approach 100%.

The devices were then irradiated with 1.8 MeV and 24 GeV protons to differing final fluences. Under both irradiation regimes the EL3 defect is introduced in the material with a characteristic energy between 0.51 and 0.56

eV, replacing the EL2 as the dominant defect. The CCE of the detector is observed to decreases with increasing fluence, however the impact on CCE after irradiation with 24 GeV protons is more extreme than with 1.8 MeV protons. This is due to creation of defects by fragmentation of the target atoms by high energy proton interactions. These defects are refered to as microinhomogeneities, and their presence is identified by a sensitive Thermally Current Stimulation (TSC) technique for defect identification.

An investigation into the effects that the introduction of radiation induced defect levels has on noise in the detectors under reverse bias concludes the experimental work.

Acknowledgements

I would like to begin by thanking everyone in the Department of Electronics and Electrical Engineering which my EPSRC funding was through, and all in the Department of Physics and Astronomy at Glasgow University, in particular those in the Detector Development Group. Huge thanks go to my supervisors, Prof. Iain Thayne of the Department of Electronics and Electrical Engineering and Prof. Ken Smith of the Department of Physics and Astronomy for giving me that well needed motivational kick when required, and more importantly the desire to learn.

Those closest to me during my research years I must thank for all the good times. So a big cheers to Keith, John, Richy, Drew, Fred, Spyros, Lee and Val. Thanks also to Tennants for being so close. However no thanks at all to some of you guys for the mornings after the nights before. A very special thanks must go to the late and sadly missed Colin Raine.

At Vilnius University in Lithuania I would like to thank Prof. J. Vaitkus, Dr V. Kazakouskas and Dr E. Gaubas. At CERN i would like to thank Maurice Glaser and in the Czech Technical University in Prague i would like to thank Stanislav, Vladimir and Ibriham. There are many others at these institutes that contributed to my work, and who made my trips who enjoyable who i would like to thank.

Gav, Steve Hamill and Santa had the misfortune of putting up me as a flat mates so to you guys i not only thank you but apologise for the mess. A further thanks goes to Alan, Andy, Charlotte, Francesca, Brian, DC, Jen, Nat, Vi and most of all the MIGHTY QM7 (all fourteen of them, you know who you are) who have all been of great support throughout. I have been very fortunate in that almost all of those mentioned above remain great friends. If i have gained anything from the experience it is such a close group of friends that i don't think i will ever loose.

Over the last two years i have been employed by ST Microelectronics Imaging and Display Division. I would like to thank ST for giving me the opportunity to put what i have learned into practice. There are many people i would like to thank for making the last five years of my life phenomenally rewarding, challenging and enjoyable. I am sure i will have missed out many people more than worthy of a mention and i apologise. Finally, to Mum, Dad, Dougie and the rest of the family, the biggest thanks of all for all the love and support.

Chapter 1

Introduction

Compound semiconductors find applications in a wide range of electronic and optoelectronic devices such as room temperature charged particle and ionizing radiation detectors [2], discrete component MESFETS [7] and laser diodes. One of the most common compound semiconductor gallium arsenide (GaAs), which is classed as a III-V semiconductor, has been studied as a radiation and charged particle detector since the 1960's when signals were observed from a GaAs detector exposed to a Co^{60} source[1][2]. Several different structures can be implemented to create a detector from this material, however the detector formed from the Schottky barrier [18],[26] is the basis of this investigation. GaAs Schottky barrier detectors find a wide range of applications such as room temperature γ-ray and X-ray detectors, and it is in the later role that the MEDIPIX single photon counting detector used for mammography and dental X-ray imaging[3] has been developed. GaAs Schottky barrier detectors have also been investigated for use in future high-energy physics experiments such as ATLAS in the Large Hadron Collider (LHC) at CERN[15].

1.1 Radiation Detectors - A review

Ionising radiation detectors were in existence many decades before the introduction of the semiconductor detector. One of the original forms of ionizing radiation detectors is based in its simplest form on the effects of charged particles passing between a pair of electrodes located in a gas chamber (containing e.g. argon). The passage of the charged particles through the gas creates ion-electron pairs, where typically 30eV is lost from the incident charged particle for every ion-electron pair generated[4]. Application of an electric field between the electrodes leads to the migration of the ions and electrons, inducing a signal in an external circuit.

The applications of this type of detector depends on the voltage applied between the electrodes. At low voltages the electric field is insufficient to guarantee prevention of recombination of ion-electron pairs and, although a signal is produced at the electrodes, it is not proportional to the incident radiation. This form of detector is known as an *ionisation detector* and is useful in an integrating mode in a high flux environment as, for example a beam monitor. As the electric field is increased the probability of recombination is reduced such that the amplitude of the induced signal becomes proportional to the energy of the incident radiation. These *proportional counters* were introduced in the 1940's. The advantage of these detectors is that, in a well calibrated system the energy of the incident radiation can be measured [8] and they are therefore useful for energy spectroscopy for identification of radioactive nuclei. As the electric field is further increased a region is reached where secondary ionisation takes place resulting in a large signal, but independent of the initial ionisation. This is the form of the *Geiger-Mueller* tube which can only be used for event counting[9].

Another form of detector is the *scintillation detector*, which operates by utilisation of a material which absorbs energy from incident charge particles and generates a number of visible and ultra-violet photons. The number of photons generated by the scintillating material is proportional to the energy of the incident charged particle. The scintillation material is then optically coupled to a photo-multiplier tube which generates an electrical pulse whose amplitude is proportional to the number of photons generated by the scintillation material, and therefore proportional to the energy of the charged particles. Scintillation detectors are commonly used in the field of gamma spectroscopy to identify radioactive nuclei, and are also found in nuclear physics to identify gamma emission during nuclear de-excitation[10].

Scintillating materials can be organic or inorganic, solid, liquid or gaseous. One of the most efficient room temperature scintillating materials is solid inorganic thallium doped sodium iodide (NaI(Tl)) which generates 38,000 photons of wavelength 415 nm per MeV of incident photons[4]. Disadvantages of this type of detector are that the NaI(Tl) crystals lifetime is reduced by moisture, the photo-multiplier tube adds bulk to the detector, and a supply voltage of kV's are required for operation.

The introduction of the semiconductor diode detector in the early 1960's overcame the problems of size and weight experienced by earlier detectors because the density of the solid state detection medium is around 1000 times greater than the gas detection medium, therefore the number of interactions required to create a signal takes place in a much reduced volume. Semiconductor diode detectors are formed by creating a high resistivity region, devoid (relatively) of free charge carriers in a manner similar to that found in a conventional reverse biased p-n diode where current flows in one direction but is prohibited in the other[27]. This high resistivity region known as the *depletion region* acts as the active detection medium in the same manner as the ionisation chamber detectors, where electron-hole pairs are created by the incident ionizing radiation, and are swept to the electrodes by an applied electric field.

One of the main advantages of the semiconductor diode detector is the much improved energy resolution over gas and scintillation detectors. Depending on the choice of semiconductor material, the energy required to form an electron-hole pair is in the range of 3 to 10 eV[4], therefore for a given quantum of energy incident on a detector, the signal formed from a semiconductor detector is greater than that from gaseous and scintillation detectors (compared to the energy in the range of 20 to 500 eV for scintillation detectors and 30 eV for gas detectors[4] to create an electron-hole pair). Due to the larger number of generated electrons, statistical fluctuations in the pulse amplitude are reduced, therefore semiconductor detectors show better energy resolution $\Delta E/E$ than gaseous and scintillation detectors.

1.2 The Radiation Environment

GaAs devices may be exposed to ionizing radiation or particles that will not cause any damage to the crystal, such as the X-ray environment in which the MEDIPIX detector operates, however in many situations detectors operate in a radiation environment that disturb the periodicity of the lattice, causing damage to the detector. Such examples are in space borne instruments where the material is exposed to cosmic radiation, and in the high radiation environment of particle physics experiments like the ATLAS experiment[15],[12]. While the project detailed in this thesis is not part of the ATLAS collaboration the conclusions of this work may play a part in the choice of GaAs detectors for future high energy experiments, therefore an explanation of the radiation environment in such an experiment is presented.

The ATLAS experiment detects collisions from the Large Hadron Collider (LHC) which collides 14 TeV protons in order to explore new physics, in particular the search for the Higgs Boson[12]. The LHC is a very high collision rate machine with bunch crossings taking place every 25 ns, and an estimated 20 proton-proton (p-p) interactions per crossing, much greater than that produced by the present Large Electron-Positron (LEP) collider at CERN. The events of interest are extremely rare, which means the experiment must be able to identify the relevant events with great efficiency, imposing stringent requirements on the detector components of the experiment. The radiation environment from the high energy p-p collisions is mainly dominated by protons, therefore the GaAs detectors proposed for use in the inner detector of the ATLAS experiment close to the proton-proton interaction point must perform as required over the 10 year lifetime of the experiment.

1.3 Choice of GaAs

The width of the depletion region in a semiconductor detector is proportional to the square root of the reverse bias voltage, and in order to create a depletion region wide enough to achieve maximum collection of generated charge, typically hundreds of volts must be applied across the semiconductor detector contacts. In the absence of ionizing radiation the detector will exhibit some finite conductivity under reverse bias, and therefore a leakage current is observed. It is also known that random fluctuations are observed which result in noise in the leakage current, and that the magnitude of this noise is directly proportional to the leakage current[9][54]. This could have the effect of obscuring the small signal current generated by an ionizing event. A major cause of leakage current in semiconductor detectors is generation current, where the generation current density J_{gen} is given by[12]:

$$J_{gen} = \frac{qn_iW}{2\tau} \tag{1.1}$$

where n_i is the intrinsic carrier density defined as the number of free carriers per cm^3, W is the width of the depletion region, q is the electron charge and τ is the mean carrier lifetime in the depletion region. Materials with larger band-gap energies E_g tend to have a lower n_i because at a given temperature more energy is required to excite electrons from the valence band to the conduction band as discussed in section 2.1.4. It is also observed from equation 2.64 that J_{gen} is directly proportional to n_i, therefore a major requirement for a semiconductor radiation detector operated at room temperature with low J_{gen} is that the band-gap energy E_g is wide enough such that thermal generation of charge carriers from the valence band to the conduction band is minimized. However, for gamma ray spectroscopy where the radiation energy is relatively low (typically in the range of 10's of KeV's), the band-gap energy E_g must be small enough to ensure that a sufficient number of electron-hole pairs are created by an absorbed quantum of ionizing radiation, such that a detectable signal is generated. A compromise is therefore necessary. A further requirement is that the detector material should have a relatively high atomic number to increase the probability of interaction with incident radiation[16].

Semiconductor detectors fabricated on Si have been used in high energy particle physics experiments since the 1970's[12]. Si detectors are well understood and have been investigated by many authors [5],[11], however in the harsh radiation environments of the inner region of high energy experiments such as ATLAS, it is observed that significant damage is inflicted on the Si components of the detector. The leakage current of these devices is seen to increase by several orders of magnitude over the operational lifetime of the experiment, leading to an increase in detector noise and heating effects, and also observed is a reduction in the detector charge collection efficiency (CCE)[14]. In many cases the effective doping density of the semiconductor material is observed to rise with time. The width of the depletion region W is proportional to the inverse square root of the doping density N_D, therefore as N_D increases, W decreases, and as a result a greater bias is required to fully deplete the detector. In light of these observations an alternative material should be investigated which exhibits the same qualities which Si possesses, but radiation hard.

The energy to create an electron-hole pair E_{e-h} is 2.9 eV for Ge, 3.6 eV for Si and 4.2 eV for GaAs[4]. This would suggest that Ge would be the most suitable choice for ionizing radiation detectors because it would produce the greatest signal for a given quantum of energy, and because Ge has an atomic number and density similar to that of GaAs and greater than Si (see Appendix) it is commonly used in high energy resolution gamma spectroscopy. It can be seen in figure 1.1 that the resolution of the Ge detector is much better than that of the NaI scintillator detector. However, Ge has a low band-gap energy E_g of 0.66 eV compared to that of 1.12 eV for Si

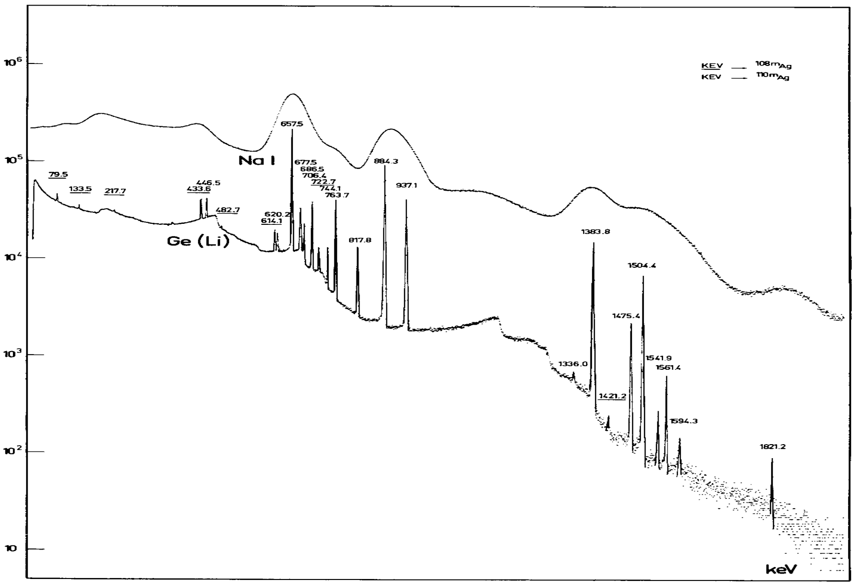

Figure 1.1: A comparison of the gamma spectra taken with a NaI scintillator and a Ge semiconductor detector

and 1.42 eV for GaAs at 300 K[13], implying that Si and GaAs exhibit lower room temperature J_{gen}. The Ge spectrum obtained in fig 1.1 is obtained at a detector temperature of 77K. For room temperature operation the wider band gaps of Si and GaAs prove a better alternative. GaAs has a greater average atomic number Z, where $Z_{Ga} = 31$ and $Z_{As} = 33$, compared to that of Si where $Z_{Si} = 14$[6] therefore on the basis of these characteristics GaAs appears to be the material of choice for semiconductor radiation detectors.

High resistivity Semi-Insulating Undoped GaAs (SI-U GaAs) was therefore proposed for such experiments, unfortunately it was also shown to suffer in the harsh radiation environment of high energy physics experiments such as ATLAS [12],[51], and in fact was found to exhibit poor macroscopic characteristics even before irradiation. This material obtains its high resistivity nature through over-compensation of the shallow carbon acceptor or silicon donor dopants by the deep EL2 defect level, thus reducing the levels of free charge carriers at room temperature. However the presence of this EL2 level means that this material also has a high concentration of deep level traps, even before irradiation. The effect of the high concentration of these deep levels is that they capture charge generated by the incident radiation, resulting in poor pre-irradiation charge collection efficiency (CCE), with a typical maximum electron CCE of 60%[12] measured by alpha particle (α) irradiation. These traps also have the effect of decreasing the charge carrier mean free lifetime τ, resulting in an increase in J_{gen}.

Although the macroscopic characteristics of Si detectors such as CCE and reverse bias leakage current degrade due to radiation damage, Si technology is well advanced and high performance detectors made from this good quality starting material are available, therefore Si was decided on as the material of choice for the ATLAS inner detector. If a form of GaAs material could be found that had good pre-irradiation characteristics and was found to be radiation hard then this may prove a suitable choice for future high radiation environments. GaAs grown by the technique of Vapour Phase Epitaxy (VPE) was suggested as such a material. VPE GaAs is a material that gains its high resistivity through growing the crystals relatively defect free, and not through compensation of shallow levels by deep levels. Therefore, although it has a lower resistivity than SI-U GaAs detectors, VPE GaAs detectors contain several orders of magnitude lower concentrations of deep level traps, resulting in pre-irradiation reverse bias leakage currents of 10's of nA over a wide range of reverse biases as reported in this thesis, compared to 100's of nA with SI-U GaAs. Pre-irradiation CCE's for an α particle source are also found to approach 100%.

1.4 Thesis Overview

The motivation of this thesis is therefore to investigate the radiation hardness of VPE GaAs and the mechanisms of radiation induced damage which occur in the lattice through irradiation with high energy protons. Investigations are carried out with protons of energy 1.8 MeV and 24 GeV over a range of fluences to analyze the dependence of the observed characteristics on irradiation energy. Of importance is the analysis of the effects of these induced defects on the noise of a reverse biased detector. While it is important that the signal from a detector be free from noise in order to obtain maximum detector sensitivity, it is also thought that analysis of noise spectra in the frequency domain may act as a technique for investigating the type of damage induced in a detector. A detailed investigation of the relationship between induced defects and noise spectra makes up a considerable percentage of the work detailed in this thesis.

Chapter 2 will give an introduction to semiconductor theory, with a particular emphasis placed on GaAs, and also Schottky barriers which are the basis of most semiconductor detectors. This chapter introduces the background to the characteristics which define detector operation.

Chapter 3 includes a brief description of the theory behind semiconductor detectors, in particular the action of the depletion region as the active detector region and signal formation within this region. The growth of VPE GaAs and the fabrication of the devices used in this investigation are also covered in this chapter.

The macroscopic characteristics of the unirradiated VPE GaAs test devices are covered in Chapter 4. Throughout a comparison is made, where possible, to detectors fabricated on SI LEC GaAs, as this is the material which has been the basis for the majority of previous investigation.

Chapter 5 follows by detailing the methods of device irradiation with 1.8 MeV and 24 GeV protons. This is then followed by an investigation of the post-irradiation characteristics of the devices, in the same manner as the investigation of the pre-irradiated devices in Chapter 4.

A key aspect of investigating radiation induced damage in semiconductor materials is the identification of the defects that are induced in the material, and how they correlate to incident particle energy and fluence. This investigation is covered in Chapter 6.

It is known that investigations of the noise of the devices under reverse bias can give information into the mechanisms taking place in the material. Chapter 7 covers the investigation of the current noise in the GaAs VPE devices before and after irradiation.

Chapter 8 summarises the investigations of the thesis, together with suggestions for future work in this area.

Chapter 2

Semiconductor Theory

In order to obtain a qualititive and quantitive understanding of the operation of GaAs Schottky diode detectors, and the mechanisms of defect introduction which lead to the degradation in GaAs detector characteristics, a detailed knowledge of the semiconductor theory relevant to these characteristics must be gained. The work described in later chapters contributes to the understanding of semiconductor detectors based on the Schottky diode structure through electrical measurements such as current-voltage, capacitance-voltage, Deep-level Transient Spectroscopy and noise power spectral density before and after proton irradiation. This chapter details the basic semiconductor theory that is relevant to the theoretical basis for the understanding of those measurements in terms of device fabrication technology, Schottky diode properties, and crystal defects. Unless otherwise stated, the theory of this chapter is a summary of the work presented by Sze[26].

2.1 The Simple Semiconductor

Theory relevant to the operation of semiconductor particle detectors is explained here with a particular emphasis on the effect of the Schottky barrier on n-type GaAs grown by the technique of Vapour Phase Epitaxy (VPE). Apart from the fact that the semiconductor detectors under investigation are based on the Schottky diode, these structures are frequently used as test devices for basic semiconductor material properties due to their relatively simple construction and the fact that the majority of the macroscopic electrical tests can give information on the characteristics of the material. Although the GaAs material investigated in this thesis is grown by VPE, the properties of semi-insulating undoped (SI-U) GaAs also require consideration due to the presence in this material of the important EL2 deep level, and due to the fact that the majority of investigations on GaAs to date have been carried out on this material.

2.1.1 Crystal Structure

The basic crystalline structure of a semiconductor is that of a regular assembly of atoms held together by a covalent bond[22]. GaAs has a zincblende structure, shown in Figure 2.1.1, which can be visualised as two inter-penetrating face-centred cubic (*fcc*) lattices where one sub-lattice is Ga (Group III, Z = 31) and the other is As (Group IV, Z = 33).

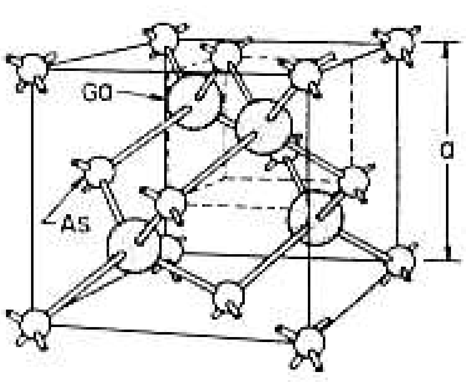

Figure 2.1: The zincblende lattice structure of GaAs, where a is the lattice constant.

2.1.2 Energy Levels

When two atoms are completely isolated from each other so that there is no interaction between them, they can have identical electronic structures. The energy levels which electrons can occupy can therefore be calculated for an atom. However as the atoms are brought together the Pauli exclusion principle, which states that no two electrons can occupy the same quantum-mechanical state, becomes important. There is thus a splitting of the discrete energy levels of the isolated atoms into new levels. In a solid where many atoms interact continuous bands are created. As the distance between atoms approaches the inter-atomic spacing of the given lattice structure the energy bands split, resulting in the production of the conduction and valence band, which are separated by an energy gap E_g [25]. The energy-momentum relationships (where the reduced wave vector q describes the momentum) for GaAs, shown in figure 2.2 result in an energy gap E_g of 1.42eV at 300K[27]. For comparison the energy gap of Si is 1.12eV at 300 K. The properties of a semiconductor are determined by the interactions of charge carriers between the valence band and the conduction band.

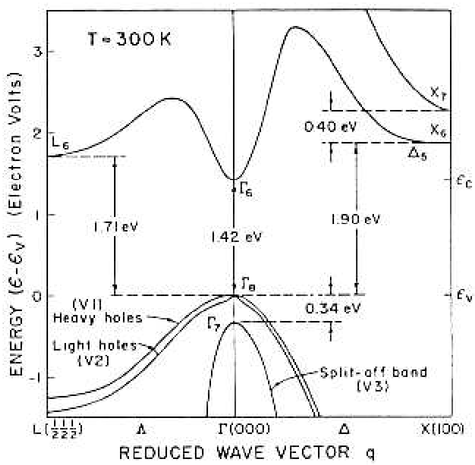

Figure 2.2: Energy-band structure for GaAs, where E_g is the band-gap

While the properties that make GaAs an attractive choice of material for semiconductor detectors were discussed in chapter 1, a further benefit is that GaAs is a *Direct Band Gap* material. Incident radiation excites the electron from the valence band to the conduction band, forming an electron-hole pair. Direct transitions between the Γ bands as observed in figure 2.2 are only the result of a change in energy. Si and Ge are not direct band gap materials (see reference [26] for their energy band structures), and therefore direct transitions between their conduction and valence bands are highly improbable. Indirect transitions can take place through intermediate levels, or through a change in momentum.

2.1.3 Effective Mass

The carriers in a semiconductor are not free particles as they interact with the crystal lattice, and therefore to treat them as classicle particles their mass is defined by an effective mass m^*. The effective mass is defined by the curvature of the Energy-band structure in figure 2.2 as:

$$m^* = (\hbar)^2 \left(\frac{d^2E}{dq^2} \right)^{-1} \tag{2.1}$$

where $\hbar$ is Planck's constant. The effective mass is therefore dependent on the curvature of the band that the charge carrier is in. In GaAs an electron in the lower conduction band valley Γ_6 will therefore have a lower effective mass that one in the higher L_6 valley.

2.1.4 Carrier Concentration

By adding controlled amounts of impurities, the properties of a semiconductor material can be dramatically modified. High purity semiconductor materials are referred to as *intrinsic* while those with impurities are known as *extrinsic*. Two types of impurity exist, donors and acceptors. A donor atom has an extra electron in its neutral state compared to the intrinsic material, which is free to contribute to the electrical conduction of the material. As a result of this contribution process, the donor atom is bound to the crystal lattice with a net positive charge. In contrast an acceptor has three valence electrons in its neutral state. An electron is accepted by this type of impurity making the acceptor negative. This process leaves a "hole" in the free electron distribution. Although the hole is not actually a particle as such, it can be mathematically described as one and is free to move in the material, and can contribute to the electrical conduction. A material in which the predominant impurity is a donor is referred to as being n-type, where electrons are referred to as majority carriers and holes as minority carriers. The inverse applies for a p-type material, where acceptors are the predominant impurity and holes are the majority carrier.

Impurities introduce energy levels into the energy band gap. The energy of the donor level is measured down from the conduction band minimum, and that of the acceptors is measured up from the valence band maximum.

The number of electrons in the conduction band (n) per cm^3 is given by:

$$n = N_C exp\left(-\frac{E_C - E_F}{kT}\right) \tag{2.2}$$

where N_C is the effective density of states in the conduction band and is equal to $4.7 \times 10^{17} cm^{-3}$ for GaAs at room temperature[26], given by:

$$N_C = 2\left(\frac{m^* kT^{\frac{3}{2}}}{2\pi\hbar}\right) \tag{2.3}$$

E_C is the energy at the bottom of the conduction band, T is the absolute temperature, m^* is the electron effective mass and k is Boltzmans constant. The Fermi level E_F is defined as the energy level at thermal equilibrium where, at temperatures above absolute zero, there is a 50% probability of occupation by an electron. The number of holes in the valence band (p) per cm^3 is given by[26]

$$p = N_V exp\left(-\frac{E_F - E_V}{kT}\right) \tag{2.4}$$

where N_V is the effective density of states in the valence band, equal to $7.0 \times 10^{18} cm^{-3}$ for GaAs at room temperature. In an intrinsic semiconductor in thermal equilibrium electrons are continually excited from the valence band to the conduction band. This process is balanced by recombination of the electrons in the conduction band with holes in the valence band. Equal values of n and p therefore exist and $n = p = n_i$ where n_i is the intrinsic carrier concentration. The intrinsic semiconductor has a Fermi level E_i given by:

$$E_F = E_i = \frac{E_C + E_V}{2} + \frac{kT}{2} ln \left(\frac{N_C}{N_V} \right) \tag{2.5}$$

It can be seen that the Fermi level of an intrinsic semiconductor lies close to the middle of the band gap. The intrinsic carrier concentration is given by

$$(np)^{\frac{1}{2}} = n_i = \left[N_C N_V exp \left(-\frac{E_g}{kT} \right) \right]^{\frac{1}{2}} \tag{2.6}$$

Equation 2.6 shows that, for given values of N_C and N_V, larger band gaps result in lower intrinsic carrier concentrations, because at a given temperature more energy is required to promote electrons into the conduction band from the valence band.

The addition of either donor or acceptor atoms will change the position of the Fermi level energy. For example, when donors are added the probability that an electron state is occupied increases, and therefore the the Fermi level E_F increases, moving towards E_C. The converse applies to addition of acceptors where the Fermi level shifts towards the valence band. Charge neutrality demands that for a crystal with donor density N_D and acceptor density N_A:

$$n + N_A = p + N_D \tag{2.7}$$

i.e. total negative charge (electrons and ionised acceptors N_A) must equal total positive charge (holes and ionised donors N_D). The electron concentration in an n-type material with only shallow dopants is given by[26]:

$$n_n = \frac{1}{2}\left[N_D - N_A + \sqrt{(N_D - N_A)^2 + 4n_i^2}\right] \quad (2.8)$$

$$p_n = \frac{n_i^2}{n_n} \quad (2.9)$$

where the subscript n denotes an n-type material. In the n-type VPE GaAs under investigation the magnitude of net dopant concentration $|N_D - N_A|$ is larger than the intrinsic concentration n_i, therefore because $N_D > N_A$, equation 2.8 can be simplified to:

$$n_n \simeq N_D - N_A \quad (2.10)$$

If $N_D \gg N_A$ then equation 2.10 can be further approximated to $n = N_D$. By rearrangement of equation 2.2 the Fermi level can then be given by:

$$E_C - E_F = \frac{kT}{q} ln\left[\frac{N_C}{N_D}\right] \quad (2.11)$$

The epitaxial GaAs material under investigation was supplied from the manufacturers with a quoted doping density of 1.7×10^{14} cm^{-3} at 300 K, and because the material is n-type the impurities are assumed to be donors. For n-type GaAs, with a donor concentration of 1.7×10^{14} cm^{-3} at 300 K, the Fermi level is located 0.205 eV below the conduction band.

2.2 Carrier Transport

2.2.1 Drift

At room temperature the electrons in the conduction band have a random thermal velocity v_{th} given by[26]:

$$\frac{1}{2}m_n^*\overline{v_{th}^2} = \frac{3}{2}kT \quad (2.12)$$

where v_{th} is of the order 10^4 ms^{-1} and m_n^* is the electron effective mass in the conduction band. A corresponding relationship to 2.12 also applies to holes. Under the application of an electric field ε a drift component is added to the thermal carrier motion. The drift velocities for electrons (v_n) and holes (v_p) due to this electric field are given by:

$$v_n = -\mu_n \varepsilon \qquad (2.13)$$

$$v_p = \mu_p \varepsilon \qquad (2.14)$$

where the mobilities ($\mu_{n,p}$) are constants of proportionality which are carrier and material dependent. The negative sign applied to v_n is because electrons flow in the opposite direction to the electric field vector. Drift velocity gives rise to a drift current density J, where:

$$J = nqv = nq\mu\varepsilon \qquad (2.15)$$

with q the electric charge. The mobility is inversely proportional to the carrier effective mass m^*, given in the appendix and defined in reference [26], therefore in GaAs the electron mobility is greater than that of holes. At low electric fields the electrons occupy the lower Γ valley in the conduction band, shown in figure 2.2, and therefore have a high mobility (8500 $cm^2V^{-1}s^{-1}$ at 300K in undoped GaAs) and high drift velocity. However at high electric fields (above 3 x 10^3 Vcm^{-1}) electrons are scattered into the indirect, upper L valley where the mobility reduces due to an increase in effective mass. This is known as the *transferred electron* effect. The average group velocity of electrons begins to fall above fields of 3 x 10^3 Vcm^{-1} as the population of electrons in the upper valley increases, as shown in figure 2.3.

It is observed in figure 2.3 that at lower fields the hole velocity is considerably lower than that of the electrons due to lower hole mobility (400 $cm^2V^{-1}s^{-1}$ at 300K in undoped GaAs), but at fields above 1×10^4 Vcm^{-1} similar electron and hole velocities can be achieved[26].

The resistivity (ρ) of a semiconductor is defined as the proportionality constant between the electric field and the drift current density J

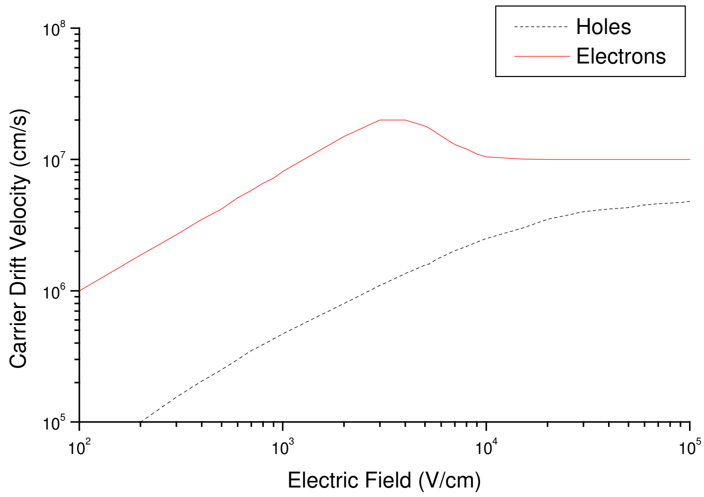

Figure 2.3: Carrier drift velocity as a function of electric field for GaAs

$$\rho = \frac{\varepsilon}{J} \tag{2.16}$$

The resistivity depends on mobility, and for semiconductors with contributions from both electrons and holes is given by:

$$\rho = \frac{1}{q\left(n\mu_n + p\mu_p\right)} \tag{2.17}$$

If $n \gg p$, as is the case with an n-type semiconductor, then equation 2.17 simplifies to:

$$\rho = \frac{1}{qn\mu_n} \tag{2.18}$$

For an n-type material where $N_D \gg n_i$ and $N_D \gg N_A$ the resistivity is given by

$$\rho = \frac{1}{qN_D\mu_n} \tag{2.19}$$

2.2.2 Carrier Diffusion

Carrier diffusion, which is proportional to the carrier concentration gradient, is an important mechanism in establishing equilibrium in many devices. The current density is given by the flux of carriers multiplied by the electron charge (q) and therefore:

$$J_n = qD_n \frac{dn}{dx} \tag{2.20}$$

$$J_p = -qD_p \frac{dp}{dx} \tag{2.21}$$

where D_n and D_p are the carrier diffusion coefficients for electrons and holes, respectively, which are directly proportional to carrier mobility and temperature[26]. Diffusion results in a change in the carrier concentration, and therefore the electric field distribution will be altered. The movement of electrons from a point A to B due to diffusion will create an electric field that will oppose this motion, and cause electrons to drift from B back to A. In equilibrium these diffusion and drift components will balance.

2.3 Trapping and Recombination

The effectiveness of a semiconductor detector is maintained only as long as the charge that is deposited in it by an ionising particle is collected at the electrodes. This will not be the case if charge carriers recombine or if electrons are removed from the conduction band, or holes from the valence band by *trapping centres* in the band gap.

All semiconductors contain impurities. They may be intentionally introduced as dopants (shallow level impurities) or deep level impurities to increase the resistivity. However many impurities are unintentionally introduced during crystal growth, device fabrication or through irradiation.

The band diagram of a perfect semiconductor consists of a conduction band and a valence band separated by the band gap E_g. When the crystal is altered by impurity atoms or crystal defects discrete energy levels are introduced into the band gap. These energy levels are referred to as traps or generation-recombination (G-R) centres, depending on their position in the band-gap, with a concentration N_t (cm^{-3}) and energy E_t.

In the presence of trapping centres four processes can occur between the conduction band, the valence band and a deep level trap, as shown in Figure 2.4.

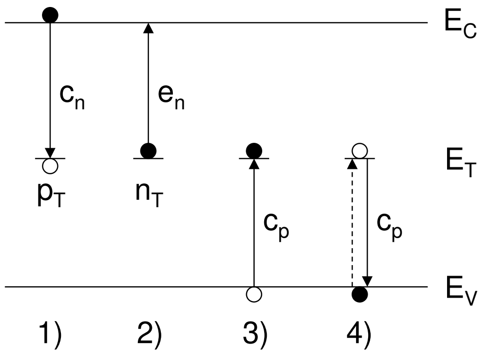

Figure 2.4: Electron energy band structure for a semiconductor with deep level impurities

1. An electron in the conduction band can be captured by the deep level with an electron capture coefficient c_n. After electron capture two processes can take place:-

2. An electron can be emitted from the defect centre back to the conduction band with an electron emission coefficient e_n or;

3. A hole can be captured from the valence band with a hole capture coefficient c_p (equivalent to electron capture by E_V from the deep level).

4. The final process is the emission of a hole back to the valence band with an emission rate e_p. This final process can also be thought of as electron emission from the valence band to the deep level trap.

Whether a mid band gap level is defined as a trap or a generation-recombination (G-R) centre tends to depend on the involvement of that level in the process taking place. A trapping event involves capture of charge carriers from the valence or conduction band and, after an interval of time, release of the charge carrier back to its initial band as given by processes 1) followed by 2), or 3) followed by 4). Trapping centres tend to be nearer to the conduction or valence band with a low energy between the trap and its nearest band. Only one of the two bands and the trapping centre take part in a single trapping event.

A defect tends to act as a G-R centre if its energy is a few kT from the Fermi level. With a G-R centre, recombination with a charge carrier of the opposite polarity takes place before re-emission takes place as given by processes 1) followed by 3), then 2) followed by 4). Both bands and the G-R centre take part in this process.

2.4 Metal-Semiconductor Contacts

GaAs particle detectors utilise the properties of the metal/semiconductor interface known as a Schottky barrier to create the depletion region, which acts as the active detector volume under reverse bias. In this section the theory relevant to the operation of a Schottky barrier is given for both ideal and non-ideal conditions. Also discussed is the Ohmic contact which is required to realize the back contact of the detector.

2.4.1 The Schottky Barrier

The Ideal Case

A rectifying Schottky barrier is formed when a metal and semiconductor material are brought into direct contact. The nature of an ideal rectifying barrier is that current flows freely in one direction but is prohibited in the other.

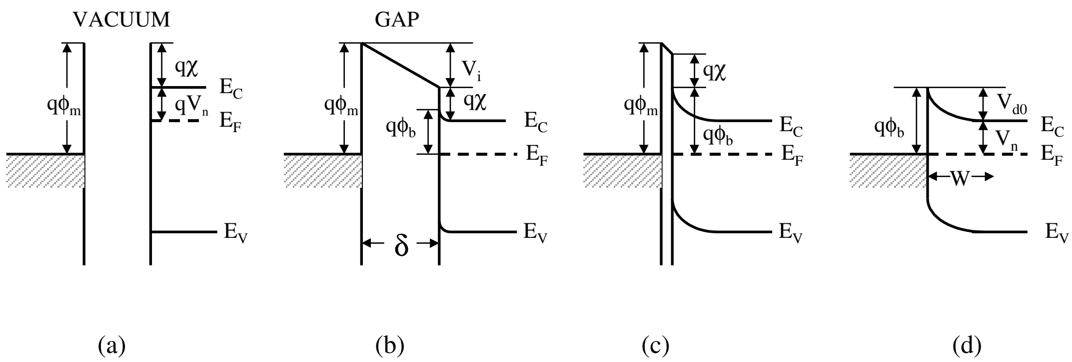

Figure 2.5: Schottky Barrier: energy band diagram of metal and semiconductor (a)both isolated (b)after electrical contact (c)separated by a narrow gap and (d) in perfect contact

The electron affinity χ of the semiconductor is the difference in energy between the bottom of the conduction band and the vacuum state, while the work function of the semiconductor ϕ_s is the difference in energy between the Fermi level and the vacuum state. For a semiconductor in the absence of an electric field, the work function and electron affinity are related by:

$$q\phi_s = q(\chi + V_n) \tag{2.22}$$

as shown in figure 2.5, where qV_n is the energy difference between E_C and E_F, and is given by[27]:

$$V_n = \frac{kT}{q} ln\left(\frac{N_C}{N_D}\right) \tag{2.23}$$

To begin with assume that both the metal and semiconductor are electrically neutral and separate from each other as shown in fig 2.5 a). To form a Schottky barrier, a metal is chosen that has a greater work function than the semiconductor. They are brought into direct contact and, because the semiconductor work function is lower than that of the metal, electrons from the semiconductor enter the metal. The presence of the conduction electrons from the semiconductor produce a negative charge in the metal and the uncompensated donors remaining in the semiconductor leave it with a positive charge. Because the concentration of uncompensated donors in the semiconductor is many orders of magnitude less than the concentration of electrons in the metal, the uncompensated donors occupy a layer of thickness W which is much greater than the region of negative charge in the metal. This region of thickness W is referred to as the depletion region.

Because the Fermi level of the two materials must remain the same, then due to the removal of electrons, the Fermi level in the semiconductor changes position relative to the conduction and valence bands, resulting in the bands being bent upwards. The barrier height qϕ_b for a perfect metal-semiconductor contact is:

$$q\phi_b = q\left(\phi_m - \chi\right) \tag{2.24}$$

The diffusion potential V_d (V_{d0} for zero bias) is defined as the difference in potential across the depletion region and is defined as:

$$V_{d0} = \phi_b - V_n \tag{2.25}$$

The shape of the potential barrier depends on the charge distribution in the depletion region. If the charge distribution (ρ in figure 2.6) is uniform up to the barrier then a Schottky barrier is produced (see Fig 2.6). The electric field ε increases linearly with distance from the edge of the depletion region towards the metal-semiconductor interface, and the potential ϕ increases quadratically. The resulting electric field in the case where a donor density N_D is present is defined by Poisson's equation as[27]:

$$\frac{d\varepsilon}{dx} = \frac{qN_D}{\epsilon_s} \tag{2.26}$$

where ϵ_s is the semiconductor permittivity. Under the approximation that the space charge density of an n-type semiconductor $\rho = qN_D$ for $x <$

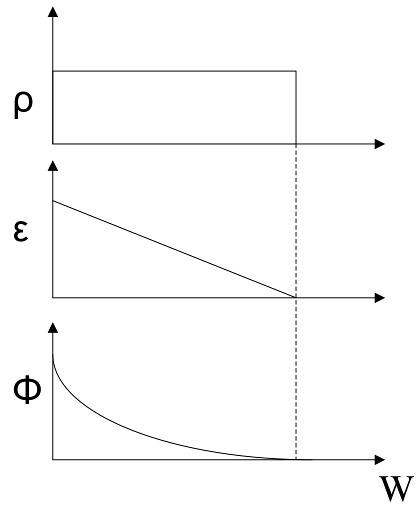

Figure 2.6: Charge density, electric field and potential of the Schottky barrier on n-type GaAs

W where W is the width of the depletion region, ϵ_s is the semiconductor permittivity and $\rho \simeq 0$ and $d\phi/\mathrm{dx} \simeq 0$ for $x >$ W, then the electric field as a function of x, obtained by solving Poisson's equation is given as:

$$\varepsilon(x) = -\frac{qN_D}{\epsilon_s}(W - x) \tag{2.27}$$

with a maximum at the metal semiconductor interface (at $x = 0$) of

$$\varepsilon_{max} = -\frac{qN_D W}{\epsilon_s} = \frac{Q_D}{\epsilon_s} \tag{2.28}$$

where Q_D is the total space charge per unit area of the uncompensated donors in the depletion region. The potential in this region, $\phi(x)$, may be found as follows

$$\begin{aligned} \phi(x) &= \int_x^W \mathcal{E}\, dx \\ &= -\int_x^W \frac{qN_D(x)}{\epsilon_s}(W - x)dx \end{aligned}$$

$$= -\frac{qN_D}{2\epsilon_s}(W-x)^2 \tag{2.29}$$

The maximum occurs at $x = 0$ with a value of

$$\phi(0) = \frac{qN_D W^2}{2\epsilon_s} \tag{2.30}$$

This difference in potential across the depletion region, the diffusion potential V_d, is equal to $\phi(0)$ - $\phi(W)$. Combining equations 2.28 and 2.30 allows V_d to be expressed as:

$$V_d = \frac{\epsilon_s \varepsilon_{max}^2}{2qN_D} \tag{2.31}$$

$$V_d = \frac{Q_D^2}{2\epsilon_s q N_D} \tag{2.32}$$

2.4.2 The Ohmic Contact

An alternative situation occurs at a metal-semiconductor contact when the work function of the metal is less than that of the semiconductor, resulting in the electrons encountering no barrier from the semiconductor to the metal. In the ideal case, if this junction is forward biased then the current is determined by the bulk resistance of the semiconductor, and not the contact properties. This is an ohmic contact as seen in figure 2.7b). For an ideal Schottky diode detector the back contact is a good ohmic contact so that all the applied bias is dropped across the junction.

2.4.3 Capacitance of reverse biased Schottky barrier

The depletion region of a Schottky barrier can behave in the same manner as a parallel plate capacitor, however the capacitance is a function of the applied bias. If the reverse bias is increased by a small increment ΔV then the electrons in the conduction band recede further from the metal contact leaving uncompensated donors, increasing the depletion region width W by an amount ΔW. A fixed charge is left, resulting in the junction having a

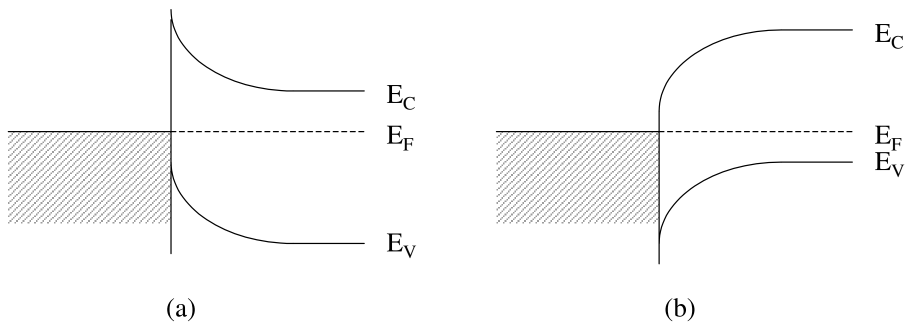

Figure 2.7: (a) $\phi_m > \phi_s$ rectifying and (b) $\phi_m < \phi_s$ ohmic

capacitance. This depletion region capacitance is of great importance in device characterisation because capacitance measurements under reverse bias can give information on semiconductor properties and barrier parameters. From equation (2.32) the differential capacitance per unit area of a Schottky barrier can be calculated, where:

$$C = \frac{dQ_D}{dV_d} = \left(\frac{\epsilon_s q N_D}{2V_d}\right)^{\frac{1}{2}} = \frac{\epsilon_s}{W} \tag{2.33}$$

Equation 2.33 can be re-written to give the depletion region width as:

$$W = \sqrt{\frac{2\epsilon_s V_d}{qN_D}} \tag{2.34}$$

which is related to the semiconductor doping density and can be re-written as

$$N_D = \frac{2}{q\epsilon_s S_e^2}\left[-\frac{1}{d(1/C^2)/dV}\right] \tag{2.35}$$

where S_e is the contact area. If N_D is constant throughout the depletion region then a plot of $1/C^2$ against V should result in a straight line with a slope of magnitude $2/(q\epsilon_s N_D)$. The donor density can therefore be found by measuring the capacitance as a function of reverse bias voltage for a metal-semiconductor junction. The depletion width of an n-type semiconductor, where $N_D \gg n_i$ can be expressed in terms of resistivity (using equation 2.18) as:

$$W = \sqrt{2\epsilon_s \mu_n \rho V_d} \tag{2.36}$$

which is of great importance in semiconductor detectors where, for a given reverse bias V, an increased resistivity ρ results in an increased depletion width W, thus increasing the probability of interaction between incident radiation and the crystal lattice. On application of an external bias V, the diffusion potential equation 2.25 for V_d is replaced by:

$$V_d = \phi_b - V - V_n \tag{2.37}$$

In an ideal device where the back contact is a good ohmic contact, all the applied bias is dropped across the junction. The equivalent circuit for a real device, shown in figure 2.8, has a resistance R_b to account for the bulk and ohmic contact resistances, in series with the junction resistance R_j. The junction capacitance is represented by a capacitor C_j in parallel with the R_j.

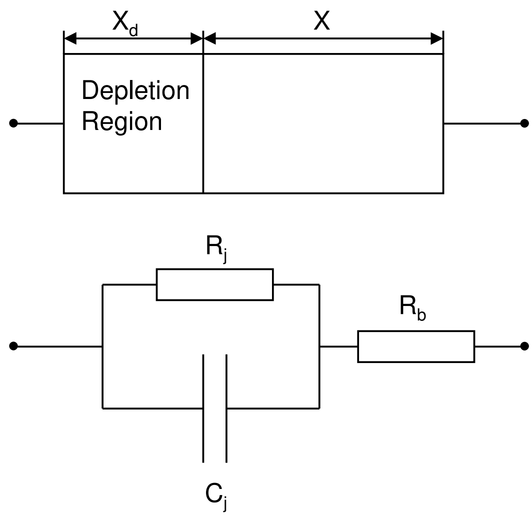

Figure 2.8: The equivalent circuit of a Schottky barrier diode with an Ohmic contact.

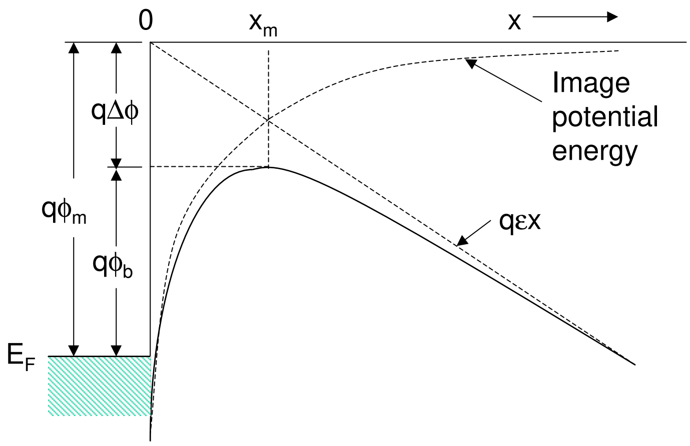

Figure 2.9: The image force lowering of a potential barrier.

2.4.4 Schottky Effect

The Schottky Effect is the image-force-induced lowering of the potential energy for charge carrier emission when an electric field is applied, as shown in figure 2.9. Consider a metal/semiconductor system where ϵ_s is the semiconductor permittivity. When an electron is at a distance x from the metal, a positive charge is induced on the metal surface. The attractive force experienced between the electron and the induced positive charge is equivalent to the force that would be experienced between an electron and an equal positive charge, referred to as the image charge, positioned at -x. The attractive force, referred to as the image force, is given as:

$$F = -\frac{q^2}{4\pi(2x)^2\epsilon_s} = -\frac{q^2}{16\pi\epsilon_s x^2} \tag{2.38}$$

Because of this attractive force the electron has a negative potential energy -qV_I relative to that of an electron at infinity where:

$$V_I = \frac{q}{16\pi\epsilon_s}\int_x^\infty \frac{dx}{x^2} = \frac{q}{16\pi\epsilon_s x} \tag{2.39}$$

Since the image potential is only of importance near the surface, then the field due to the Schottky barrier is regarded as constant with a value of ε_{max}

where:

$$\varepsilon_{max} = \left(\frac{2qN_DV_d}{\epsilon_s}\right)^{\frac{1}{2}} \tag{2.40}$$

The maximum potential energy occurs at a position x_m where the field due to the image force is equal and opposite to the field in the depletion region, causing the resultant field to vanish, where:

$$\frac{q}{16\pi\epsilon_s x_m^2} = \varepsilon_{max} \tag{2.41}$$

The Schottky barrier is lowered by an amount $\Delta\phi_{bi}$ given by:

$$\Delta\phi_{bi} = x_m\varepsilon_{max} + \frac{q}{16\pi\varepsilon_s x_m} = 2\varepsilon_{max}x_m \tag{2.42}$$

Combining equation 2.41 with 2.42 results in:

$$\Delta\phi_{bi} = \left(\frac{\varepsilon_{max}q}{4\pi\epsilon_s}\right)^{\frac{1}{2}} \tag{2.43}$$

Substituting with $\varepsilon_{max}$from equation 2.40 and V_d from equation 2.37 results in:

$$\Delta\phi_{bi} = \left[\frac{q^3N_D}{8\pi\epsilon_s^3}\left(\phi_b - V - V_n - \frac{k_BT}{q}\right)\right]^{\frac{1}{4}} \tag{2.44}$$

$$x_m = \frac{1}{4}\left(\frac{q}{2\pi^2\epsilon_s N_D}\right)^{\frac{1}{4}}\left(\phi_b - V - V_n - \frac{k_BT}{q}\right)^{-\frac{1}{4}} \tag{2.45}$$

In the VPE GaAs material under investigation where $N_D = 1.7\times10^{14}cm^{-3}$, an applied electric field of $\varepsilon_{max} = 1\times10^5Vcm^{-1}$ will result in an image barrier lowering of $\Delta\phi_{bi} = 0.33$eV. Measurements carried out in section 4.2.4 result in a barrier height of 0.905 eV, therefore the barrier lowering of 0.033eV results in a decrease of ϕ_b of 3.6% at ε_{max}.

The image force barrier lowering for a maximum electric field $\varepsilon_{max} = 1\times10^5Vcm^{-1}$ in GaAs is 0.033V in a device with $N_D = 2\times10^{14}cm^{-3}$, which is a lowering of 3.9% on a Schottky contact made from titanium on n-type GaAs, where the barrier height is 0.83 eV.

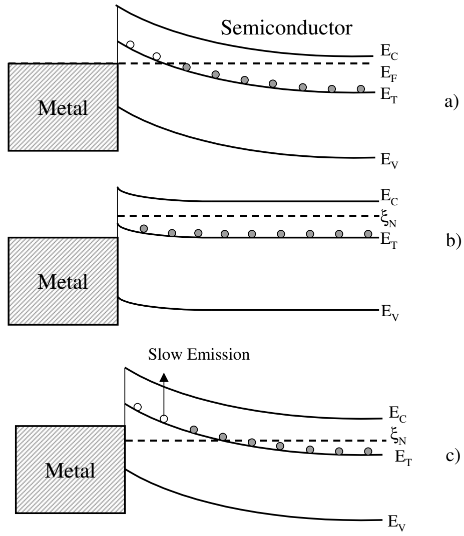

Figure 2.10: Metal-Semiconductor junction under a)zero bias, b)forward bias and c)reverse bias.

2.4.5 Time Dependence of Carrier Emission

In an unbiased Schottky barrier all electron states are occupied in accordance with the equilibrium Fermi level E_F. A deep level in the bandgap with energy E_T will follow the curvature of the conduction band as in figure 2.10a). In thermal equilibrium, where the deep level falls below the Fermi level it is occupied by an electron, and above E_F the level is empty. When a voltage is applied the minority carrier densities on both sides of the junction are changed. Under application of a forward bias (almost flat band situation) the deep level is below the electron quasi-Fermi level ξ_n which replaces E_F under non-equilibrium conditions as in figure 2.10b). Provided the forward-bias time is long compared to the characteristic electron filling time τ given by:

$$\tau = (\sigma_n v_{th} n)^{-1} \tag{2.46}$$

then all the levels become filled. If the forward bias is now removed and a reverse bias applied, then the depletion region expands uncovering the electron occupied deep levels (Figure 2.10c). The response time of the electrons is relatively slow and temperature dependent. A steady state situation is reached when all the deep levels above ξ_n lose their electrons, and all below it remain full. When the electrons are emitted to the conduction band they leave behind a net positive charge, which increases the space charge density. Under application of a constant voltage this causes the diode capacitance to increase as seen in figure 2.11, causing the depletion layer width to reduce. Under the simple case where $n_T = N_T$ at t = 0 and $n_T = 0$ at $t = \infty$, electron emission following a reverse bias is given by[30]:

$$\frac{dn_T}{dt} = -e_n n_T \tag{2.47}$$

Thus

$$n_T = N_T exp(-e_n t) \tag{2.48}$$

The trapped electron density decays with a time constant $(e_n)^{-1}$ and the positive space charge, and therefore capacitance builds up as $(1-exp(-e_n t)$[30]. The time constant $(e_n)^{-1}$ depends critically on the energy of the level, E_T, and the temperature T, given by:

$$e_n = T^2 \sigma_n exp\left(\frac{-E_T}{k_B T}\right) \tag{2.49}$$

where σ_n is the electron capture cross section of the trap. The temperature dependence of e_n is usually dominated by the exponential term, so by performing the sequence given in figure 2.11 a set of transients are obtained. The temperature dependence of these transients is the basis for the Deep Level Transient Spectroscopy (DLTS) technique discussed later in chapter 4.

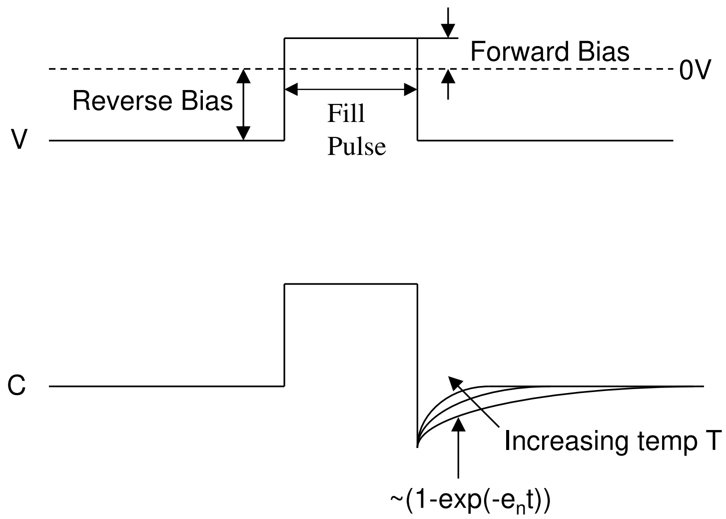

Figure 2.11: Temperature dependence of the capacitance transient.

2.5 Current Transport

The forward and reverse bias leakage currents inherent in semiconductor Schottky barrier devices are known to be strongly dependent on the properties of the semiconductor material. The quality of the material therefore has strong implications on the performance of the Schottky barrier as a detector. These currents are products of the current transport in the device.

Measurement of the current characteristics as a function of bias, and an understanding of the four major processes in a forward biased barrier, as discussed below, allow an analysis of the mechanisms which contribute to the observed current in GaAs Schottky detectors, such as identification of the properties of deep level defects.

The four conduction processes for a forward biased metal-semiconductor junction as shown in figure 2.12 are[27],[12]:

1. transport of electrons from the semiconductor over the top of the potential barrier into the metal.

2. quantum mechanical tunnelling of electrons through the barrier.

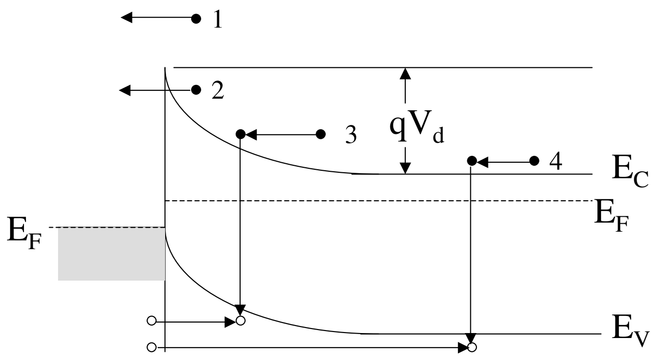

Figure 2.12: Conduction processes in the forward biased Schottky barrier.

3. recombination in the depletion region.

4. recombination in the neutral region (hole injection from the metal to the semiconductor).

It is possible to make 'nearly ideal' Schottky diodes where (1) is the predominant process. The other processes cause a departure from ideality. Under reverse bias the current characteristics are defined by the reverse of the first three processes.

Transport of electrons over the barrier is the most important process in defining ideal Schottky device operation and therefore this will be described in detail. Recombination in the depletion region under forward bias, and its opposite, generation current under reverse will also be discussed. The effects of tunneling and hole injection are not discussed in detail. However for a detailed analysis of these processes, refer to [28].

2.5.1 Emission over the barrier

The transport of electrons is a result of either drift and diffusion processes, or by emission into the metal. These two processes effectively act in series with each other and the resulting current is determined by which of the two processes is the more dominant. The first process gives is governed by diffusion theory and the second is addressed by Bethe's thermionic emission theory.

Diffusion Theory

Diffusion theory states that the concentration of electrons in the conduction band of the semiconductor remains independent of applied bias. This is the case when the quasi-Fermi level ξ_n in the semiconductor drops down from the level in the depletion region to that at the barrier such that it coincides with the metal Fermi level.

The current dependence on bias voltage as predicted by the diffusion theory in the rectifying metal-semiconductor junction is given by[28]:

$$J = qN_c\mu\varepsilon_{max}exp\left(\frac{-q\phi_B}{kT}\right)\left[exp\left(\frac{qV}{kT}\right) - 1\right] \tag{2.50}$$

where ε_{max} is given by equation 2.28. Equation 2.50 differs from the ideal rectifier characteristic given by equation 2.56 for thermionic emission because ε_{max} is dependent on bias voltage.

Thermionic Emission Theory

In thermionic-emission theory the current is primarily defined by the rate of transfer of electrons across the metal/semiconductor interface, consisting of two components: the flow of electrons from the semiconductor to the metal, and the flow of electrons from the metal to the semiconductor where the work function ϕ_m is replaced by the barrier height ϕ_b. The quasi-Fermi level is flat in the depletion region and coincides with the Fermi-level in the bulk of the semiconductor, therefore, qξ_n = E_F. The current density from the semiconductor to the metal is:

$$J_{sm} = \frac{v_{th}nq}{4} \tag{2.51}$$

$$= \frac{qN_cv_{th}}{4}exp\left(\frac{-q(\phi_b - V)}{kT}\right) \tag{2.52}$$

where v_{th} is the average electron thermal velocity in the semiconductor with effective mass m^* given by[26].

$$v_{th} = \left(\frac{8kT}{\pi m^*}\right) \tag{2.53}$$

There is also a flow of electrons from the metal to the semiconductor (J_{ms}) which is assumed to be bias independent, because ϕ_b seen from the metal is unchanged (assuming no bias dependence of ϕ_b). For zero bias there is no net current, therefore:

$$J_{ms} = J_{sm}(V = 0) = \frac{qN_c v_{th}}{4} \exp\left(\frac{-q\phi_b}{kT}\right) \tag{2.54}$$

When an external bias is applied, the net current flow is equal to the difference between the currents J_{sm} and J_{ms}, thus:

$$J = \frac{qN_c v_{th}}{4} \exp\left(\frac{-q\phi_b}{kT}\right)\left[\exp\left(\frac{qV}{kT}\right) - 1\right] \tag{2.55}$$

Substituting N_c from equation 2.3 and v_{th} from equation 2.53 gives:

$$J = J_0\left[exp\left(\frac{qV}{k_BT}\right) - 1\right] \tag{2.56}$$

where the saturation current J_0 is given by:

$$J_0 = A^*T^2 exp\left(-\frac{q\phi_b}{k_BT}\right) \tag{2.57}$$

and the Richardson constant A^* is given by[27]:

$$A^* = \frac{4\pi m^* q k_B^2}{h^3} \tag{2.58}$$

where m_* is the electron effective mass.

While ideal devices with good Schottky contacts will possess low voltage I-V characteristics defined by equations 2.56 and 2.57, in a real device the presence of other current transport processes will mean that the measured characteristics deviate from theory. These deviations from ideality are characterised by the *Ideality Factor* n, such that equation 2.56 is modified to:

$$J = J_0 \left[exp\left(\frac{qV}{nk_BT}\right) - 1 \right] \tag{2.59}$$

For an ideal device where thermionic emission is dominant process, n tends to unity.

Combined Theory

The diffusion and thermionic emission theories can be combined by placing the thermionic and diffusion currents in series resulting in the complete expression for the current:

$$J = J_s \left[exp\left(\frac{qV}{k_BT}\right) - 1 \right] \tag{2.60}$$

where

$$J_s = A^{**}T^2 exp\left(\frac{-q\phi_b}{k_BT}\right) \tag{2.61}$$

where A^{**} is the effective Richardson constant. For GaAs Schottky barrier diodes the current is predominantly due to thermionic emission of majority carriers, therefore, the diffusion current does not play a major part in the current characteristics.

2.5.2 Recombination and Generation

It was discussed in section 2.3 that the effect of charge recombination can reduce the effectiveness of a semiconductor because it limits the probability of the charge generated by an incident particle reaching the electrodes. Recombination is a process that occurs in Schottky devices under a forward bias, and the probability of recombination taking place is defined by the the energy of deep level acting as a recombination centre as shown in figure 2.4. Schockley-Reed-Hall statistics, discussed in reference [26], state that under a forward bias the maximum recombination rate occurs when the trap energy is near the middle of the band gap. Chapter 4 discusses that SI-U GaAs and GaAs material grown by the VPE technique exhibit defects with such deep level defects, predominantly the well known EL2 level. Chapter 5 discusses that the concentration of such defects also increases with proton irradiation.

Recombination current is given by [12],[26]:

$$J_r = J_{r0}\left[exp\left(\frac{qV}{2kT}\right) - 1\right] \tag{2.62}$$

where

$$J_{r0} = \frac{qn_iW}{2\tau} \tag{2.63}$$

where W is the thickness of the depletion region, n_i is the intrinsic carrier concentration and τ is the carrier lifetime in the depletion region.

Generation in the depletion region is the opposite process to forward biased recombination. Because semiconductors operate under reverse bias then this process is of great importance. Generation current J_{gen}, discussed in more detail in [27], is given as:

$$J_{gen} = \frac{qn_iW}{2\tau} \tag{2.64}$$

J_{gen} in a function of applied bias due to its dependence on depletion width W, and therefore from equation 2.34:

$$J_{gen} \propto V_d^{\frac{1}{2}} \tag{2.65}$$

Because of the temperature dependence of n_i and τ, J_{gen} has a temperature[27] dependence of:

$$\begin{aligned} J_{gen} &\propto \frac{n_i}{\tau} \\ &\propto v_{th}\sqrt{N_C N_V} exp\left(-\frac{E_A}{kT}\right) \\ &\propto T^{\frac{2}{3}}T^{\frac{1}{2}} exp\left(-\frac{E_A}{kT}\right) \end{aligned} \tag{2.66}$$

where E_A is the generation activation energy. Under high reverse bias where current increases from ideality due to recombination, measurement of the reverse bias current as a function of temperature can result in identification of the activation energy E_A of the main generation centre. These measurements are carried out in chapter 4.

A theoretical estimate can now be made of the reverse and forward bias current in a GaAs Shottky diode detector. The reverse bias characteristics are observed in figure 2.13. The thermionic current is calculated using equation 2.60 and 2.61 where N_D is 1.7×10^{14} cm^{-3}, ϕ_b is 0.905eV and A^{**} is 117A$cm^{-2}k^{-2}$, and T is 300K. Barrier lowering is calculated using equation 2.44 and generation current J_{gen} is calculated as a function of depletion width using equation 2.34 and 2.64 with τ equal to 6ns. It is observed that the effect of barrier lowering as discussed in section 2.4.4 increases the current density, and that generation current does not become the predominant source of current until the reverse bias is over 10V. The values for N_D, ϕ_b and A^{**} are taken from measurements carried out in chapter 4, while τ is as calculated by Vaitkus et-al in [73].

Forward bias characteristics are given in figure 2.14, where again the current at low voltages can be explained by thermionic emission. As the forward bias is increased and the forward current increases there is an increase in the electron density in the material which causes a change in the bulk resistivity of the material. This is shown by the dotted line deviation from the thermionic curve.

2.6 The EL2 level

The EL2 level is a mid-gap level present in GaAs. It was originally postulated in 1961 [33] and while much debate has taken place as to its exact origin it is the accepted view today that this level is an arsenic antisite defect (an arsenic atom an a gallium lattice site, denoted by As_{Ga}). The EL2 level is a deep level double donor with three charge states; neutral when

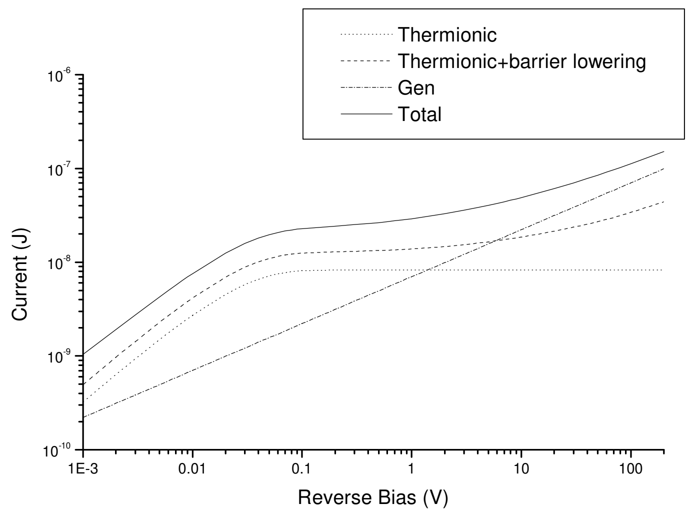

Figure 2.13: Theoretical reverse bias current characteristics of a GaAs Schottky detector at room temperature.

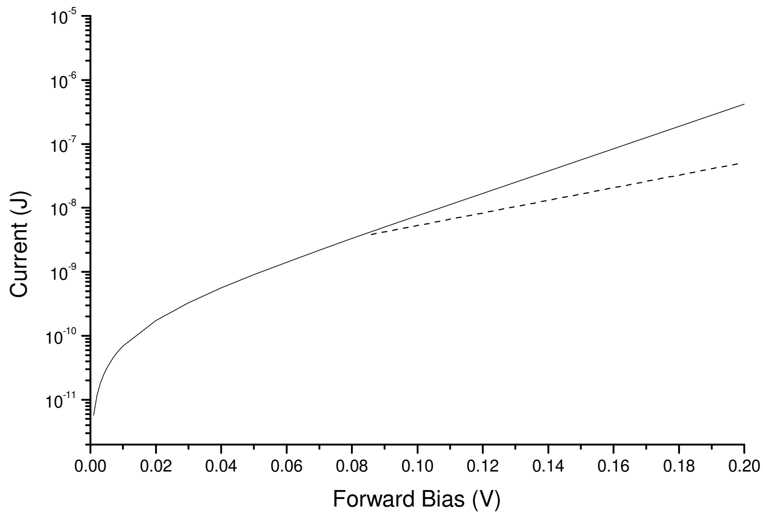

Figure 2.14: Theoretical forward bias current characteristics of a GaAs Schottky detector at room temperature.

occupied by electrons, plus one, and plus two when it has donated both of its electrons. These three charge states give rise to two electrical energy levels, one at 0.75 eV below the conduction band, and the other at 0.52 eV above the valence band[18]. It has also been known for some years that high concentration of EL2-like defects are introduced in GaAs after proton and neutron irradiation[35]. These irradiation induced defects appear to differ from grown-in EL2 centres because they can be annealed out at temperatures between 500 and 600 K unlike the grown-in centres which are stable up to 1200 K. They also do not exhibit *photoquenching*, the property whereby the EL2 centres can be excited into an inert metastable $EL2^*$ state[71], discussed in more detail in chapter 6.

A high resistivity material is required for semiconductor detectors to ensure a large active depletion region at low reverse bias. Pure intrinsic GaAs has a resistivity of $3 \times 10^8 \Omega cm$ calculated using equation 2.17 with a value of $n_i = 1.79 \times 10^6 cm^{-3}$. Such a pure material cannot realistically be grown due to contamination from impurities including the EL2 level. However the EL2 level can be utilised to solve this problem by the use of the technique of over-compensation, resulting in a very low carrier concentration and therefore a very high resistivity $\geq 10^8 \Omega cm$. Over-compensation results in such a low carrier concentration by transferring all the free carriers from the net shallow acceptors (usually carbon in LEC GaAs) to the deep levels where the probability of thermal excitation is low. The resistivity of semi-insulating GaAs is strongly dependent on stoichiometry where it is seen in figure 2.15 that high resistivity is achieved with an arsenic atom fraction greater than 0.48 in the melt[18].

2.7 Field Enhanced Electron Capture

The electron emission rate and capture cross sections mentioned in section 2.4.5 are a function of the electric field. The emission rate increases with increasing electric field according to the Poole-Frenkel [12] effect as a result of a lowering of the Coulomb potential barrier as shown in figure 2.16. The electron energy diagram at zero electric field is given in the figure by the solid

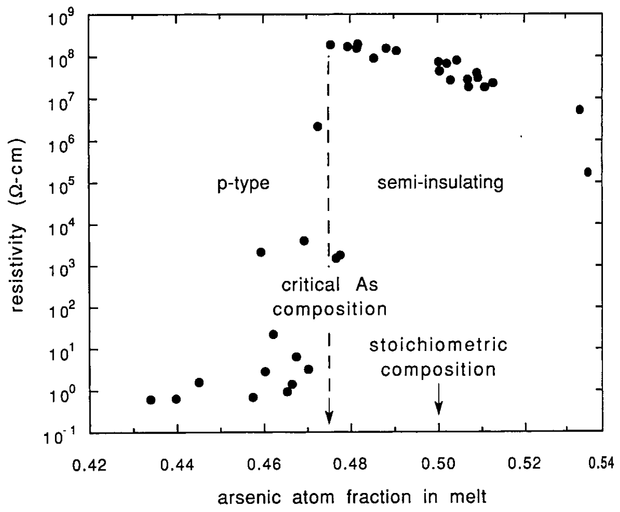

Figure 2.15: Resistivity of LEC GaAs as a function of arsenic atom fraction in the melt

lines. An energy E_c - E_t is required to emit an electron from the trap. In the presence of an electric field the bands are slanted as given by the dotted lines, and the emission energy is reduced by ΔE. The reduction in energy ΔE_{PF} due to the Poole-Frenkel effect is given by the following:

$$\Delta E_{PF} = \sqrt{\left(\frac{q\epsilon}{\pi\varepsilon_s}\right)} \tag{2.67}$$

The electron capture cross section is found to increase with increasing electric field only at high electric fields ($> 10^5 V cm^{-1}$). The effect of this, discussed in more detail in reference [17], is that there is a fall in the $EL2^+$ concentration with increasing electric field, which at a critical field strength results in zero net charge in the depletion region. In SI GaAs where the EL2 concentration is high ($N_{EL2} = 10^{16} cm^{-3}$), a constant field distribution, as displayed in figures 2.6 b) and 2.17 is found. This effect is not found in unirradiated VPE GaAs where the EL2 concentration is low, and therefore the change in compensation between the shallow donors and the EL2 level due to field enhanced increase of the electron capture cross-section is insignificant.

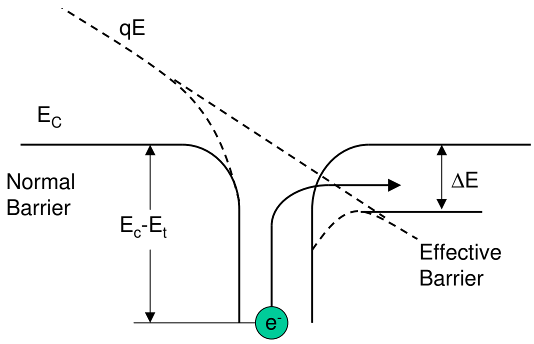

Figure 2.16: Electron emission due to the Poole-Frenkel effect.

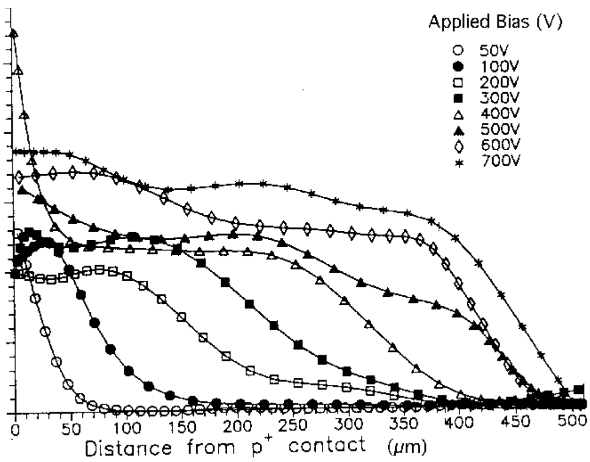

Figure 2.17: Measured electric field distribution of SI GaAs reverse biased Schottky diode for different reverse biases[36]

Chapter 3

Device Fabrication and Detector Theory

This chapter gives a brief introduction to the operation of semiconductor radiation and charged particle detectors. The devices used for all the experimental work reported in this thesis were fabricated in the Department of Electronics and Electrical Engineering at the University of Glasgow, and therefore the processes involved in the fabrication of these devices are briefly covered. The choice of detector material is based on the requirement for low defect levels to minimise recombination, and thick layers to ensure that incident particles liberate enough electron-hole pairs to give a sufficient signal. A brief explanation of the theory behind these requirements for the operation of a detector is also given.

3.1 Detector Theory

A semiconductor detector operates in the same manner as a conventional ionisation chamber detector where incident particles, or ionising radiation generate electron-hole (e-h) pairs, which under application of an electric field drift to their relevant contacts where a signal is produced, as seen in figure 3.1. For a semiconductor detector this is obtained by applying a voltage across two

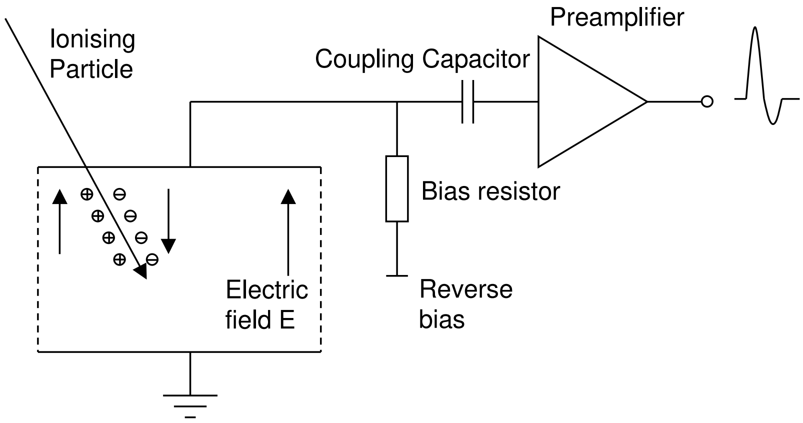

Figure 3.1: Generation of e-h pairs in semiconductor detector

metal contacts fabricated on opposite sides of the semiconductor. A means however is required to ensure that when an electron or hole is collected at one electrode the same carrier species is not injected at the opposite electrode otherwise no signal would be detected. The Schottky contact is a blocking contact that meets this requirement where charge carriers are removed by the application of an applied electric field and are not replaced at the opposite electrode. A further requirement is that when a reverse bias is applied the dc current level must be low enough to ensure that shot noise (discussed in chapter 7) is minimised. This situation is obtained by implementation of the Schottky contact.

3.1.1 The Depletion Region

In the Schottky contact, described in detail in section 2.4, a potential barrier is formed at a metal-semiconductor interface. The depletion layer at the metal-semiconductor interface is similar to that of a one-sided *pn* junction[27], where on application of a reverse bias, the high resistivity depletion region extends into the semiconductor material. This is the active region of a semiconductor detector. The width of the depletion region W is proportional to

$V^{\frac{1}{2}}$, where V is the applied reverse bias, as given in equation 2.34. A requirement for an efficient detector is that the depletion region is wide enough to ensure that a sufficient number of e-h pairs are generated to induce a measurable charge at the contacts. It is this charge that is measured to determine the energy of the incident radiation. As seen from equation 2.34 the depletion width is also proportional to $N_D^{-\frac{1}{2}}$. A pure material with low doping density N_D is therefore required to deplete the detector fully at low voltages. A bias of 47 V is required to obtain a depletion width of 20 μm, when $N_D = 1.7\times10^{14}cm^{-3}$. This is the range of the 5.5 MeV α particles from an Am^{241} source that are used to determine the detector characteristics.

3.1.2 Signal Formation

The number of e-h pairs produced in a semiconductor detector by the interaction of incident ionising radiation is directly proportional to the energy deposited by the ionising radiation. On average an energy deposition of 4.2 eV is required in GaAs to create an e-h pair [18], so, for example the 5.5 MeV α from the Am^{241} source, which is the source used for CCE measurements described in the next chapter, will produce 1.31×10^6 e-h pairs. Under the influence of the electric field these charges drift towards the contacts as shown in figure 3.1.

The current signal at the electrodes does not, however, begin when the charge reaches the electrode. It begins when the induced charge begins to move in the detector. When an e-h pair is created, both the positive and negative charges couple to the electrodes and induce mirror charges of equal magnitude . Ramo's theorem states that the charge at contact due to the motion of electrons Q_e is given by the following equation[4]

$$Q_e = q\frac{x_0}{W} \tag{3.1}$$

and due to the motion of holes Q_h is

$$Q_h = q\left(1 - \frac{x_0}{W}\right) \tag{3.2}$$

where W is the separation of the electrodes (in semiconductor detectors with a good ohmic contact this seperation is the depletion region width), and x_0 is the position of creation of the e-h pair with respect to the Schottky contact. It can be observed from these two equations that the total charge induced at both electrodes $Q_e + Q_e$ by the creation of one e-h pair is equal to q. It can further be seen that the charge carrier that traverses the greatest distance in the detection medium contributes more to the total charge. As an example, irradiation with the 5.5 MeV α used for CCE measurements incident on the Schottky contact induces charge 20μm under the Schottky contact. Electrons travel the greatest distance in a 50μm detector, therefore they contribute to the total charge 60%.

Various methods of signal acquisition are possible but the basic philosophy is based on the creation of a voltage from the induced charge by the use of a capacitance where;

$$V = Q/C \tag{3.3}$$

3.2 Growth of VPE GaAs

Most of the work carried out on GaAs detectors by previous authors is based on material made by bulk growth techniques. The method of Liquid Encapsulated Czochralski (LEC) is one of the most common bulk growth techniques used, where high purity arsenic and gallium are melted in a high temperature vessel and slowly cooled to produce a large single crystal from a seed crystal[20]. This material contains high levels of carbon which acts as a shallow acceptor, and also deep level impurities such as the well studied EL2 As_{Ga} defect[40]. The semi-insulating nature of LEC GaAs is obtained through over compensation of the shallow levels with the deep level EL2, as discussed in section 2.6.

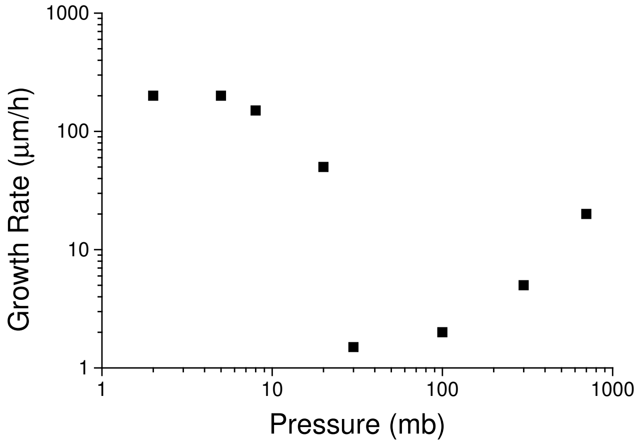

Figure 3.2: Change in growth rate of VPE GaAs with pressure

The advantage of the growth of high purity GaAs layers using the Vapour Phase Epitaxy (VPE) method is that impurity levels in the order of $1 \times 10^{14} cm^{-3}$ can be achieved. R. L. Adams describes the Low-Pressure VPE growth system manufactured by the *Aixtron Corporation* used to produce material for this work in reference [20]. The epitaxial GaAs layers are produced using the following reaction. Hydrogen gas is forced through liquid $AsCl_3$ into a reaction furnace holding a container of Ga source material creating a Ga and As mix in the vapour phase. The GaAs substrates are then loaded into the reaction furnace where they are brought into contact with the vapor phase Ga and As mix. A reaction then takes place which forms layers of high purity GaAs[18]. It was observed in reference [20] that the growth rate of the VPE layers depended on the pressure under which the growth chamber was held. As the pressure of the chamber decreased from atmospheric pressure the growth rate reduced, until the pressure reached about 50 mbar. Below these pressures the growth rate increased rapidly, reaching value of $\sim 100 \mu$m/h at 1 - 10 mbar, as seen in figure 3.2. It is availabilty of these thick layers which make VPE GaAs a suitable material choice for radiation detectors.

3.3 Device fabrication

The detectors used in this investigation were grown on epitaxial GaAs supplied by AIXTRON and fabricated by Mr D. Meikle in the Dept. of Electronics and Electrical Engineering at the University of Glasgow. The epitaxial layers were grown onto a heavily doped, 600 μm thick SI-LEC substrate. The substrate was doped with 1×10^{18} silicon atoms cm^{-3}, to enable the production of an ohmic n^{+} back contact as described in section 2.4.2.

The topology of the front side (VPE side) showed a large variation throughout the different devices. The samples were therefore polished with a chemo-mechanical polish of $H_2 0_2$: NH_4 solution of pH 7.9 $\pm$ 0.1, to make the surfaces more uniform and to remove any surface defects. This process removed approximately 30μm from the VPE layer, resulting in a VPE layer of thickness 50μm.

The diodes were then fabricated with a 3mm diameter pad contact, surrounded by a 200μm guard ring, separated from the pad contact by 10μm, as shown in figure 3.3. The contacts were evaporated on both the front and backside of the detector using a *Plassys MB430* Evaporator. The metallisation, as shown in figure 3.3, was a Ti/Pd/Au multi-layer. Au diffuses very quickly into GaAs, therefore the Pd layer is introduced to prevent this. Ti is used to improve the adhesion of the metal to the GaAs. The metallisation on the front VPE layer creates the Schottky contact, while that on the back creates an ohmic contact due to the n^{+} nature of the substrate. DC measurements carried out in chapter 4 result in the back contact resistance of around 1Ω while the junction resistance is in the range of 10's of MΩ's.

3.3.1 The Guard Ring

The guard ring, which is fabricated around the main pad structure, has several functions.

1. When the guard ring is held at the same potential as the pad then the area of the depletion region under the pad is uniform, as the edge

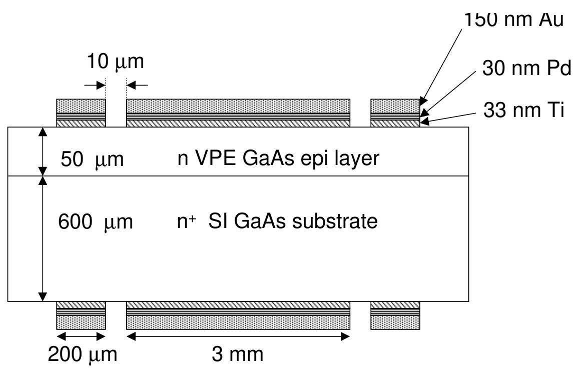

Figure 3.3: Cross section of VPE diode fabricated on front and back with Ti/Pd/Au contact

effects of the electric field are found around the guard ring only.

2. The guard ring also has the effect of removing current generated by surface states.

The separation between the guard ring and the pad must be similar to or less than the thickness of the depletion region for 3) to be effective. The guard ring structure is therefore only used in high resistivity materials with a large depletion region.

3.4 Summary

Given the availability of suitable material, the technology and expertise exists in-house to fabricate semiconductor detectors based on the Schottky contact. The important feature of these structures is that the analysis of their characteristics allow a detailed analysis of the material properties.

Chapter 4

Characterisation of Non-Irradiated GaAs Detectors

A detailed investigation of the macroscopic electrical characteristics of the semiconductor detector gives vital information about the material properties. For a Schottky diode detector to operate at its optimum signal-to-noise ratio, the leakage current must be low enough under the required high reverse bias that both shot noise, (as covered in chapter 7), and heating effects are minimised, and charge collection efficiency (CCE) is maximised. The macroscopic characteristics for unirradiated detectors are presented in this chapter. An investigation of these characteristics after proton irradiation is described in chapter 5. Throughout a comparison is made to devices fabricated on SI-U GaAs.

The devices under investigation were fabricated on a 3" wafer grown by *AIXTRON AG*, and identified as AX1221. The wafer consists of a 50 μm thick (after surface polishing) Vapour-Phase Epitaxy (VPE) layer grown on an LEC substrate. The growth and fabrication techniques are described in chapter 3. For comparison, I-V measurements with identical contact geometries were carried out on SI GaAs detectors under similar test conditions. The devices are fabricated with a 200μm wide guard ring separated from the pad by 10μm. Unless otherwise stated, all measurements are carried out at

300K.

These measurements are of importance in that they will act as a direct reference for the changes in macroscopic characteristics as a function of proton fluence investigated in later chapters.

4.1 Capacitance-Voltage Characteristics

Measurements of the capacitance characteristics of a reverse biased diode as a function of voltage provide information about the material properties. Assuming a uniform doping concentration, a plot of $1/C^2$ against V will give a straight line where, using equation 2.35 of section 2.4.3, the gradient is equal to $2/(q\varepsilon_s N_D)$. In an ideal defect free n-type material where $N_D \gg N_A$ this allows the measurement of the donor density N_D. If there were shallow acceptors then N_D would be replaced by $N_D - N_A$ throughout.

In a real device, however, the presence of deep-level defects in the material means that C-V measurements do not give a true measure of N_D, but actually give the effective impurity concentration N_{eff} in the depletion region. The ionised shallow-level donors in the depletion region are positively charged and $N_{eff} = N_D^+ - n_T^-$ for deep-level acceptor impurities that are negatively charged when occupied by electrons. When occupied by holes, the deep levels are neutral and $N_{eff} = N_D^+$. For shallow-level donors and deep-level donor impurities occupied by electrons $N_{eff} = N_D^+$, and for deep level donors occupied by holes $N_{eff} = N_D^+ + p_T^+$ [64]. For the following work the effective space-charge ionised impurity concentration will be referred to as N_D.

The capacitance characteristics were measured using a Hewlett Packard multi-frequency LCR meter and a Keithley 237 bias supply. Both instruments were controlled with a *Labview*^{TM} program. The LCR meter is capable of measuring the capacitance by applying a small signal a.c. voltage across the biased detector with modulation frequency ω, ranging from 100 Hz to 100 kHz. The meter also has the ability to compensate for the capacitance of the cables and connectors.

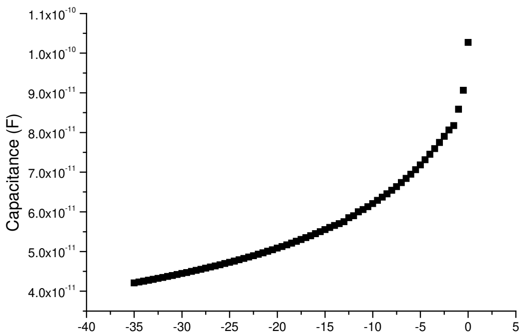

(a) The reverse bias capacitance characteristic at 293K with a modulation frequency of 100 kHz.

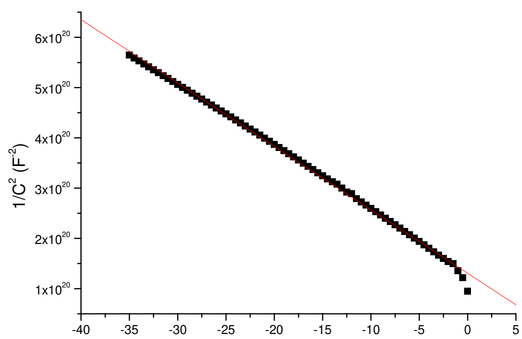

(b) The plot of $1/C^2$ against V, resulting in a doping density N_D of $1.72 \times 10^{14} cm^{-3}$

Figure 4.1: The C-V characteristics of AX1221-9

A C-V measurement was carried out on device AX1221-9 over the full range of modulation frequencies ω accessible with the LCR. The resultant C-V with a modulation frequency of 100 kHz is shown in figure 4.1(a). The plot of C^{-2} against V, as given in figure 4.1(b), gave a value of N_D of $(1.72 \pm 0.01) \times 10^{14} cm^{-3}$, close to the value of $1.7 \times 10^{14} cm^{-3}$ quoted by the manufacturers. The error is due to the uncertainty in the linear fit to the data. The measured capacitance of the VPE devices is independent of modulation frequency of the LCR meter.

For comparison the C-V plot for SI-LEC GaAs device G175-5A is given in figure 4.2, where it can be seen that the measured capacitance is now dependent on sample frequency ω. There are two possible explanations for this.

The device capacitance is measured by the application of the small signal a.c. voltage of sample frequency ω across the biased detector. In this modulated C-V measurement, it is assumed that the detector junction capacitance is the only significant element in the circuit and that the measured out of phase current I (90^0 phase shift if this assumption is true) gives the true

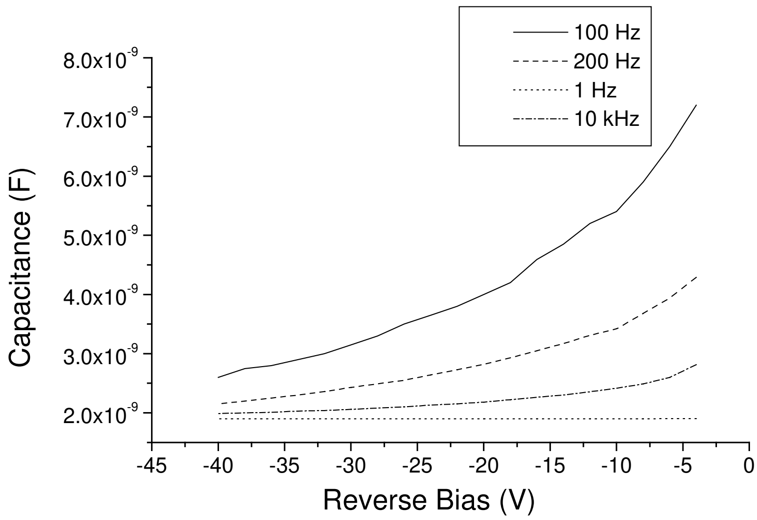

Figure 4.2: C-V characteristic at 300Kfor LEC device G175-5A

capacitance as a function of bias[18], where the depletion width capacitance is given by:

$$I = \frac{V}{Z} = j\omega VC \tag{4.1}$$

where Z is the detector impedance, ω is the modulation frequency and V is the applied reverse bias. In reality, diodes have a significant resistance between the junction and the ohmic contact, as shown by R_b in figure 2.8, and modulated C-V measurements can give false results regarding the active region width. The high resistivity of SI-LEC GaAs creates a condition where the C-V measurements show no change in capacitance with voltage for frequencies over 1 kHz. When the Schottky diode is regarded as a resistance R_j in parallel with a capacitance C_j in the depletion region, and a resistance R_b in parallel with a capacitance C_b in the substrate then the impedance across the diode can be described by:

$$Z = \left[\frac{R_j}{1 + j\omega R_j C_j} + \frac{R_b}{1 + j\omega R_b C_b}\right] \tag{4.2}$$

When the substrate resistivity becomes comparable with the depletion region resistivity, then the impedance reduces to:

$$Z \approx \frac{\rho(L_j + L_b)}{A(j\omega\rho\varepsilon_s + 1)} \tag{4.3}$$

where ρ is the resistivity, L_j and L_b are the lengths of the depletion region and the substrate respectively. The current is approximated by:

$$I \approx V_R \left(\frac{1}{(R_j + R_b)} + j\omega C_T \right) \tag{4.4}$$

where C_T is the series combination of C_j and C_b and is equivalent to the parallel plate capacitance between the Schottky and Ohmic contact. The effect is that the detector appears to have a constant capacitance C_T between the contacts.

The second explanation is that the presence of high concentrations of the deep EL2 level also contributes errors in the C-V measurements. It is often assumed that a change in bias will result in an immediate change in depletion thickness. This is the case as long as the carrier emission rate is greater than the modulation frequency ($e_n > \omega$), i.e. for most shallow level impurities. However this is not the case in materials with high concentrations of the deep EL2 level. The EL2 level has a room temperature electron emission rate of 0.045 s^{-1}[40], indicating that the modulation frequency must approach this rate to avoid false conclusions from the C-V measurements. The observed change in capacitance may be due to a contribution from both of the effects discussed.

An estimation is made as to the effective doping density N_D of a SI-U LEC device with a sample frequency of 120Hz. From a plot of $1/C^2$ against V, N_D was measured as $(7.70 \pm 0.02) \times 10^{15} cm^{-3}$. It must be remembered that this is only an estimate and that the true value is likely to be higher due to incomplete emptying of the traps. An EL2 concentration in the order of $10^{16} cm^{-3}$ was reported in [12].

4.2 Current-Voltage Characteristics

A requirement for optimum detector operation is that it exhibits low leakage current under the reverse bias required for full depletion to ensure minimum noise. Investigation of the current-voltage (I-V) characteristics can also give information on the carrier transport mechanism occurring in the material as well as identification of the mechanisms responsible for deviation from ideality. I-V measurements were carried out on VPE GaAs pad detectors under both forward and reverse bias directions, and over a series of voltage ranges. The measurements were carried out in a variable temperature environmental chamber using the Keithley 237 voltage source controlled by a $Labview^{TM}$ program.

4.2.1 Ideality Factor

The ideality factor n defined in equation 2.59 is used to characterise a device's deviation from ideality where processes other than thermionic emission are present. While at higher biases recombination currents and bias dependence of barrier heights are a common cause of departure from ideal behaviour of the device, the usefulness of n at low voltages is really as a measure of the contact quality. Measurements here are therefore restricted to low forward biases.

The value of n may be obtained by plotting ln(J/[1-exp(-qV/kT)]) against V. The gradient of the line is $\frac{q}{nkT}$. Shown in figure 4.3 are the results for AX1221-9 at 293 K. The fit was only performed on data between forward bias of 50 mV and 200 mV, and results in a value of n equal to 1.02 $\pm$ 0.05. The devices used in the work presented here are selected to have similarly high quality contacts. These are of a higher quality than the SI-U devices used in experiments by other authors where n was measured as 1.04 [12].

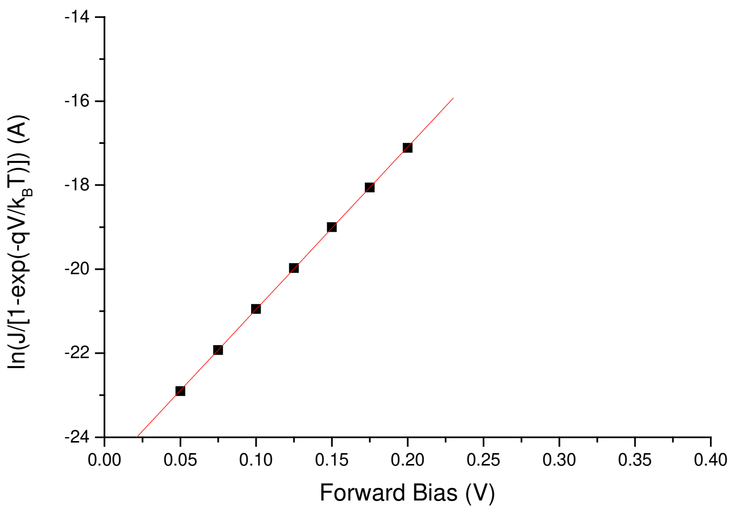

Figure 4.3: Low voltage forward bias I-V calculation of ideality factor n for AX1221-9

4.2.2 High Voltage Reverse Bias Measurements

The high voltage reverse bias characteristics of AX1221-9 are shown in figure 4.4. It can be seen that the leakage current is extremely low when the guard ring is held at the same bias as the pad, in the order of tens of nA's over a wide range of reverse biases. The increase in leakage current between reverse bias of -1V to -150V is observed to be almost linear. Beyond this voltage the current begins to increase, and breakdown eventually occurs at around -200V. The current increases when the guard ring is disconnected due to an increase in surface currents and possibly an increase in lateral spreading of the depletion region. The I-V characteristic of the VPE GaAs diode is in stark contrast to that obtained from diodes fabricated on SI-LEC material, as shown in figure 4.5. It can be seen here that the measured current in SI-U LEC devices increases rapidly until it reaches a plateau region in the order of 0.1 μA at a bias of about -10V. This characteristic is of importance for irradiated VPE devices, as will be discussed in chapter 5. The steep increase in current in the reverse bias range of 0 to 25 V is assumed to be due to

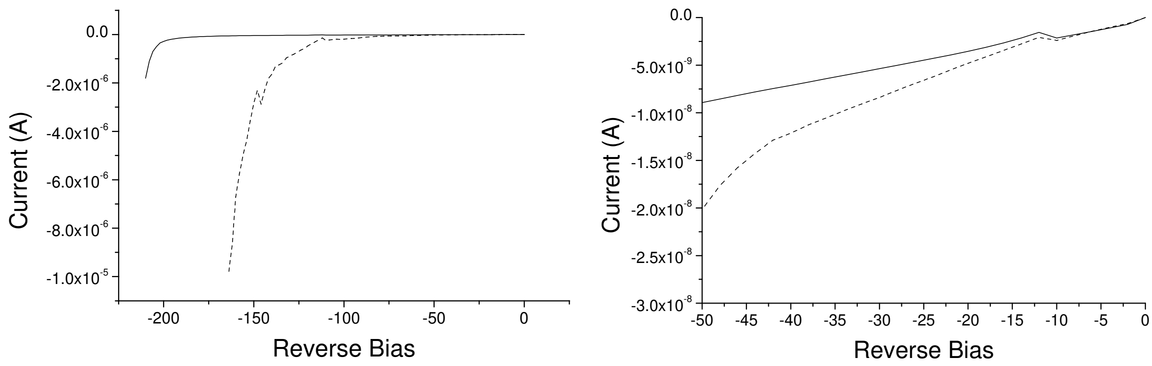

(a) High voltage range

(b) Zoom in of the lower voltage range

Figure 4.4: Reverse bias IV for diode AX1221-21 fabricated on VPE GaAs. Solid line: guard ring connected, dashed line: guard ring disconnected

generation in the depletion region through the EL2 level. It was explained in equation 2.66 from section 2.5.2 that:

$$J_{gen} \propto T^2 exp\left(-\frac{E_A}{kT}\right) \tag{4.5}$$

Under reverse bias a plot of ln(I/T^2) against 1/T will allow the evaluation of E_A of the active generation centre responsible for the current.

The presence of the EL2 level as a generation centre was verified by a measurement of the activation energy of SI-U GaAs device G175-5A, as a function of temperature at a reverse bias of -10 V to be $E_a = 0.75 \pm 0.02$ eV [12]. This corresponds to the EL2 energy of $E_t = 0.75$ eV as reported in reference [38][12]. As equation 2.64 suggests, generation current should increase proportionally to depletion width W, and therefore as the square root of reverse bias voltage V, however it is observed to plateau as in figure 4.5. This plateau in reverse current has been suggested as being due to space charge limiting effects involving the field enhanced electron capture cross-section of the EL2 level, as discussed by M. Rogalla et al in reference [17], and section 2.7 of this thesis. A further increase in reverse bias beyond -10V

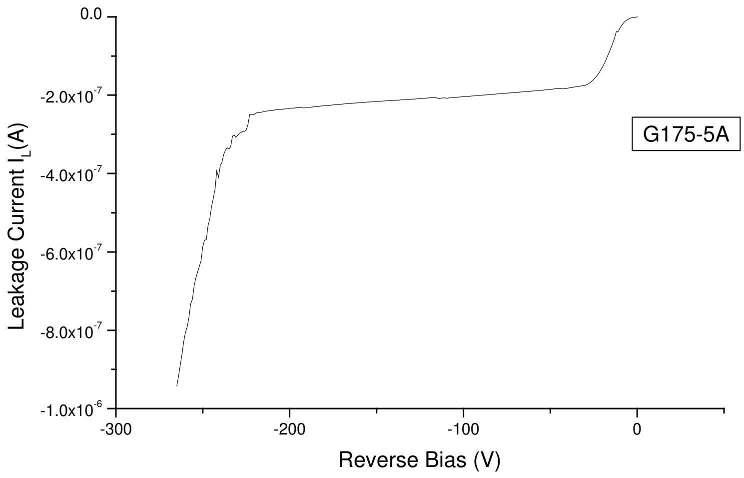

Figure 4.5: The high voltage reverse bias IV for diode G175-5A fabricated on SI-LEC GaAs

results in no significant change in the magnitude of the electric field. This results in a saturation of the drift velocity, and therefore no increase in drift current.

Measurements were also carried out on VPE device AX1221-9 at -10V. The activation energy of the the device was measured as 0.73 ± 0.02 eV and was therefore also identified as the EL2 centre.

These measurements give no details as to the concentration of the EL2 centre, however C-V measurements carried out in section 4.1 identified that the defect concentration in reverse biased SI-U LEC devices was orders of magnitude greater than in VPE devices. It is therefore assumed that the plateau in reverse bias I-V characteristics found in the SI-U devices is a direct result of high concentrations of the EL2 level.

4.2.3 Device Resistivity Measurements

The junction and bulk resistances R_j and R_b can be calculated separately by fitting the low voltage I-V characteristics to the ideal diode equation 2.60:

$$J = P(1)\left[exp\left(\frac{V - IP(2)}{P(3)}\right) - 1\right] \tag{4.6}$$

where P(1), P(2) and P(3) are free parameters, I is the measured current and V is the applied voltage as described in detail in reference[34]. Assuming that the measured current I passes through R_j and R_b, then the voltage dropped across the junction is V - IR_b. The free parameters are altered until the fitted curve matches the measured curve to less than 0.1 % at 0.01V (kT/2). The value of P(2) gives R_b.

At very low voltages it is found that the I-V relationship is linear, and therefore the effective device resistance R_{eff} can be calculated using Ohm's law. The junction resistance is now simply $R_j = R_{eff} - R_b$.

The measurements carried out on AX1221-9 at 300 K, corrected for a cable resistance of 0.3Ω, as shown in figure 4.6, result in $R_b = 1.27 \pm 0.05\Omega$, and $R_j = 23.39 \pm 0.5 M\Omega$.

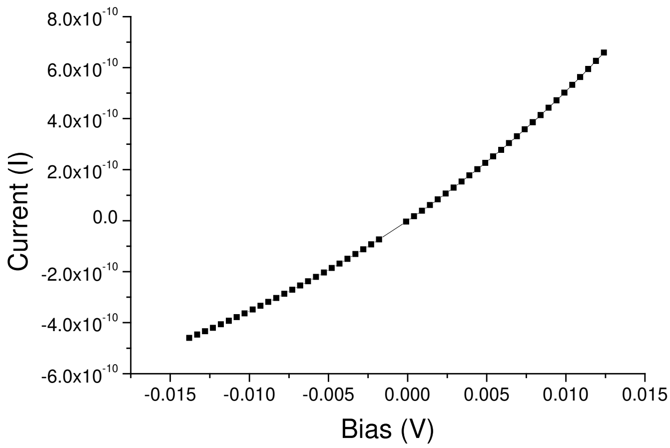

Figure 4.6: Fit to data for low voltage forward and reverse bias I-V's for analysis of bulk and junction resistances, where box: measured data, solid line: theoretical fit

The value of R_b is the resistance of the heavily doped substrate in series with the undepleted epitaxial region. A substrate of thickness 600μm, area of

0.0706cm and doping density 1 $\times 10^{18}$ cm^{-3} results in a theoretical resistance of 0.62mΩ using equation 2.19. Because the measurements are carried out over a very low voltage range it is assumed that the majority of the epitaxial layer remains undepleted. The 50μm epitaxial layer with a measured doping density 1.7 $\times 10^{14}$ cm^{-3} results in a theoretical resistance of 0.3Ω, much lower than the measured value of 1.27Ω. This may be due to a reduction in electron mobility μ_n due to the presence of traps or scattering centres in the bulk. To verify this a measurement of μ_n is necessary. This was not carried out as part of this investigation. It is further observed that, because R_b constitutes so little of the overall effective resistance R_{eff} then this measurement is only useful in measuring R_j. This situation defines an ideal radiation detector where the low substrate resistivity ensures long carrier lifetime of the generated charge in the substrate.

4.2.4 Measurement of Barrier Height

There are several methods for determining the device barrier height using its current dependence on applied voltage. The barrier height can be determined by measuring the forward current dependence on temperature. By multiplying the current density of equations 2.60 and 2.61 by the electrically active area S_e, the following expression is obtained:

$$ln\left(\frac{I}{T^2}\right) = lnA^{**}S_e - \frac{q}{k_BT}(\phi_b - V) \tag{4.7}$$

A plot of ln(I/T^2) against 1/T should give a straight line with gradient q(ϕ_b - V)/k_B, where V is the actual bias applied across the device, if n is constant. AX1221-9 was measured between 233 K and 293 K under 0.15V forward bias. The data are plotted in figure 4.7 and ϕ_b is measured as 0.915 $\pm$ 0.002 eV. The error quoted is from the error in the linear fit to the data. When recombination current is significant, the temperature variation of the forward current can show two barrier heights. At high temperatures the activation energy tends to the value $\phi_b - V$, characteristic of the thermionic-emission component, and at low temperatures it approaches a value of $(E_g -$

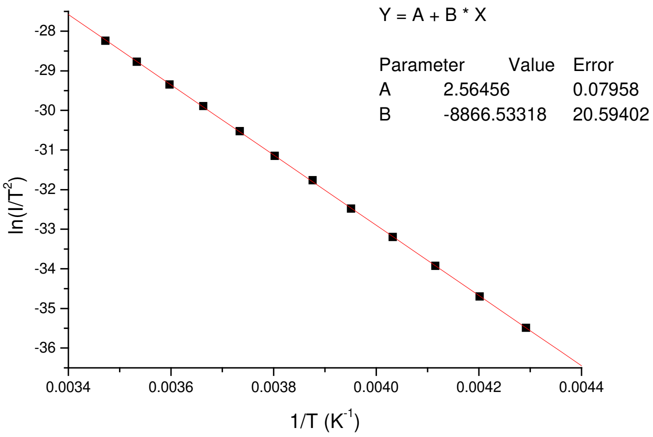

Figure 4.7: The activation energy plot used to determine the barrier height of AX1221-9 VPE GaAs diode under forward bias of 0.15V

$V)/2$, which is characteristic of the recombination component [65]. It is seen in figure 4.7 that only one energy dominates, that of the thermionic-emission component. The effect of recombination is therefore assumed to be negligible. This is also reflected in the value of n close to unity reported in the previous section. The validity of these measurements is based on the assumption that the junction resistance is much higher than that of the bulk, and therefore, all of the applied voltage is effectively dropped across the junction. The results presented in section 4.2.3 prove that this is a valid assumption. The measurement system is calibrated before carrying out measurements to account for voltage drops across cables and connectors.

The slope of the plot in figure 4.7 cuts the y-axis at 2.565 which, for a 3mm pad diode shorted to 200μm guard ring, and therefore an active surface area S_e of $0.0908cm^2$ gives a value for the Richardson constant A^{**}[26] of 117.3 ± 3.5 A$cm^{-2}K^{-2}$ where the error is due to the uncertainty in the point where the slope cuts the y-axis.

The second technique for determination of the barrier height involves

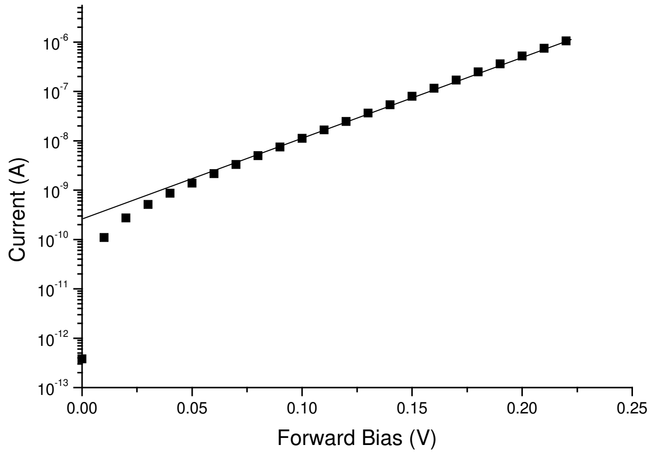

Figure 4.8: The low voltage I-V characteristic used to determine barrier height ϕ_b from the saturation current density J_s

extrapolation of the log of the current density at zero voltage to extract the saturation current density J_s as observed in figure 4.8 for unirradiated device AX1221-9. The ideal current equation 2.61 of section 2.5 is modified to:

$$\phi_b = \frac{kT}{q} ln \left(\frac{A^{**}T^2}{J_s} \right) \tag{4.8}$$

Using the values of A^{**} and S_e from the previous method, ϕ_b was calculated as 0.905 $\pm$ 0.005 eV. For a barrier height of 0.905 eV the theoretical reverse bias I-V characteristic compared to the measured characteristic for AX1221-9 between 1mV and 200V at a temperature of 293K is shown in figure 4.9. It can be seen that over the full voltage range the measured current is greater than that given by theory. This increase can be explained by taking into the account the effects of image force barrier lowering $\Delta\phi_{bi}$, given by equation 2.44 in section 2.4.4. The displayed current with the effect of barrier lowering assumes a value for N_D of 1.7 $\times 10^{14} cm^{-3}$ and ϕ_b is again 0.905 eV. Generation current is also fitted to the measured reverse bias I-V plot, and using equation 2.64 τ is calculated to be 1ns. While this differs

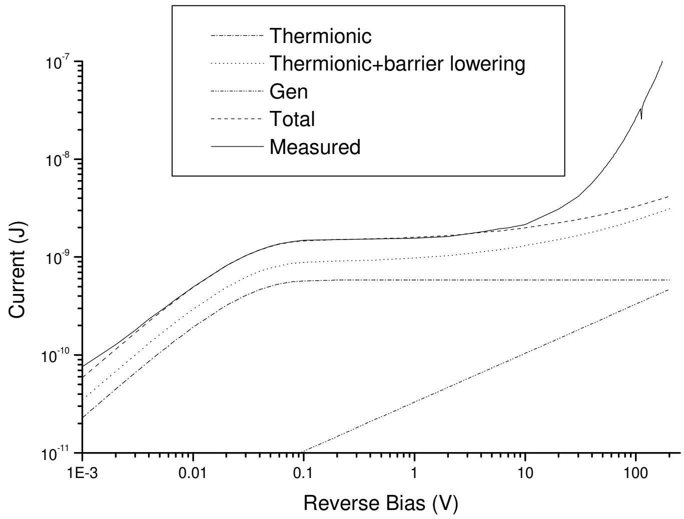

Figure 4.9: Fits of theoretical contributions to reverse bias current density against measured current density for AX1221-9

from the value of 6ns reported in [73], the fit carried out here is only applicable over a short voltage range before breakdown begins, and also the the exact doping density of the material used in [73] is not given.

The electrical breakdown which results in the increase in current found at high reverse bias is caused by avalanche multiplication. This occurs when the electric field is high enough to accelerate movable charge carriers strongly enough between collisions with lattice atoms to cause production of electron-hole pairs. Another reason for this high reverse bias breakdown is due to hole injection through the ohmic contact when the depletion region extends to that contact. The breakdown seen in the measured currents on application of high reverse bias is caused by impact ionisation under the high electric field causing an avalanche of e-h pairs. While reverse bias breakdown can be measured, it is a subject that is the basis for a project in itself and is therefore not included here.

4.3 Charge Collection Efficiency

It was explained in chapter 3.1.2 that the total charge induced at the electrodes by generation of an e-h pair is q, and that the charge carrier which contributes most to this is the one that travels the greatest distance in the detection medium. This property allows measurement of the effectiveness of the Schottky diode to operate as a particle detector by measuring the charge collection efficiency (CCE), defined by[12],[2]:

$$CCE = \frac{Q_{meas}}{Q_0} \times 100\% \tag{4.9}$$

where

$$Q_0 = q\frac{E}{\varepsilon} \tag{4.10}$$

where Q_{meas} is the charge measured at the electrodes, Q_0 is the charge expected from a particle depositing energy E, q is the electron charge and ε is the mean energy required to create an electron-hole pair, given as 4.2 eV in chapter 1 and in reference [31].

The electron and hole charge collection of the detector was investigated using 5.5 MeV alpha particles from an Am^{241} source. The detector was reverse biased using a Keithley voltage source via an Ortec pre-amplifier which was used to measure the charge. The back Ohmic contact was held at ground and a negative potential applied to the front Schottky contact to reverse bias the detector. The detector was placed in a metal box for electrical screening, with a hole in it to allow irradiation of the front contact. Due to the short range of alpha particles in air the detector was held in an evacuated chamber at a pressure of around 30 mbar. The Am^{241} source is held over the hole, and the orientation of the device in the box is chosen such that the front or the back contact can be irradiated. The signal is read out using the Ortec pre-amplifier connected to a post amplifier with a 500 ns shaping time. The pulse height spectrum is analysed using the *Maestro* PC-based multi-channel analyser software[37].

The system is calibrated using a known voltage pulse applied to a 1.8 pF capacitance on the front end of the pre-amp. The calibration was verified using a fully depleted, 100% efficient Si detector. The peak in the pulse height spectrum was obtained at the channel that corresponds to 1.5×10^6 electrons, as expected for the deposition of 5.5 MeV in Si, where ε_{Si} is 3.6 eV[11].

Given that the energy required to create an electron-hole pair in GaAs is assumed to be 4.2 eV [31], an alpha particle with an energy of 5.5 MeV will therefore generate 1.31×10^6 electrons, corresponding to a charge of 0.21 pC. The charge collected at the electrodes of the GaAs detector is measured with respect to reverse bias voltage for electrons and holes.

The CCE is also defined in reference [12] as:

$$CCE = \frac{\lambda_e}{W}\left(1 - exp\left[-\frac{(W - x_0)}{\lambda_e}\right]\right) + \frac{\lambda_h}{W}\left(1 - exp\left[-\frac{x_0}{\lambda_h}\right]\right) \tag{4.11}$$

where it can be seen that the CCE depends on the mean free drift lengths of the electrons and holes λ_e and λ_h respectively, and on the position x_0 that the charge carriers were generated with respect to the irradiated surface.

The measured CCE for α particles incident on the front contact of the unirradiated device AX1221-9 is given in figure 4.10. It is observed that the CCE increases with increasing reverse bias, and therefore depletion width, approaching 98% at a bias of 50V. According to simulations carried out using SRIM[39] monte carlo software for 5.5 MeV α particles in GaAs, the maximum range of the α particles is 19.8μm as shown in figure 4.11(b). Using equation 2.34 of section 2.4.3 the depletion width of a device with $N_D = 1.7 \times 10^{14}\ cm^{-3}$ under a reverse bias of 50V is 20.5μm, approximately equal to the range of α particles in GaAs, therefore all of the charge generated is collected under the applied electric field. Under these conditions, with reference to equation 4.11, irradiation of a reverse biased Schottky diode with 50 μm epitaxial layer, with 5.5 MeV α results in the charge generated being predominantly due to the transport of holes as they traverse the greater

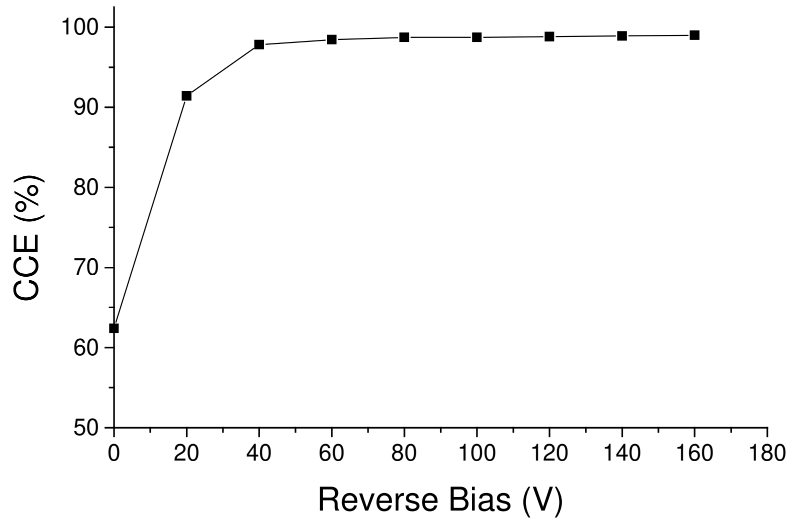

Figure 4.10: The charge collection efficiency of AX1221-9 measured with 5.5 MeV α's as a function of reverse bias.

distance. In LEC devices the signal and therefore CCE due to the transport of holes is usually obtained from α particles incident on the back contact. In these devices there is no signal until the device is fully depleted and the depletion region extends to the back contact. In the VPE devices, beacause the 600μm thick substrate is heavily doped with 10^{18} Si atoms cm^{-3}, the depletion region will not extend to the back contact. The fixed space charge density is zero and therefore the electric field is zero. Non-equilibrium charge carriers generated by incident radiation in this region will not be separated and swept to the relevant contacts. Because of this, α particles incident on the back contact of VPE devices result in no signal.

In order to asses the contribution from electron and holes in this situation where the hole contribution cannot be directly measured, only electron motion is considered first, and equation 4.11 modifies to:

$$CCE = \frac{\lambda_e}{W}\left(1 - exp\left[-\frac{(W - x_0)}{\lambda_e}\right]\right) \tag{4.12}$$

When W = 50μm and x_0 = 20.5μm, the CCE due to electrons saturates

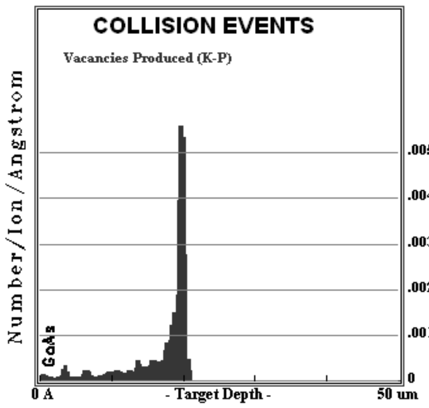

(a) Ionization of 5.5 MeV α particles

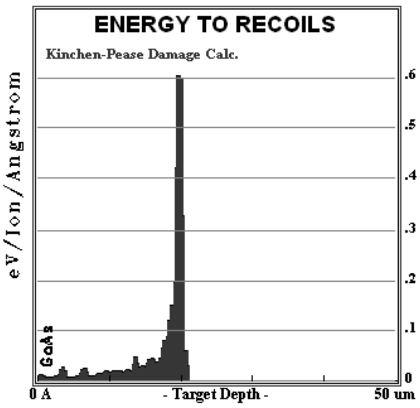

(b) Range of 5.5 MeV α particles

Figure 4.11: SRIM simulations for 5.5 MeV α particles in GaAs with contacts as defined in section 3.3

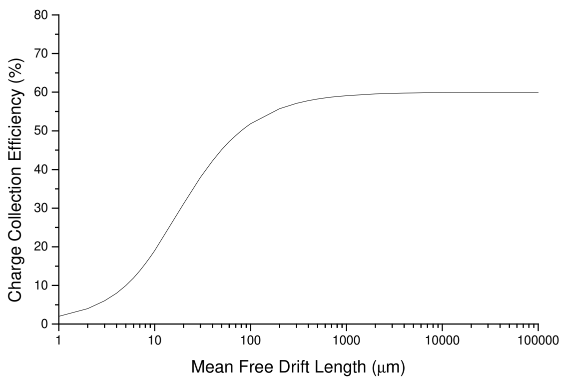

Figure 4.12: The charge collection efficiency as a function of mean free drift length of electrons for a 50 μm thick detector irradiated on the Schottky contact with 5.5 MeV α particles from equation 4.11

at a value of 60% as shown in figure 4.12 with increasing mean free drift length, therefore the remaining percentage of induced charge must be due to the collection of electrons. Both electrons and holes therefore contribute to the CCE in VPE GaAs devices. It is further observed from figure 4.10 that at zero bias the CCE is 62%. The diffusion potential at zero bias given by equation 2.25 results in V_{d0} equal to 0.7 eV. This results in a depletion width W of 2.44 μm. Because the majority of the charge from a 5.5 MeV α particle is deposited at 19.8μm this large CCE is probably due to drift and diffusion of charge in the depletion region. However, it is also observed in figure 4.11(a) that charge is deposited at shallower depths, therefore this loss of energy from the α may contribute to the CCE.

4.4 Capacitance DLTS

The method of defect analysis known as Capacitance Deep Level Transient Spectroscopy (Capacitance DLTS)[64] is a well used and respected technique which utilises the temperature dependence of carrier emission as described in section 2.4.5 to identify energy levels. A series of pulses are applied to the device (a single pulse is shown in figure 2.11) while it is swept through a range of temperatures, usually in the range of 100 to 450K. The emission rate is temperature dependent and characteristic of each type of defect. The DLTS processing technique is to sample the capacitance transients at two different times t_1 and t_2 as shown in figure 4.13. The difference in capacitance between t_1 and t_2, ΔC, is then measured and averaged over many repetitions of the pulse. As the temperature is varied a sharp maximum is produced in a plot of ΔC against T. This peak occurs at the temperature which causes the emission constant e_n^{-1} of a particular defect to be matched to the time difference ΔT = t_1 - t_2. Because each defect has a unique emission time constant e_n^{-1}, each defect present in the material will produce a separate peak in the spectra.

Various hardware set *rate windows* can be selected, such that the temperature can be found that gives a defect in question a particular emission

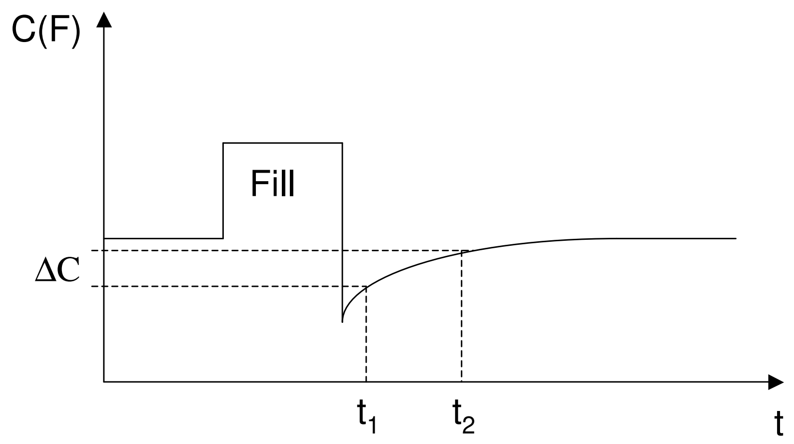

Figure 4.13: Change in capacitance over measured time difference on removal of filling pulse

constant. For example the DLTS plot for AX1221-9 in figure 4.14(a) shows that this device has a defect which has an emission of 1000 s^{-1} at 425degC and $400s^{-1}$ at 405degC. The change in emission time constant with temperature allows evaluation of the activation energy of the deep level defect by plotting $\ln(e_n/T^2)$ against 1/T.

The Arrhenius plot given in figure 4.14(b) for unirradiated device AX1221-9 results in a level with energy $E_t = 0.79 \pm 0.02$ eV, where the error is due to the uncertainty in the straight line fit. This deep level is attributed to the EL2 level.

The deep level trap concentration is calculated follows[30]:

$$N_T = \frac{6\Delta C_{max}}{C_{ques}} N_{eff} \tag{4.13}$$

where the quiescent capacitance C_{ques} is the capacitance of the Schottky diode at the reverse bias that the experiment will pulse to, gained from a simple C-V experiment, N_{eff} is the effective doping density at that bias and ΔC_{max} is the peak value of ΔC. The concentration of the EL2 level is calculated as $(2.36 \pm 0.13) \times 10^{14} cm^{-3}$. The EL2 concentration is greater than the measured value of effective doping density of $1.7 \times 10^{14} cm^{-3}$ using the

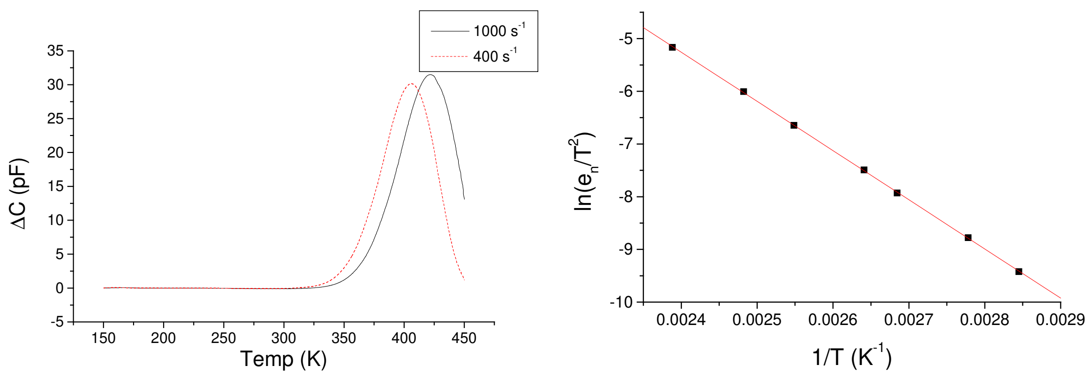

(a) DLTS plot of unirradiated device AX1221-9

(b) Arrhenius plot of AX1221-9

Figure 4.14: Capacitance DLTS results for AX1221-9

C-V technique. This is reasonable if some level of compensation takes place in the pure epitaxial material between the shallow level donors and deep level EL2. The C-V technique measures an effective doping density N_{eff} as reported in section 4.1, while the DLTS technique measures the change in capacitance through trap emptying and is more likely to report the true concentration of the EL2 defect.

4.5 Summary

The results presented in this chapter have shown that growth of high purity epitaxial layers grown by the VPE technique on highly doped LEC substrates enables fabrication of good quality devices with CCE approaching 100 %, but with macroscopic characteristics very different from the most commonly investigated devices formed on SI-U GaAs material.

The high voltage reverse bias I-V characteristics of the VPE material do not exhibit the plateauing feature found in the SI-U LEC material which is thought to be due to field enhanced electron capture by the EL2 level. Activation energy measurements have shown that the EL2 level is indeed present in the VPE GaAs material implying that this plateau should therefore be observed, but DLTS measurements show that the EL2 concentration of 2.36 x 10^{14} cm^{-3} in VPE material is much lower than that of 10^{16} cm^{-3} in the SI-U LEC material.

A further feature of the reverse bias I-V measurements is that the reverse bias leakage currents between -10V and -150V are an order of magnitude lower in the epitaxial GaAs devices than in the SI-U GaAs devices. While the high resistivity of the SI-U material is obtained through compensation of the EL2 level, the high concentration of this level also acts as generation centres, thus increasing the reverse bias current. It is expected that this will result in lower levels of noise in the device.

It is an interesting point to note that the EL2 level has been identified in the VPE GaAs material, and yet CV measurements on this material showed no frequency dependence as detailed in section 4.1. It was explained in that section that the frequency dependence of CV measurements may be a result of a combination of a high concentration of defects with slow emission times and of the junction and bulk resistances becoming comparable. In 4.2.3, for VPE GaAs R_j was measured as 23.29MΩ and R_b as 1.27 Ω, a ratio of 18 $\times 10^6$ to 1. The resistances for SI-U material given in reference [12] results in R_j equal to 122M$\Omega$and R_b equal to 16MΩ, a ratio of 7.6 to 1. It is the high bulk resistivity of the SI-U material which causes the frequency dependence of the measured capacitance in SI-U material. This has an unfortunate side affect in that it is not possible to analyse the SI-U GaAs by the capacitance DLTS technique, because the 1MHz sample rate of the capacitance meter used in the DLTS system is too high.

Chapter 5

Device Irradiation and Characteristics

It is well known that the performance of GaAs semiconductor detectors is severely degraded by sustained operation in a high radiation environment of colliding beam accelerator experiments such as that described in chapter 1. As a contribution to the detailed understanding of the nature of this degradation, the performance of GaAs Schottky diode detectors has been investigated after irradiation with high fluences of 1.8 MeV and 24 GeV protons. This chapter details the methods of irradiation utilised in both cases to achieve the required fluences and discusses the theory of radiation damage in semiconductor target materials, with a particular emphasis on GaAs. The details of the procedures used to irradiate the GaAs Schottky devices with 1.8 MeV and 24 GeV protons to the required fluences, and the methods of confirming these fluences are also explained. Details of the investigations carried out into the changes in macroscopic characteristics due to proton irradiation are then given, followed by an analysis of the mechanisms causing these changes.

5.1 Radiation Theory

The effect that radiation has on a target material, and therefore on the operation of a semiconductor device depends on the energy and type of radiation, and the material from which the device is made. Radiation-induced defects result in a change in the concentration of equilibrium charge carriers, a reduction in the lifetime of non-equilibrium charge carriers and, therefore, a reduction in charge collection efficiency. The effects relevant to the study detailed in this thesis that incident ionising radiation have on a device are characterised as follows[12]:

- **Transient Ionisation Effects**: A high energy particle creates electron-hole pairs when it passes through a material. For a detector these electron-hole pairs generate the signal which identifies the passage of such a particle. This effect causes no damage.

- **Displacement Effects**: Atoms can be displaced from their normal lattice sites via interatomic collisions. These displacements interrupt the periodicity of the lattice and introduce long lived changes to the device.

- **Nuclear Transmutations**: In some materials incident radiation can cause nuclear interactions to take place in the material. Due to fragmentation, fission and spallation, dopant isotopes may be created in the material which can form both deep and shallow levels. These defects take place when the energy of the incident radiation is high enough to overcome the Coulomb potential (4-5MeV) and the nuclear reaction threshold (40-50MeV)of the target atom[43].

For semiconductor detectors Transient Ionisation Effects are non-damaging. Nuclear Transmutations and Displacement Effects do, however, cause significant radiation induced defects in semiconductor detectors.

5.1.1 Displacement Effects

The process of producing displacement effects by the interaction of high-energy particles in virtually all crystalline materials can be expressed in terms of the following rules [35]:

1. The incident particles will give up energy to the lattice by the creation of interstitial atoms and vacancies (Frenkel defects) by forcing host atoms off their sites. The absorbed energy required to knock an atom from its lattice site is about 10 eV in GaAs. This is known as the Wigner energy E_w. The value of E_w is roughly the same for both sub-lattices in GaAs and is about half of that required in Si ($E_{wSi} = 21$ eV [40][52]).

2. If these primary defects recombine where they were created or elsewhere in the lattice, following diffusion of either or both of the interstitials or vacancies, the damage is removed and the host lattice is said to have undergone “self healing”. After such primary defect recombination the material will show no evidence of the original damage and the material is then said to be “radiation hard”.

3. If the primary defects are not annihilated in this way, the material will retain evidence of the damage. If the residual defect centres introduce energy levels in the band gap then they are electrically active. Electrical characterisation of the device after irradiation will show that the crystal is damaged and, therefore, is not radiation hard. If the defects are not electrically active then non-electrical characterisations (such as optical absorption) may reveal damage even though the material is electrically radiation hard.

4. In semiconductors much of the primary damage is self-healed by the rapid recombination of the interstitial-vacancy Frenkel defects. However, residual damage can occur either by the trapping of some of these defects by impurity atoms, their gathering into complexes or, in the case

of compound semiconductors like GaAs, by reactions between atoms of one sub-lattice and vacancies of the other. The level of this damage is therefore dependent on the initial lattice state. It is possible to produce secondary defects such as As_{Ga} or Ga_{As} (an arsenic atom on a gallium site and a gallium atom on an arsenic site respectively) by interactions of interstitials from one sub-lattice with vacancies of the other. The first of these secondary defects is known to occur in both irradiated and unirradiated SI-U LEC GaAs as the well studied EL2-centre.

5. Under irradiation by a high particle fluence, further gathering of primary and secondary defects can result in larger defects such as dislocations (and associated stacking faults), precipitates and voids.

5.1.2 Primary Damage

If the incident irradiating particle has sufficient energy the target atom will be knocked out of its normal lattice position, creating a primary knock-on atom (PKA). If the PKA has sufficient energy it will move through the lattice displacing additional atoms, resulting in a cascade. As the PKA interacts it loses energy through ionisation and displacement generation, and the mean free path reduces. The result is a higher density of lattice defects towards the end of the path. Terminal clusters are formed with a high density of displacement defects when the mean free path of the recoil atom is less than the range of the lattice distortion as shown in figure 5.1.

The form of energy loss from the incident particle that is channelled into creation of PKA's is non-ionising and is referred to the Non-Ionising Energy Loss (NIEL [45]). It has been reported by several authors that the observed damage to GaAs devices is proportional to the NIEL because the number of primary displaced atoms is proportional to the NIEL of the incident particle[40],[42],[45]. Such damage has been observed in GaAs particle detectors irradiated with MeV neutrons[48] and fast protons and pions[51]. It has been observed, however, that GaAs particle detectors are able to with-

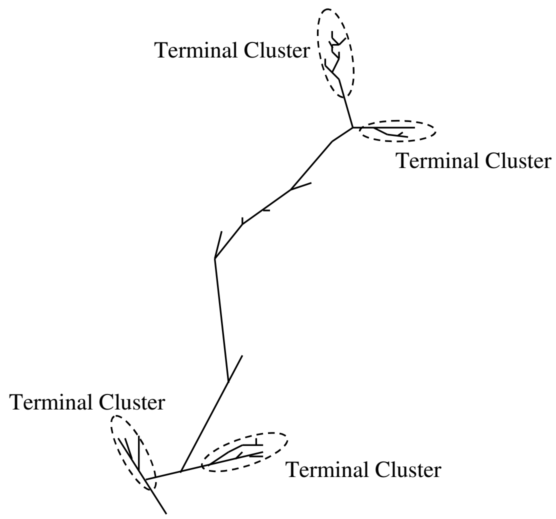

Figure 5.1: Tracks and clustering produced in a semiconductor material by recoil atoms

stand large doses of gamma radiation (up to 1MGy) with almost no observable damage because the gamma radiation produces little NIEL.

The NIEL caused by a particle is determined by the probability of interaction between the incident particle and the lattice atom, and the energy transferred to the recoil atoms or fragments. At low energies the interactions are mainly due to elastic Rutherford scattering where small energy transfers between incident particle and lattice atom are more probable than high energy transfers, while at high energies inelastic processes become more predominant and the lattice atom can fragment, creating several smaller PKAs with lower mass.

The majority of NIEL measurements have been carried out for Si because most particle detectors are made from this material[46],[47]. Measurements for charged particles in GaAs only exist for protons with kinetic energy up to 1 GeV. A theoretical estimate of the NIEL for protons in GaAs has been made up to 24GeV[32]. 24GeV is of great importance in this investigation as this is the proton energy at which many irradiations are carried out. The resulting

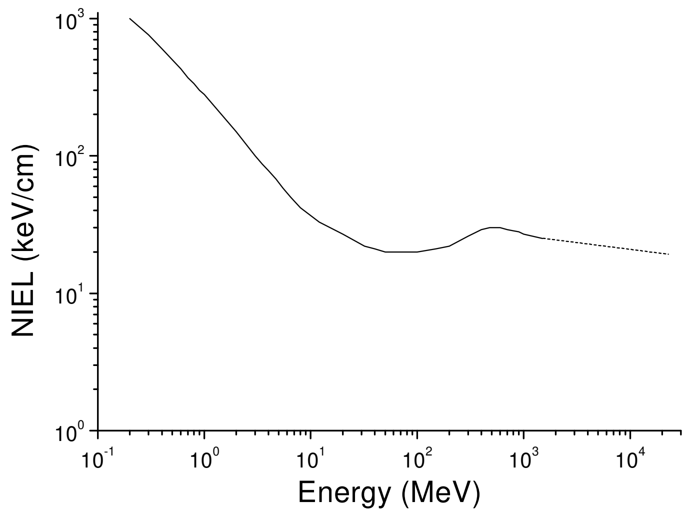

Figure 5.2: NIEL for protons in GaAs in units of keV/cm.

extended NIEL values for protons in GaAs are shown in figure 5.2[40], where it is observed that the NIEL for 1.8 MeV protons is 200 keV/cm and for 24 GeV protons is 20 keV/cm..

The range of damage in GaAs is strongly dependent on the energy of the incident radiation, because as the energy of the PKA increases, a greater number of subsequent interactions takes place before the mean free path reduces to the terminal cluster point. From SRIM simulations[39] the range of 1.8 MeV protons in GaAs is 27.7 μm as observed in figure 5.3. 24 GeV protons are observed to pass through the entire thickness of the epitaxial layer plus substrate.

5.2 1.8 MeV proton Irradiations

GaAs devices fabricated as described in chapter 3 were irradiated in the Van de Graaff accelerator at the Charles University in Prague with protons of kinetic energy 1.8 MeV. The primary beam current in this accelerator of 1.5 μA is equivalent to a fluence of 6.25×10^{12} protons $cm^{-2}s^{-1}$. This was too

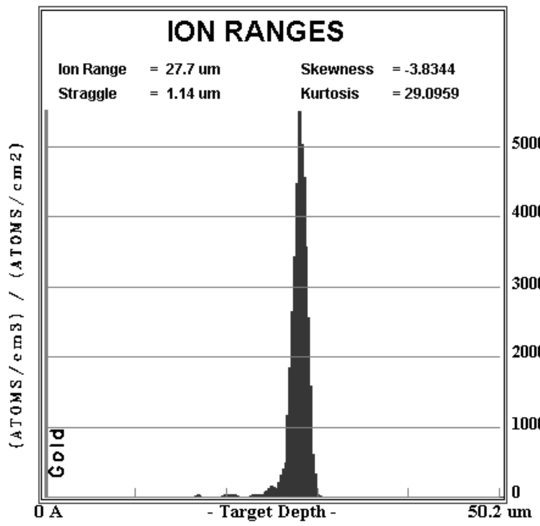

Figure 5.3: Range of 1.8 MeV protons in GaAs.

large to attain the desired fluences, within the range of 5×10^{12} protons cm^{-2} and 1×10^{14} protons cm^{-2}, with any realistic accuracy. Rutherford scattering of the primary proton beam on a gold foil target was therefore used to attain the desired fluences by placing the detectors around the scattering area at well defined Rutherford scattering angles. Good descriptions of the theory of Rutherford scattering are found in references [10] and [68].

5.2.1 Rutherford Scattering

With knowledge of the primary beam current and the thickness of the gold foil, an estimate can be made of the scattered proton intensity as a function of scatter angle θ. The thickness of the gold foil was determined by measuring the ionisation loss of α particles through it using a Si detector calibrated at the Czech Technical University with $\sim$ 100% CCE. A pulse height spectrum of a three line source (Am+Cm+Pu) was first measured without the gold foil. The same measurement was then carried out with the gold foil in the path of the proton beam. Both spectra are shown in figure 5.4. Based on the calibration of channels/keV for the multi-channel analyser using that

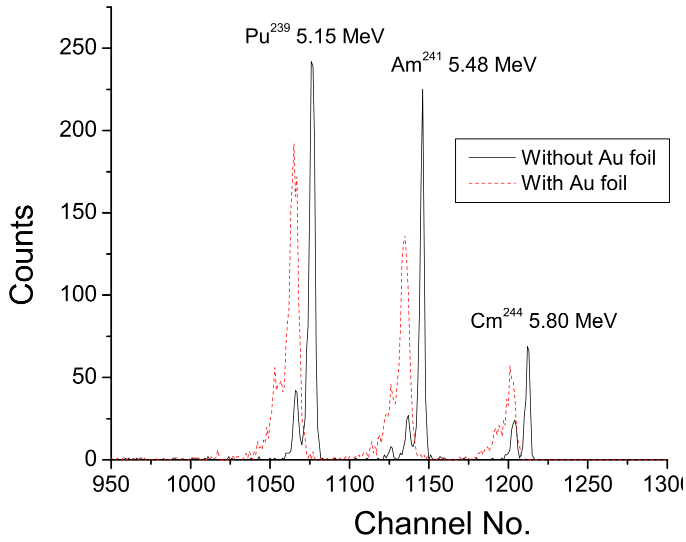

Figure 5.4: The α spectra of a three line source (Am+Cm+Pu). The given peak energies are attributed to the main peak with no gold foil

Si detector, the mean ionisation loss due to the gold foil is calculated as 50.1 $\pm$ 2.5 keV, where the error is the accuracy with which an energy can be identified as in a particular channel . Using the published value of $\frac{-dE}{dX}$ = 41.17 MeV/(cm^2/g) for 1.8 MeV α particles in gold[39], the resultant thickness of the gold foil is calculated as 6.32 $\times 10^{-5}$cm, which corresponds to $n_s = 3.72 \times 10^{18}$ gold atoms cm^{-2}. The Rutherford scattering cross-section formula is given by[10]:

$$d\sigma = \left(\frac{\alpha}{4T}\right)^2 \frac{d\Omega}{sin^4 \frac{\theta}{2}} \tag{5.1}$$

where T is the proton energy, θ is the scattering angle, and:

$$\alpha = \frac{1}{4\pi\epsilon_0} Z_1 Z_2 q^2 \tag{5.2}$$

where the magnitude of the charges of the incident and target particles are Z_1q and Z_2q respectively, with Z_1 = 1 and Z_2 = 79, α = 1.818 $\times$

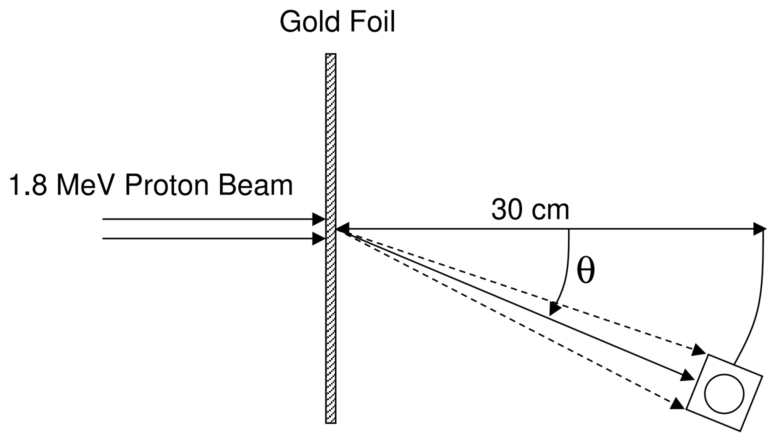

Figure 5.5: Scattering of 1.8 MeV protons from a gold foil.

$10^{-24} FC^2/cm$, q the electronic charge and ϵ_0 the permittivity of free space. The beam flux after scattering, as a function of solid angle $\Delta\Omega$, is given by:

$$\Delta N = N \times n_s \times \frac{d\sigma}{d\Omega}\Delta\Omega \tag{5.3}$$

where N is the primary beam flux, n_s is the number of gold atoms per cm^3 and the solid angle $\Delta\Omega$ is given by[69]:

$$\Delta\Omega = \frac{S}{R^2} \tag{5.4}$$

where S is the surface area of the chosen irradiation surface, and R is the distance from the gold foil target to the detector (R = 30cm) as shown in figure 5.5. The solid angle for an area of 1 cm^2 (based on fluence measurements at a distance of 30cm from the gold foil) is 1.11×10^{-3} steradians. The scattered beam distribution as shown by equation 5.1 and in figure 5.6 as a function of scatter angle θ is proportional to $1/sin^4\frac{\theta}{2}$. The actual fluence as a function of angle was tested with a collimated Si detector with an area 5×10^{-3} cm^2. Throughout the angular range of interest the error between measurement and theory was found to be less than 10%.

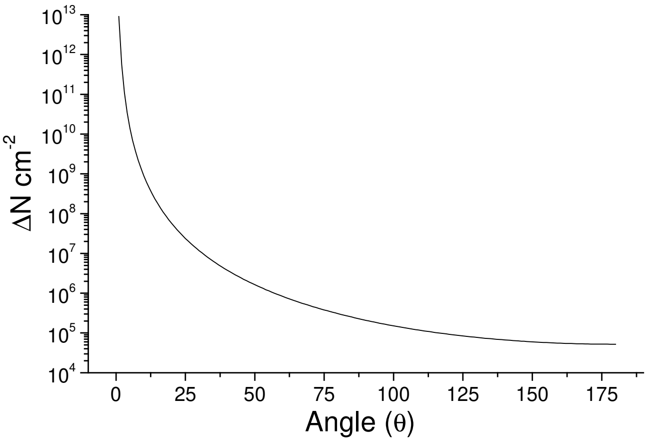

Figure 5.6: The scattered proton intensity after Rutherford scattering from a gold foil, as a function of scattering angle.

5.3 24 GeV Proton Irradiations

The irradiation of devices by 24 GeV protons was carried out at the CERN PS-T7 proton beam. The proton beam operates in bursts of 14.4s in which 1-3 spills of about 400 ms are delivered. The maximum beam intensity is $2 - 4 \times 10^{11}$ protons/spill. The proton beam is uniform to $\pm 10\%$ over a surface area of several square centimetres [44].

The irradiation zone is fitted with a remote controlled shuttle to move the samples for irradiation from the control room to the irradiation area. The shuttle moves on a rail inside an iron conduit with a section of $40 \times 25cm^2$ and a length of 15 m. The conduit has three chicanes to avoid secondary particles coming out of the beam zone. It is estimated that the PS beam will deliver a fluence of 1×10^{13} protons/cm^2 for every 1100 seconds, however due to variations in the dose per spill delivered to the detector and short periods of beam down time, a more accurate method of dose analysis was required. High purity aluminium foils cut to the size of the GaAs sample were positioned in the sample holder immediately in front of and behind the detectors. A standard method known as the *foil activation technique* was used to calculate the 24 GeV proton dose delivered to the detectors by the PS beam. Proton irradiation of aluminium creates gamma emitting radionuclides, and therefore the induced activity of the foil analysed with a Ge(Li) gamma spectrometer allows calculation of the proton fluence.

The sample holder within the shuttle is able to move in the horizontal and vertical direction, covering an area of $10 \times 10cm^2$. This allowed mapping of the beam profile using a GaAs detector as seen in figure 5.7, and therefore confirmation of the quoted beam uniformity.

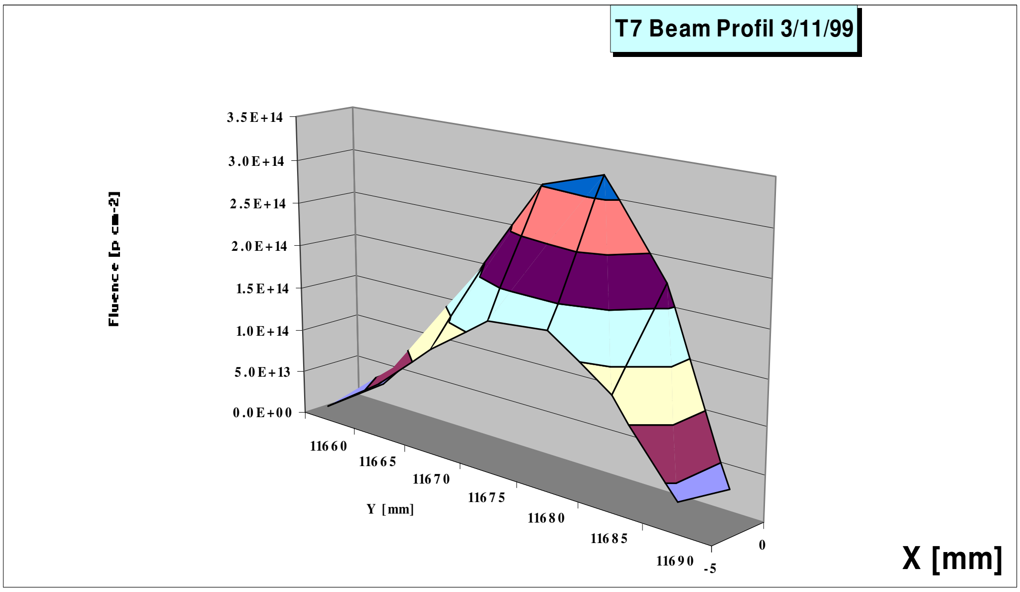

Figure 5.7: The profile of the PS-T7 proton beam at CERN .

5.4 Characteristics of Irradiated GaAs Diodes

The effects of 1.8 MeV and 24 GeV proton irradiation on AIXTRON VPE GaAs Schottky diodes were investigated in terms of the changes in the macroscopic characteristics as a function of particle fluence, such that a comparison can be made with the characteristics of unirradiated devices as described in chapter 4. An analysis is therefore made of the mechanisms of defect introduction in the material, which degrade the detector performance in a high proton fluence environment. The devices were irradiated as discussed in the previous sections. Unless otherwise stated, all measurements were carried out at 300 K.

5.4.1 Current-Voltage Characteristics

The observed change in the reverse bias leakage current characteristics of the devices after irradiation with 24 GeV protons is displayed in figure 5.8 where it is observed that as the proton fluence increases the reverse bias leakage current increases over the full range of reverse biases. The variation in reverse bias current is plotted in figure 5.9 as a function of proton fluence at fixed biases of -50V, -75V and -100V. It is observed that the current rises in an exponential manner as the proton fluence increases. If it is assumed that the reverse bias current is generation current then, from equation 2.64, the current is directly proportional to charge carrier lifetime τ. It was reported by M. Rogalla in reference [40] that the electron lifetime in SI-LEC GaAs material reduces with increasing 24 GeV proton induced EL2 concentration, as observed in figure 5.10. If the introduced defects are of a similar nature to the EL2 level then this would explain the current trend observed in figure 5.9. In order to verify this explanation, a detailed analysis is required to identify the energy, concentration and distribution of these induced defects.

In order to analyse in detail the defects introduced in the material during irradiation, which lead to this increase in current, a plot of ln(I/T^2) against 1/T is made to measure the activation energy E_a, as discussed in section 4.2.2. In the unirradiated VPE GaAs device the activation energy is measured as E_a = 0.73±0.02 eV , corresponding with the energy of the EL2 defect. Measurements on AX1221-5A irradiated with 5×10^{12} 24 GeV protons/cm^2 result in an activation energy of E_a = 0.59±0.04 eV, and E_a for device AX1221-20 irradiated with 1×10^{13} 24 GeV protons/cm^2 is measured as 0.61± 0.05 eV. No significant change in activation energy is found with further

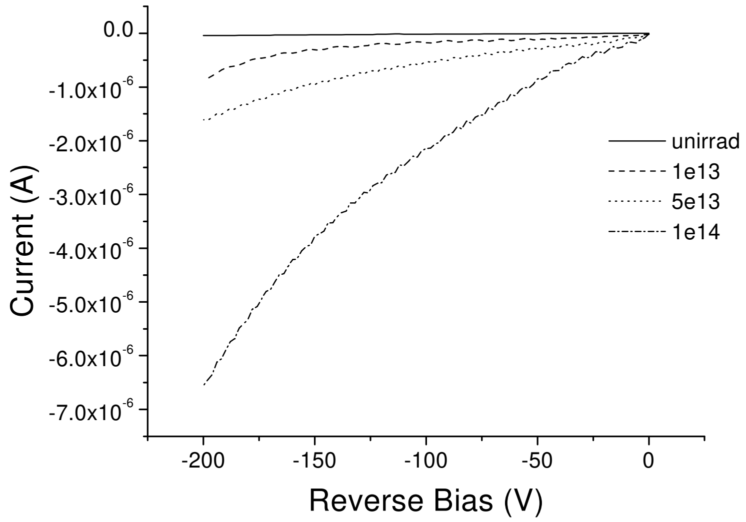

Figure 5.8: AX1221-10:Unirradiated, AX1221-20: $1\times10^{13}pcm^{-2}$, AX1221-22: $5\times10^{13}pcm^{-2}$, AX1221-1: $1\times10^{14}pcm^{-2}$

increases in proton fluence as shown in table 5.1. This implies that even under low 24 GeV proton/cm^2 fluence the lattice has been altered such that another defect has become the more predominant reverse bias current mechanism. An electron trap introduced by 1 MeV electron irradiation of VPE grown GaAs has been found with an energy of 0.5 eV[62],[12]. This trap was reported to contribute to only 5% of the electron trap concentration found after electron irradiation. However, electron irradiation causes point-like defects, therefore it is reasonable to assume that proton irradiation will result in a higher concentration of such defects in VPE GaAs. An electron trap known as the EL3 is reported in reference [38] with an energy of 0.51 ± 0.07 eV, and also in reference [76] with energy of 0.56 eV. In the latter reference the EL3 defect is identified as a complex defect of an As interstitial As_i, and an As vacancy V_{As}.

A comparison is made of the low voltage forward bias current of VPE GaAs devices before and after irradiation in figure 5.11. It is observed that as the 24 GeV proton fluence increases the forward current decreases. In

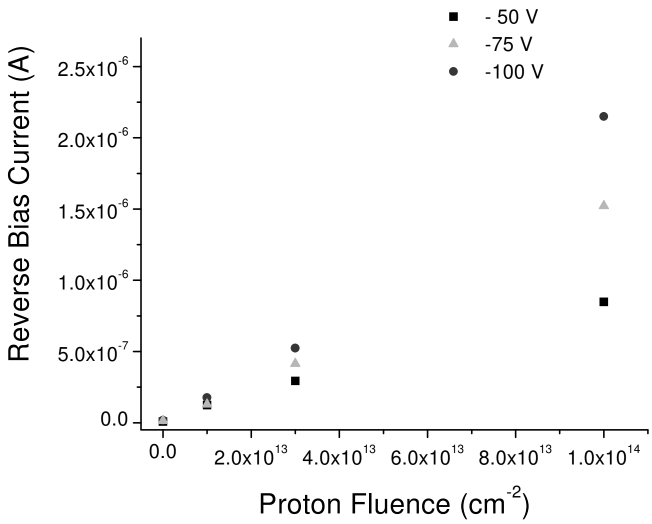

Figure 5.9: Reverse bias currents as a function of 24 GeV proton fluence at -50V, -75V and -100V

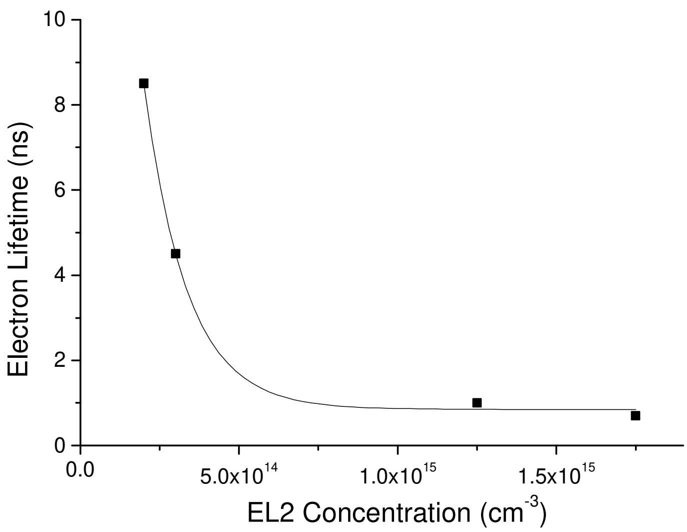

Figure 5.10: The reduction in electron lifetime with increasing EL2 concentration in SI-U LEC GaAs

Fluence cm^{-2}	E_a(eV)
5×10^{12}	0.59 ± 0.04
1×10^{13}	0.61 ± 0.05
5×10^{13}	0.62 ± 0.03
1×10^{14}	0.61 ± 0.03

Table 5.1: Activation energies of reverse biased VPE GaAs Schottky diodes as a function of 24 GeV proton irradiation

the unirradiated device the current is 2.8×10^{-6}A at a forward bias of 0.25 V, and after irradiation with 1×10^{13} 24 GeV protons/cm^2 the current at the same bias has reduced to 4.6×10^{-8}A. This reduction in current with increasing proton fluence implies that the resistivity of the material (as given in equation 2.18) is increasing. This may be due to a reduction in mobility caused by a radiation induced increase in the number of defects acting as scattering centres[50]. This could be confirmed with irradiation VPE GaAs test structures fabricated solely for the purpose of mobility measurements. It is observed in equation 2.18 that ρ is inversely proportional to the free electron density n in the conduction band. While proton irradiation has the effect of introducing defects into the material, these defects may act as electron traps, thus reducing n. An investigation into the properties of the defects induced in VPE GaAs will be discussed in detail in chapter 6.

The reverse bias leakage current characteristic after irradiation with 1.8 MeV protons is quite different from the 24 GeV proton case, as shown in figure 5.12. The obvious difference here is the initial steep rise in reverse bias leakage current at low voltages, followed by a plateau as the reverse bias voltage increases. This is similar to the observed characteristic of an unirradiated SI-LEC Schottky diode, suggesting that the electron emission constants of the induced defects are being enhanced by the electric field as discussed in sections 2.7 and 4.2. An alternative explanation for this effect may be due to the introduction of defects that result in a reduction in electron lifetime, in the same manner as the EL2 level discussed in reference [40], such

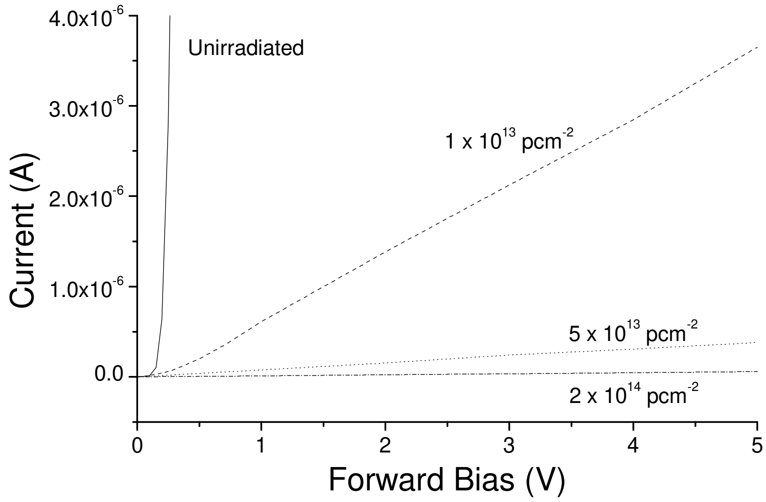

Figure 5.11: Forward bias characteristics of VPE GaAs devices before and after irradiation with 24GeV protons

that generation current increases as given by equation 2.64. Through SRIM simulations it was observed that the range of 1.8 MeV protons in GaAs is 27 μm. The reverse bias current would increase as given by equation 2.64 only in this 27μm region. A comparison is made in figure 5.13 between the reverse bias currents of AX1221-22 irradiated with 5×10^{13} 24 GeV protons cm^{-2} and AX1221-6 irradiated with 5×10^{13} 1.8 MeV protons cm^{-2} in the bias range 0 to -15V. The currents under both irradiation regimes are very similar, and it is therefore accepted that the same mechanism responsible for the increase in current after 24 GeV proton irradiation is induced in only the first 27μm. The voltage range of this steep increase is 16V. If the depletion width at this bias is the range of damage in the material, using equation 2.34 N_D is now reduced to $3.18 \times 10^{13} cm^{-3}$.

Measurement of the activation energy at a reverse bias of -10 V on AX1221-12, irradiated with 1×10^{12} 1.8 MeV protons cm^{-2} results in E_A = 0.60 ± 0.04 eV, and AX1221-6 irradiated with 5×10^{13} 1.8 MeV protons cm^{-2} results in $E_A = 0.59 \pm 0.06$ eV. These are similar to the activation en-

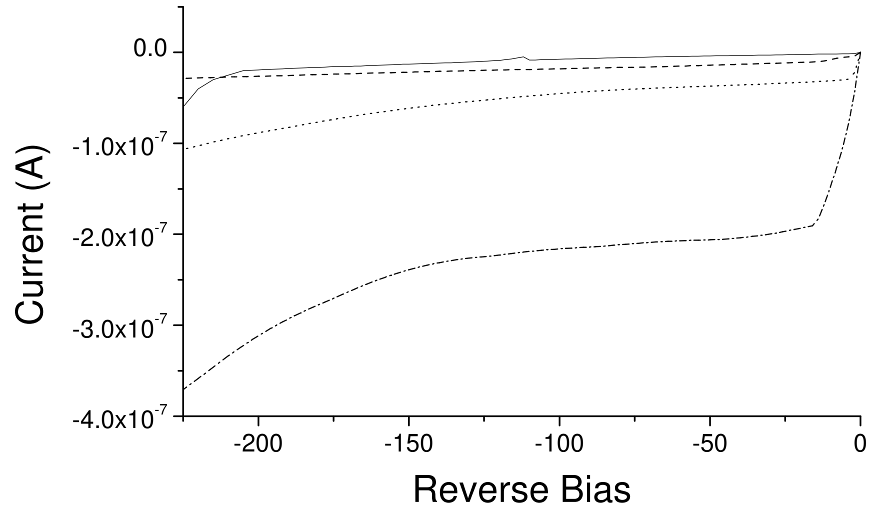

Figure 5.12: I-V characteristics of VPE GaAs devices after irradiation with 1.8 MeV protons. Solid line: Unirradiated, dashed line: $1 \times 10^{12} pcm^{-2}$, dotted line: $1 \times 10^{13} pcm^{-2}$, dash-dotted line: $5 \times 10^{13} pcm^{-2}$.

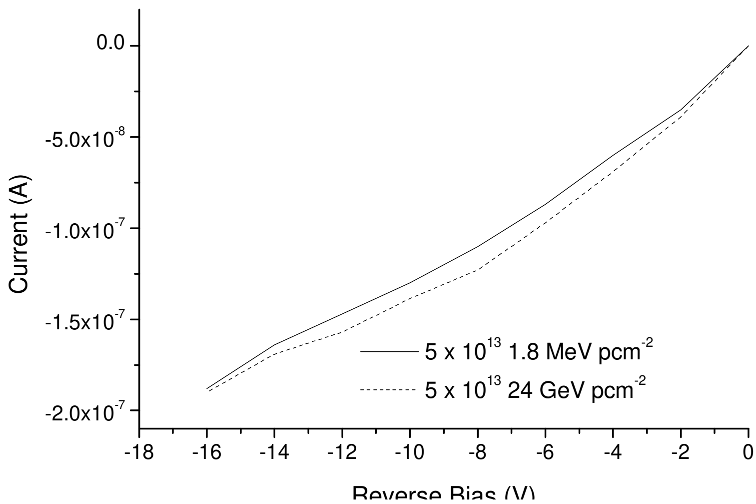

Figure 5.13: Comparison of low voltage reverse bias current after irradiation with 5×10^{13} 24GeV protons cm^{-2} and 5×10^{13} 1.8 MeV protons cm^{-2}

Fluence cm^{-2}	Ratio I(24GeV)/I(1.8MeV)
1×10^{12}	1.27
1×10^{13}	1.22
5×10^{13}	1.14

Table 5.2: Ratio of measured current at a reverse bias of -10V between devices irradiated with 24GeV protons and 1.8MeV protons as a function of fluence

ergies found in the 24 GeV irradiated devices, therefore it is assumed that the same defect, the EL3, is introduced by both 1.8 MeV and 24 GeV protons, and is responsible for the increase in generation current.

Plotted in figure 5.14 is a comparison of the reverse bias leakage currents at -10V for devices irradiated with either 24 GeV protons or 1.8 MeV protons. The ratio of measured currents as a function of fluence is given in table 5.2. It is observed that the current ratio is consistently around a value of 1.2 with increasing fluence. It was noted in section 5.1.2 that the damage found in GaAs devices is believed to be proportional to the NIEL. Since it is also clear from figure 5.2 that the NIEL for 1.8 MeV protons is an order of magnitude greater than that for 24 GeV protons, the NIEL hypothesis is incompatible with the results presented in figure 5.14. This would suggest that the increase in reverse bias leakage current after irradiation with 24 GeV protons has its origin elsewhere than the non-ionising energy loss. A comprehensive understanding of the damage effects from irradiation with high energy protons may require more detailed consideration of the processes of spallation, fragmentation and fission, although their specific contributions remain unseen by the techniques discussed so far.

One test that could shed light on the relevance of the NIEL hypothesis would be a comparison of devices irradiated with 24GeV and around 10-20MeV protons. For these energies the NIEL values are rather similar, while only in the 24 GeV case are the more complex high energy processes likely to occur.

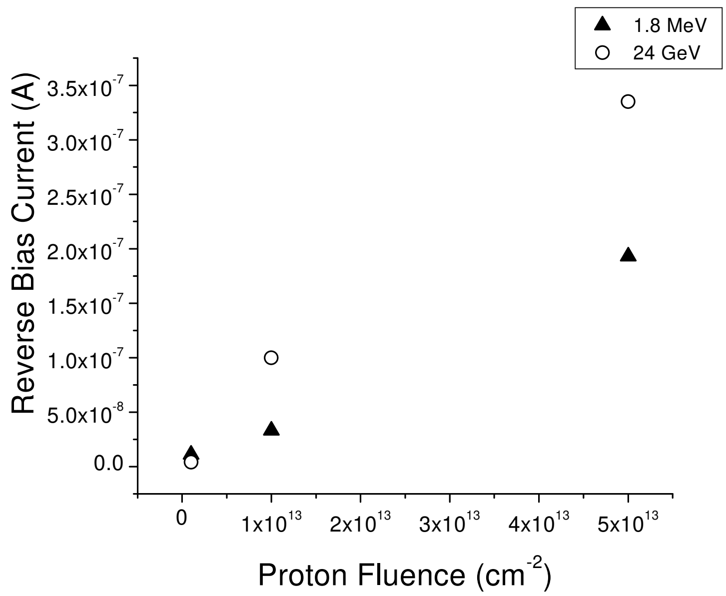

Figure 5.14: The reverse bias leakage current as a function of 24 GeV and 1.8 MeV proton fluence at -10V bias.

5.4.2 Capacitance-Voltage Characteristics

The capacitance-voltage (C-V) characteristics of AX1221-20, irradiated with 1×10^{13} 24 GeV protons cm^{-2}, are displayed in figure 5.15. It is immediately obvious that the capacitance is now dependent on the modulation frequency of the LCR meter, unlike the behaviour of non-irradiated VPE GaAs diodes, but similar to the LEC diodes as discussed in section 4.1. It was suggested in section 4.1 that there were two possible reasons for this frequency dependent behaviour; the presence of defects with slow carrier emission constant e_n, or when the junction resistance R_j becomes comparable with the substrate resistance R_b.

Although the majority of damage to GaAs by 24 GeV protons is through electronic and inelastic nuclear interactions, there is a significant amount of damage due to NIEL as discussed in section 5.1, and as identified through activation energy measurements in the previous section. SRIM simulations[39]

Fluence cm^{-2}	$R_j(\Omega)$	$R_b(\Omega)$
5×10^{12}	35.48×10^{6}	31
1×10^{13}	50.11×10^{6}	120
1×10^{14}	92.40×10^{6}	324

Table 5.3: Measurements of R_b and R_j for devices irradiated with 24 GeV protons

show that 24 GeV protons pass through the entire thickness of the detector causing uniform damage due to NIEL. The modulation frequency dependence of the capacitance suggests that the atomic displacements induced by 24 GeV proton irradiation are similar to the EL2 defect, with respect to its slow carrier emission constant e_n of 0.045 s^{-1}. More detailed analysis of the emission times and concentrations of the induced defects, which are required to comment with confidence on this topic, are made in chapter 6. However, measurement of junction and bulk resistance, R_b and R_j respectively, using the techniques of section 4.1 and given in tables 5.3 and 5.4 for irradiation with 24 GeV and 1.8 MeV protons respectively, confirm that R_b does not become comparable with R_j. It is therefore assumed that the introduction of defects with slow emission time is responsible for the frequency dependence of the capacitance.

Due to the frequency dependence of the device capacitance as a function of voltage after 24 GeV proton irradiation, it is now impossible to use the DLTS technique to investigate the introduction of defects with slow emission times. The high frequency of the capacitance meter used in DLTS experiments means that no change in capacitance of the reverse biased Schottky diode is measured on removal of the filling pulse.

Post-irradiation C-V's characteristics for 1.8 MeV protons are shown in figure 5.16. The profile of the characteristics are seen to differ from those on devices irradiated with 24 GeV protons. It is not possible to measure the effective doping concentration using CV measurements in this case, however the plateau in capacitance between 3 and 15 V is thought to be caused by

Fluence cm^{-2}	$R_j(\Omega)$	$R_b(\Omega)$
$1{\times}10^{13}$	$26.27{\times}10^6$	31
$5{\times}10^{13}$	$43.6{\times}10^6$	57

Table 5.4: Measurements of R_b and R_j for devices irradiated with 1.8 MeV protons

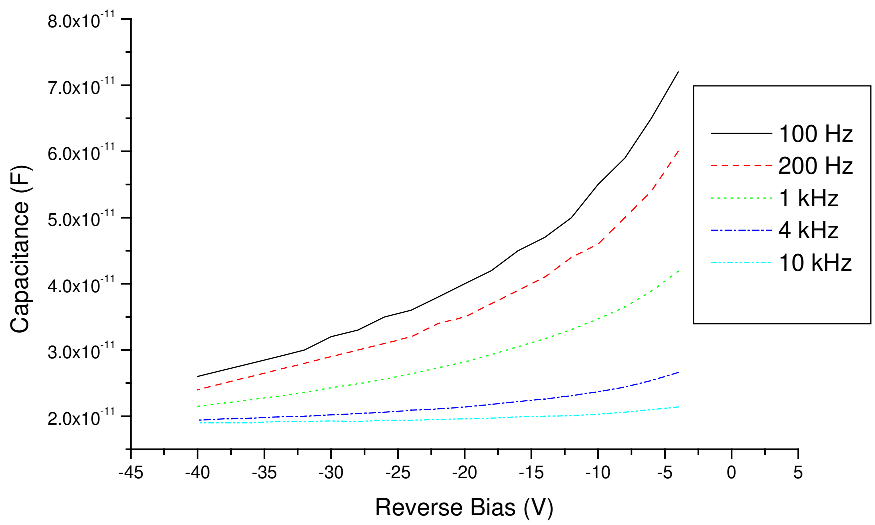

Figure 5.15: The C-V plot for AX1221-20 after irradiation with 1×10^{13} 24 GeV protons cm^{-2} for a range of modulation frequencies of the LCR meter

an increased doping concentration within a localised volume of the detector, as observed in the 1.8 MeV irradiation reverse bias characteristics of section 5.4.1. The SRIM simulations state that the damage caused by 1.8 MeV protons occurs within a depth of 27μm, and is due to NIEL. If these induced defects have a similar slow emission time constant as the defects introduced with 24 GeV protons, where e_n is slower than the sample frequency, then in this region of damage there will be no change in capacitance as described previously. When the device is depleted past this area of damage then the capacitance will change as expected by theory.

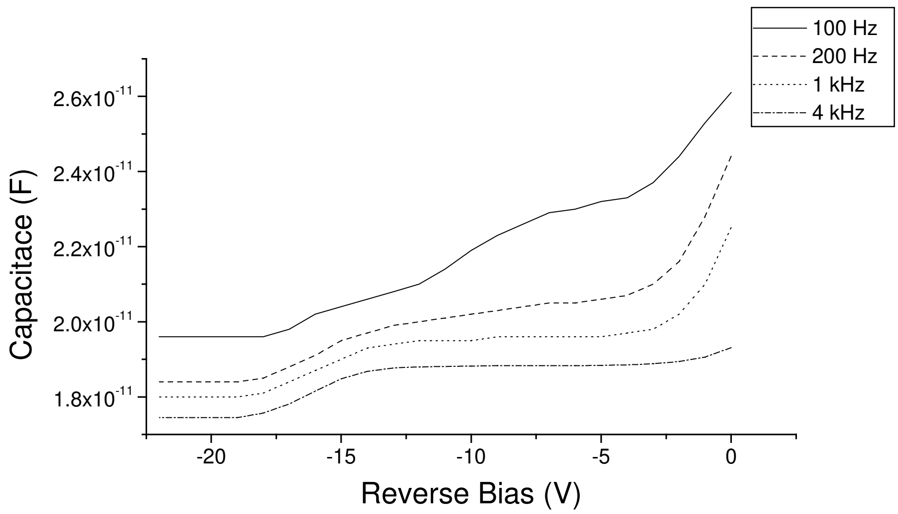

Figure 5.16: C-V plots for AX1221-6 after irradiation with 5×10^{13} 1.8 MeV protons cm^{-2} for a range of modulation frequencies of the LCR meter

5.4.3 Charge Collection Efficiency

The detectors were characterised under reverse bias using 5.5 MeV α particles from an Am^{241} source incident on the front contact, as discussed in section 4.3. The CCE of devices irradiated with 24 GeV protons is displayed in figure 5.17. Again, due to the substrate thickness, it was only possible to measure the electron CCE. The CCE is observed to deteriorate significantly with increasing proton fluence such that at zero reverse bias the CCE is 0% indicating a great reduction in drift and diffusion of charge carriers. The range of reverse bias under which these measurements were carried out is limited to 200 V because of the onset of noise in the pulse height spectra which made it impossible to observe the α peak. Analysis of this noise in the frequency domain is known to give important information on defects and their distribution, and therefore justifies a complete discussion and analysis as given in chapter 7. The variations in CCE with increasing fluence are shown in figure 5.18 for different reverse bias voltages, where it is observed that the rate of degradation of CCE is equal at all biases, indicating uniform damage throughout the depletion region. At fluences over $1 \times 10^{14} cm^{-2}$ there is very little change in CCE with further increasing fluence. It is in this regime that the beam profile measurement described in section 5.3 was carried out.

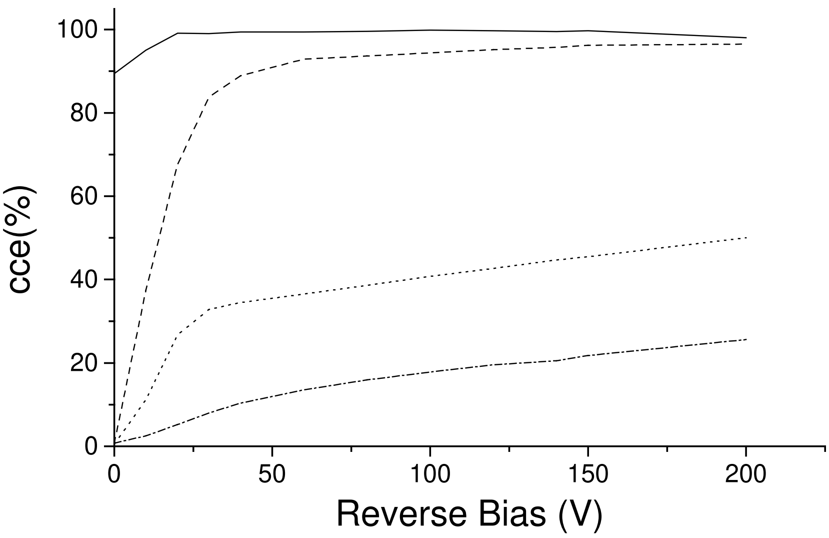

Figure 5.17: Charge collection efficiencies of VPE GaAs Schottky diodes after irradiation with 24 GeV protons. Solid line: unirradiated, dashed line: 1×10^{13} protons cm^{-2}, dotted line: 5×10^{13} protons cm^{-2}, dot-dashed line: 1×10^{14} protons cm^{-2}.

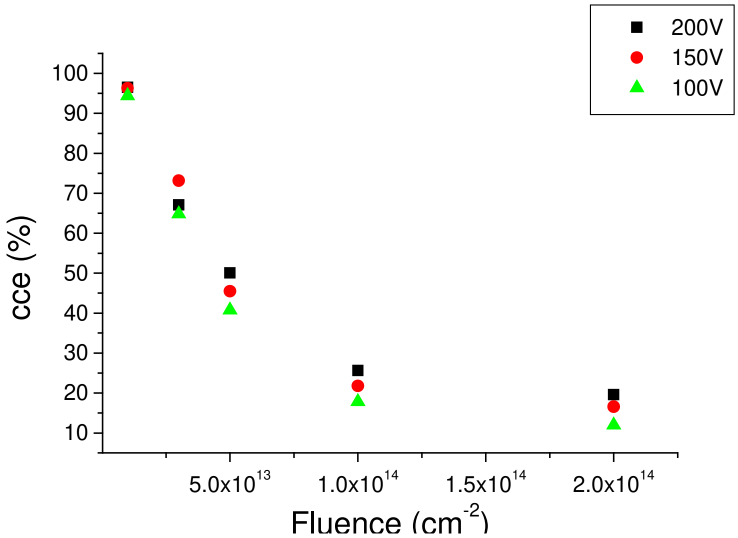

Figure 5.18: Charge collection efficiencies of 24 GeV proton irradiated GaAs devices as a function of fluence at different reverse bias voltages

The signal loss that leads to a reduction in electron CCE with increasing 24 GeV proton fluence is thought to stem from electron trapping due to introduction of deep level defects. The much-reduced CCE at low biases is due to incomplete penetration of the depletion region at low biases. Experimental limitations imposed by the thick substrate mean that no information can be gained on the introduction rate of hole traps, and therefore it is not known whether 24 GeV proton irradiation introduces predominantly hole or electron traps. The reduction in electron CCE with increasing fluence could be explained however by introduction of the EL3 defect as identified in section 5.4.1, with a capture cross section quoted in the range of 0.8-1.7 $\times 10^{-13} cm^2$ in reference [75]. In section 4.4 the predominant defect found in the non-irradiated GaAs devices was identified as the EL2 defect with an energy measured as $E_t = 0.79 \pm 0.02$ eV and concentration of $(2.36 \pm 0.13) \times 10^{14} cm^{-3}$. The EL2 capture cross-section, reported in [38] as 8 $\times 10^{-14} cm^2$, is lower than that of the EL3 defect, therefore it is reasonable to assume that this EL3 level would play a more dominant role in the trapping of generated charge. This is further verified by the fact that the CCE of non-irradiated VPE GaAs, where the EL3 defect is not present is $\sim$ 100%, therefore this defect plays almost no role in electron trapping. It is therefore assumed that after low fluences the predominant defect in reduction of CCE has become that which was identified as the EL3, consistent with the results reported in section 5.4.1.

Shown in figure 5.19 are the CCE's for the VPE GaAs devices irradiated with 1.8 MeV protons to fluences of 1×10^{13} protons cm^{-2} and 5×10^{13} protons cm^{-2}. It is observed here that the degradation of the CCE is considerably greater than that found in the 24 GeV irradiation by between 5 and 10 times. This would suggest that the CCE corresponds to the theory that the damage to GaAs devices is proportional to the NIEL.

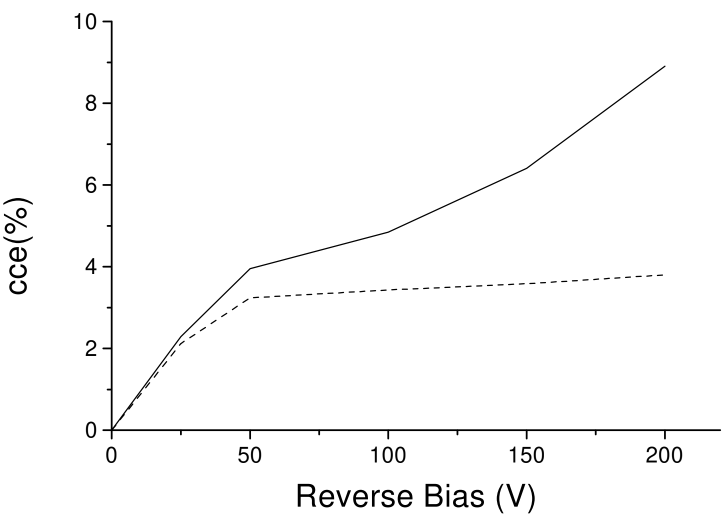

Figure 5.19: Charge collection efficiencies of VPE GaAs Schottky diodes after irradiation with 1.8 MeV protons. Solid line: 1×10^{13} protons cm^{-2}, dashed line: 5×10^{13} protons cm^{-2}.

5.5 Summary

The work carried out in this chapter detailed the mechanisms which lead to the degradation in macroscopic characteristics of the Schottky diode detector.

The overall macroscopic behaviour of VPE GaAs Schottky devices after irradiation with 1.8 MeV and 24 GeV protons seems to emulate that of unirradiated LEC GaAs devices. It is observed by measurement of the activation energies that irradiation with protons of both energies induces the same defect. This is the EL3 level, with energy between 0.51 and 0.56 eV and capture cross section σ_n between 0.8 and 1.7×10^{-13} cm^2, which has been identified as a complex defect of As_i and V_{As}. In both materials under a reverse bias, this is observed as the predominant activation energy, replacing the EL2 level for proton fluences as low as 5×10^{12} cm^{-2}. This EL3 level is uniformly distributed throughout the epitaxial layer by 24 GeV protons, but not by 1.8 MeV protons as suggested by SRIM simulations. It further has the effect of reducing the electron lifetime in a similar manner to that of the EL2 level in SI-U GaAs, such that reverse bias leakage current is dominated by generation current.

It is reported by several authors that the damage observed in GaAs is proportional to the NIEL. The reverse bias leakage current variation as a function of fluence at a fixed bias of -10 V suggests that this is not the case however when comparing 1.8 MeV protons to 24 GeV protons. The damage due to 1.8 MeV protons is expected to be an order of magnitude greater than that due to 24 GeV protons, however this is not observed, as leakage currents due to 24 GeV protons are double that due to 1.8 MeV protons. This implies that some other kind of defect is also induced in the material by irradiation with 24 GeV protons. CCE measurements suggest however that the capture cross sections of any such defects are such that they do not play a major part in electron capture, as 24 GeV and 1.8 MeV proton irradiation CCE measurements are compatible with the NIEL hypothesis. Completely new analysis methods may well be required to resolve this apparent conflict between the CCE support for the NIEL hypothesis and the apparent incompatibility of the leakage current measurements.

One important potential source of error in the comparisons of the NIEL ratio is that NIEL is a function of depletion volume. Because the effective doping concentration N_{eff} cannot be accurately measured due to frequency dependence of the CV measurements then accurate calculation of the depletion width cannot be made.

It is further observed that, post-irradiation, the measured capacitance as a function of reverse bias becomes sample frequency dependent. Measurements of junction resistance R_j and substrate resistance R_b prove that they do not become comparable with each other. It is therefore concluded that the frequency dependent capacitance is due to the increased presence of defects with slow emission times e_n. Due to this frequency dependence it becomes impossible to carry out capacitance DLTS measurements, as described in section 4.4 on these irradiated devices, and therefore the presence of such defects cannot be examined. The fast sample frequency of the capacitance meter means that no change in frequency δC is measured on removal of the filling pulse.

The next chapter details an investigation of the analysis of Thermally Stimulated Current (TSC), a more sensitive technique that may clarify defect introduction in proton irradiated GaAs.

Chapter 6

Defect Analysis

Defects present in GaAs detectors introduce energy levels into the band gap which may or may not be electrically active. These defects may be introduced during crystal growth by impurities in the Ga and As mix, or during the device fabrication. As discussed in chapters 5 they may also be introduced through irradiation by charged particles. The detailed analysis of this latter type of defect introduction is the basis of this chapter. Capacitance DLTS discussed in section 4.4 is a common technique utilised for quantative defect analysis in semiconductor materials. This technique can be utilised for high purity epitaxial GaAs but not for SI-U LEC GaAs due to the high EL2 concentration. There is clear evidence that VPE GaAs Schottky devices behave in the same nature as SI-U devices after irradiation with protons as discussed in chapter 5. Chapter 5 also details an investigation into the change in macroscopic characteristics of proton irradiated VPE GaAs devices which lead to the identification of activation energy and concentration of the principal defect level, further leading to an increase in leakage current and reduction in CCE. These investigations, however, give no detailed information on the other levels present in the bandgap and therefore a more sensitive defect analysis technique is required. The analysis of Thermally Stimulated Current (TSC) is such a technique used to identify single defect levels.

6.1 Defect Investigation through Analysis of Thermally Stimulated Currents

6.1.1 Theoretical Description

TSC is a technique used to identify single defect levels by measurement and analysis of currents which are generated by thermal emptying of charge carriers from traps initially filled under reverse bias. Light excitation from a 10 mW HeNe laser with quantum energy of 1.08 eV (sub-bandgap) excites the EL2 level to a metastable state. Further deep level defects are identified in a repetitive temperature scan. This light excitation can have the effect of introducing *metastable modification* which under the correct conditions reduces the donor concentration in the sample, whereby it may become the case that holes become the majority carriers. The theoretical explanation of this process is discussed in detail in reference [66]. Correct illumination therefore allows a detailed investigation of both electron and hole traps[70].

Short excitation pulses in the range of 1-3s result in non-metastable transformation of the EL2 centre to the $EL2^0$ and $EL2^+$ charge states, which remain electrically active[70], while excitation of several minutes results in metastable transformation to the neutral $EL2^*$ state[71]. The heating routine which allows measurement of TSC is carried out as follows [74]:

1. A reverse bias is applied to the diode (15-20V)

2. The sample is then excited as described above to transform the EL2 level to the metastable state.

3. The diode is kept in the dark to ensure recombination of free carriers.

4. The sample is then subjected to cycles of heating at a rate β of approximately 0.14K/s up to a point where no further increase in current is observed. The temperature is then lowered and the scan repeated. An example of raw unanalysed measured TSC current is given in figure 6.1.

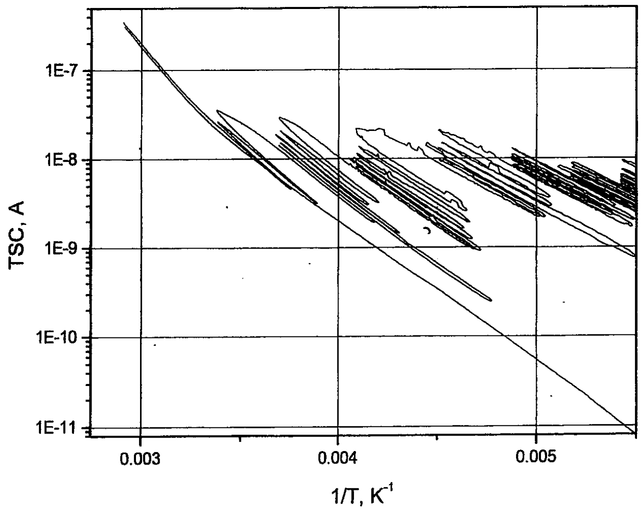

Figure 6.1: Measured TSC current as a result of repetitive temperature scans

In every heating cycle the shallower levels are fully (or partially) emptied of the initially captured electrons. These thermally generated electrons produce a current, I in the external circuit, which, when a graph is plotted of log(I) against 1/T produces a slope that defines the activation energy E_t of a particular level, where $I = exp\left(-E_t/kT\right)$[72]. The initial occupation n_{t0} is calculated from the following formula which is defined in reference [72]:

$$I_m = \frac{qLA\beta n_{t0}E_t}{2kT_m^2}exp\left(-\frac{E_t}{E_t + kT_m}\right) \tag{6.1}$$

where I_m is the maximum current for a given level, T_m is the temperature at which the maximum current for that level occurs, L is the thickness of the active region of the Schottky diode, defined for the samples investigated here as the 50μm thickness of the epitaxial layer and A is the sample area.

The trap capture cross section σ_n is calculated from the following formula, given in reference [66]:

$$\frac{E_t}{kT_m^2} = \frac{v_{th}\sigma_n N_C}{\beta}exp\left(\frac{E_t}{kT_m}\right) \tag{6.2}$$

where N_C is the effective density of states at the bottom of the conduction band and v_{th} is the electron thermal velocity.

From the characteristics obtained from TSC spectra it is also possible to obtain estimates of further trapping centre parameters $\tau_{emission}$ and $\tau_{capture}$[73], where:

$$\tau_{capture} = \frac{1}{v_{th}\sigma_n n_{t0}} \tag{6.3}$$

and

$$\tau_{emission} = v_{th}\sigma_n N_C exp\left(\frac{E_t}{kT}\right) \tag{6.4}$$

6.1.2 TSC Results

Normally the metastable transformation of the EL2 level described above is caused by an excitation wavelength of 1-1.5μm. The effectiveness of this transformation in identifying electron and hole traps, however, also depends on the relative concentrations of other levels present, i.e. on the compensation of the EL2 level. It is observed that after illumination of several hundreds of seconds (ensuring full level filling) there is very little difference in the influence of the EL2 level on the low temperature spectra compared to illumination by a short pulse, and therefore it is assumed that the influence of hole traps in the samples is not observed.

The TSC plot for unirradiated device AX1221-11 is given in figure 6.2 under excitation of wavelength 1 - 1.5 μm for several minutes. The slopes reveal defect levels with a wide distribution of energies between 0.13 and 0.72 eV, as shown in figure 6.3 and in table 6.1, a considerably greater number of levels than found with the capacitance DLTS technique of defect characterisation. As can be seen the energy levels are reasonably uniformly distributed between 0.13 and 0.51 eV with concentrations between $2 \times 10^{12} cm^{-3}$ and $6 \times 10^{14} cm^{-3}$. The next level occurs at 0.72 eV with a concentration of $2 \times 10^{15} cm^{-3}$.

After irradiation with 5×10^{12} 24 GeV protons cm^{-2} the energy distribution changes considerably as observed in figure 6.4 and in table 6.2. 24

E_t (eV)	$\sigma_n(cm^2)$	$\tau_{capture}(s)$	$\tau_{emission}(s)$
0.132	2.27×10^{-22}	46.84	0.03
0.144	3.56×10^{-21}	5.97	0.01
0.179	2.06×10^{-19}	0.26	2.21×10^{-4}
0.206	1.01×10^{-16}	2.10×10^{-5}	1.28×10^{-6}
0.243	1.05×10^{-22}	405.26	5.17
0.251	4.52×10^{-21}	0.23	0.16
0.303	9.13×10^{-12}	2.33×10^{-8}	6.04×10^{-10}
0.311	8.39×10^{-20}	0.02	0.09
0.327	7.12×10^{-20}	0.02	0.19
0.354	2.60×10^{-19}	4.09×10^{-4}	0.15
0.410	2.42×10^{-19}	8.79×10^{-4}	1.42
0.481	4.40×10^{-17}	1.21×10^{-6}	0.12
0.506	9.31×10^{-15}	3.26×10^{-9}	0.01
0.718	3.83×10^{-14}	2.78×10^{-10}	1.33

Table 6.1: Trapping centre parameters for unirradiated device AX1221-11

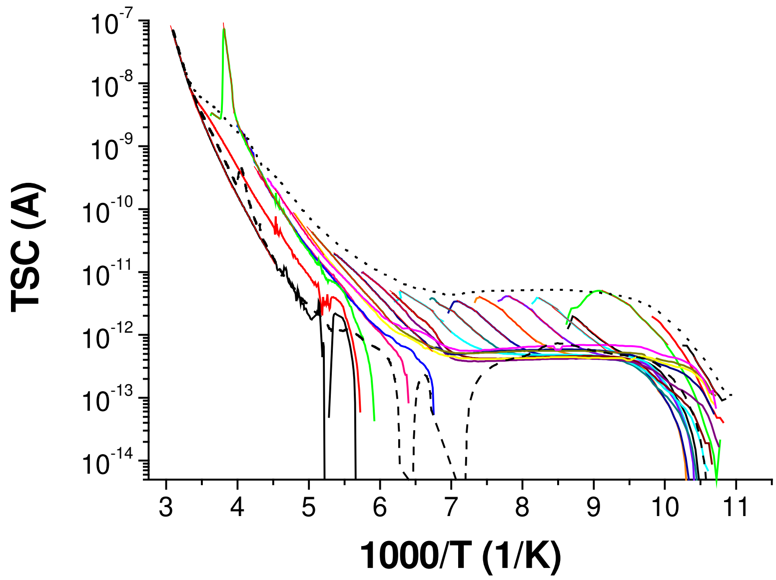

Figure 6.2: Experimental TSC curve for unirradiated device AX1221-11 obtained by fractional heating after excitation by light of wavelength 1 - 1.5 μm. The dark current caused by the generation from the EL2 level is denoted by the dashed line. The TSC measured in the single heating regime is given by the dotted line.

GeV proton irradiation causes the majority of uniformly distributed defects in the energy range 0.13 to 0.51 eV to disappear, but results in the creation of a series of levels tightly grouped between 0.31 and 0.38 eV with concentrations between $1.5 \times 10^{11} cm^{-3}$ and $1 \times 10^{14} cm^{-3}$. Levels are also found at 0.27, 0.59 and 0.76 eV with concentrations $2 \times 10^{11} cm^{-3}$, $1 \times 10^{15} cm^{-3}$, and $3 \times 10^{15} cm^{-3}$ respectively. As the fluence increases to 5×10^{13} 24 GeV protons cm^{-2} the energy range of this tight group reduces to 0.26 to 0.35 eV, the level at 0.59 eV reduces to 0.56eV and the level at 0.76 eV reduces to 0.70 eV. A further increase in fluence to 1×10^{14} 24 GeV protons cm^{-2} reduces the energy range of this group to 0.18 to 0.29 eV, the 0.56 eV level remains unchanged, and the highest energy level at 0.70 eV is now at 0.66 eV. With increasing fluence the trend for the tightly packed group of levels

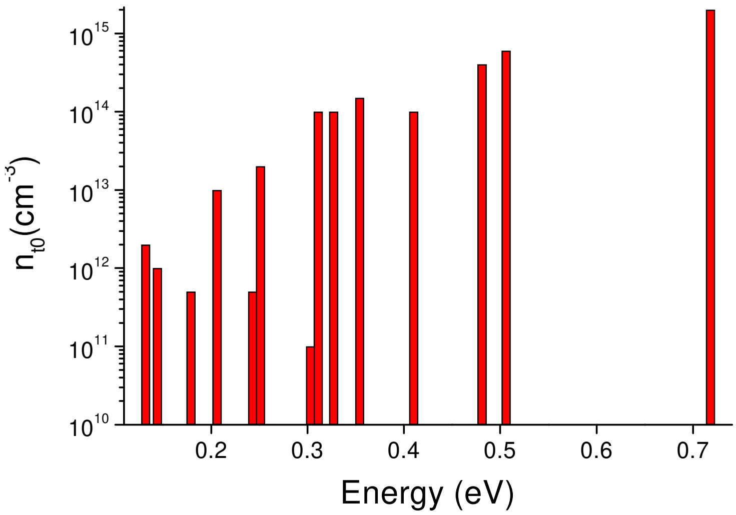

Figure 6.3: Defect energy level distribution of unirradiated device AX1221-11

is an increase in n_{t0} for all levels, where after 1×10^{14} 24 GeV protons cm^{-2} the spread in n_{t0} for this group is between 2×10^{12} and 5×10^{14} cm^{-3}, while the concentration of the level initially found at 0.59 eV increases to 3×10^{15} cm^{-3}. The initial concentration of the level at around 0.7 eV remains almost constant, fluctuating around $1 \times 10^{17} cm^{-3}$.

Irradiation with 5×10^{13} 1.8 MeV protons cm^{-2} induces levels with an energy distribution given in figure 6.5 and table 6.3. The main difference is the introduction of a level with energy of 0.57 eV and concentration of 2×10^{14} cm^{-2}. The level with energy 0.67 eV and concentration $1 \times 10^{16} cm^{-3}$ is assumed to be the same level found in the unirradiated material with energy 0.72 eV. The energy distribution of the levels in the range 0.21 to 0.51 eV remains uniform throughout with increasing fluence, however there is a slight increase in the number of levels and the concentrations of these levels increase slightly. Irradiation with an increased fluence of 1×10^{14} 1.8 MeV protons cm^{-2} causes a reduction in the energy range of the levels to 0.20 to 0.64 eV. The highest energy level doubles in concentration to 2×10^{16} cm^{-2}, however

E_t (eV)	$\sigma_n(cm^2)$	$\tau_{capture}(s)$	$\tau_{emission}(s)$
0.272	1.02×10^{-14}	1.04×10^{-5}	1.63×10^{-7}
0.313	2.36×10^{-15}	4.50×10^{-5}	3.43×10^{-6}
0.323	2.41×10^{-13}	8.82×10^{-7}	4.95×10^{-8}
0.334	3.15×10^{-18}	0.01	0.05
0.341	7.98×10^{-16}	1.33×10^{-6}	3.00×10^{-5}
0.343	1.97×10^{-19}	0.01	0.13
0.354	3.23×10^{-14}	6.58×10^{-7}	1.22×10^{-6}
0.355	8.25×10^{-15}	2.86×10^{-6}	4.98×10^{-6}
0.357	6.66×10^{-16}	3.19×10^{-4}	6.67×10^{-5}
0.359	4.85×10^{-16}	2.19×10^{-6}	9.90×10^{-5}
0.359	8.78×10^{-14}	2.42×10^{-9}	5.46×10^{-7}
0.362	1.35×10^{-18}	0.01	0.04
0.592	8.90×10^{-15}	2.39×10^{-9}	0.04
0.761	2.86×10^{-13}	2.47×10^{-11}	0.93

Table 6.2: Trapping centre parameters for AX1221-ukn2 after irradiation with 5×10^{12} 24 GeV protons cm^{-2}

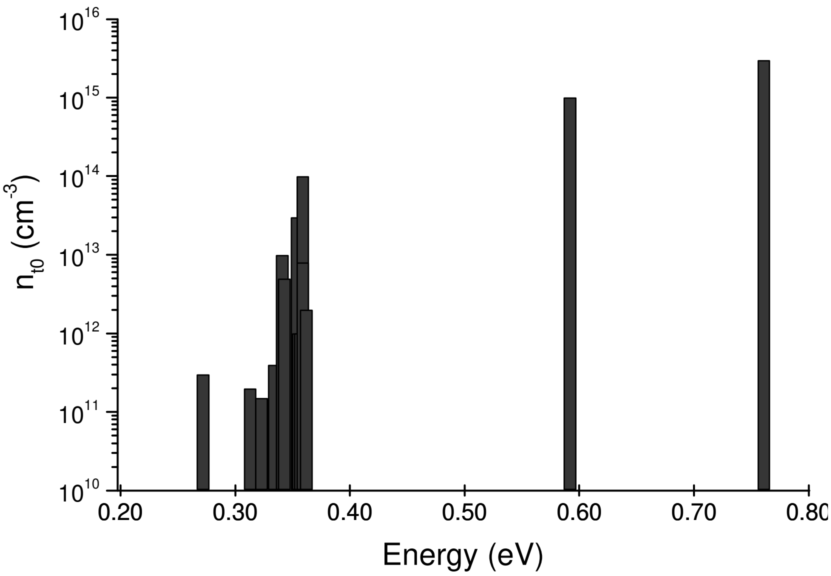

Figure 6.4: Energy distribution of defects in AX1221-ukn2 after irradiation with 5×10^{12} 24 GeV protons cm^{-2}

there is a significant increase in the concentration of the second highest energy level to 7×10^{15} cm^{-2}.

6.2 Gamma Spectroscopy

Further identification of defects present in proton irradiated GaAs can be carried out by gamma-ray (γ) spectroscopy. After irradiation by protons with an energy high enough to penetrate the target nucleus, causing spallation, fragmentation and fission reactions, as discussed in section 5.1, the remnant nucleus is often left in an excited state, from which it will de-excite by γ emission. Analysis of the γ spectra of a material after proton irradiation can therefore give information about the nuclei present in the material.

The γ spectrum of the devices irradiated with 24 GeV protons was analysed by Guy Roubaud of the CERN Radiation Protection Group, using a high purity Ge detector with *Genie 2000* multi-channel analyser software.

E_t (eV)	$\sigma_n(cm^2)$	$\tau_{capture}(s)$	$\tau_{emission}(s)$
0.210	1.80×10^{-14}	1.68×10^{-6}	8.42×10^{-9}
0.219	2.79×10^{-14}	2.54×10^{-6}	7.69×10^{-9}
0.274	7.02×10^{-13}	5.05×10^{-8}	2.56×10^{-9}
0.282	8.72×10^{-12}	8.13×10^{-9}	2.80×10^{-10}
0.289	2.80×10^{-15}	2.53×10^{-6}	1.14×10^{-6}
0.342	5.64×10^{-12}	4.19×10^{-10}	4.41×10^{-9}
0.348	8.02×10^{-13}	3.31×10^{-9}	3.91×10^{-8}
0.355	2.72×10^{-13}	1.11×10^{-8}	1.51×10^{-7}
0.368	6.00×10^{-16}	4.43×10^{-6}	1.13×10^{-4}
0.382	3.01×10^{-13}	3.53×10^{-9}	3.88×10^{-7}
0.393	1.10×10^{-13}	2.15×10^{-8}	1.63×10^{-6}
0.408	8.12×10^{-14}	1.74×10^{-8}	3.92×10^{-6}
0.422	2.14×10^{-15}	2.48×10^{-7}	2.56×10^{-4}
0.465	3.65×10^{-15}	1.45×10^{-7}	7.91×10^{-4}
0.466	1.21×10^{-15}	1.95×10^{-7}	0.02
0.469	2.51×10^{-16}	4.25×10^{-7}	0.01
0.484	1.71×10^{-16}	2.07×10^{-7}	0.04
0.574	1.15×10^{-15}	4.63×10^{-8}	0.16
0.668	1.67×10^{-14}	1.27×10^{-10}	0.44

Table 6.3: Trapping centre parameters for AX1221-6 after irradiation with 5×10^{13} 1.8 MeV protons cm^{-2}

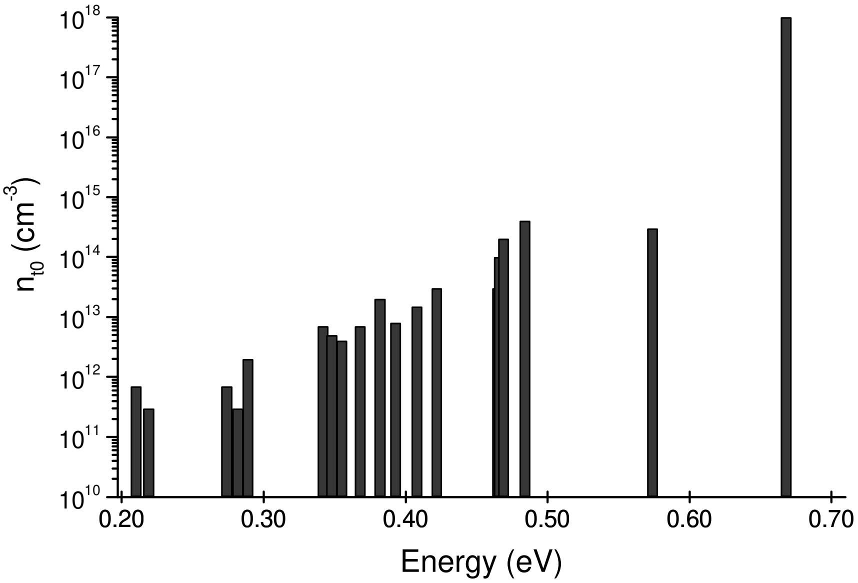

Figure 6.5: The distribution of energy levels in VPE GaAs device AX1221-6 after irradiation with 5×10^{13} 1.8 MeV protons cm^{-2}

The analysis of the devices irradiated with 1.8 MeV protons was carried out by Vladimir Lindhard at the Czech Technical University in Prague, using a high purity Ge detector controlled by *Maestro* multi-channel analyser software.

After 24 GeV proton irradiation the radio-isotope defects found with γ spectroscopy are: Be^7, Na^{24}, Mg^{28}, K^{42}, Sc^{43} Sc^{44}, Sc^{46}, V^{48} and Cr^{51}. Of these levels, the only identifications are that the Mg defect is a A_{Ga} with energy E_v + 28.7 meV, and the Cr defect is an A_{Ga} defect with energy E_v + 790 meV[75]. Both of these are acceptors. The effect of these levels is that they may act as micro-inhomogeneities responsible for drift-recombination barrier modification, however without suitable characteristic identification this can only be speculated at.

The defects identified above were measured 12 hours after removal of the device from the 24 GeV proton beam. The gamma spectra taken immediately after removal contained many unidentified peaks that were not present in the spectra taken after 12 hours. This suggests that 24 GeV proton irradiation created many defects that anneal rapidly.

An analysis of the devices irradiated by 1.8 MeV protons show that, as expected, there is no significant peak in the γ spectrum from the device because the proton energy is below the nuclear threshold, and therefore the only defects are transient ionisation effects and displacement effects.

6.3 Discussion

Irradiation with 24 GeV protons results in both destruction and creation of defect levels in the bandgap. The wide distribution of levels found in the range 0.13 and 0.51 eV in the unirradiated sample disappear after a fluence of 5×10^{12} 24 GeV protons cm^{-2}, to be replaced with the tight group of levels around the 0.31 to 0.38 eV range. The large number of TSC characteristic defect levels within this group is misleading as their energies probably do not correspond to different centres. Microscopic doping and compensation inhomogeneities, referred to in this thesis as micro-inhomogeneities can be introduced during the crystal growth process or by irradiation. In a crystal with such *micro-inhomogeneities*, small fluctuations in compensation lead to a different modulation of electrical potential in the bulk that causes the appearance of different drift-recombination barriers, causing the measured activation energy E_a to be modified to (E_t - ϕ) where ϕ is the height of the drift-recombination barrier[66],[72],[74]. In some electric fields these barriers may be reverse biased, causing an increase in measured energy. Many radio-isotopes are identified by the analysis of the gamma ray spectra from a device after irradiation, a vast number of which anneal out rapidly. It is probable that these radio-isotopes act as micro-inhomogeneities, however further investigations would be to extract their concentrations as a function of proton fluence, and comparisons made with Monte Carlo simulations of radioactive isotope production.

The levels between 0.31 - 0.38 eV are thought to be due to modification by micro-inhomogeneities of either the E3 $V_{As} - As_i$ electron trap with $E_c - E_t$ = 0.3 eV,[74] and capture cross section σ_n quoted as 6.2×10^{-15} cm^2 in reference [63], or to the EL6 complex $As_{Ga} - V_{As}$ defect with $E_c - E_t = 0.33$ eV and σ_n quoted in reference [76] as 2.8×10^{-14} cm^2. Calculation of the capture cross section using equation 6.2 as shown in table 6.2 gives a result for the principle defect of this cluster at 0.36 eV of $\sigma_n = 8.7 \times 10^{-14}$ cm^2. This suggests that this defect is more likely to be the EL6, however due to the difficulty in assigning the measured cross-section to a particular defect with confidence it may be that case that the cluster of defects comprises both the E3 and EL6 defect. The highest energy level in this range is assumed to be the EL2 level whose concentration remains unaffected by 24 GeV proton irradiation. This is confirmed by measurement of $\sigma_n = 2.8 \times 10^{-13}$ cm^2, compared to the value quoted in reference [38] 8×10^{-14} cm^2.

The defect concentrations induced by lower energy protons, where no nuclear interactions take place, and kinetic energy and momentum are conserved in these elastic processes, are easier to estimate than with higher energy protons. The defect in figure 6.5 with energy of 0.67 eV and concentration of $1 \times 10^{16} cm^{-3}$ is assumed to be the EL2 present in the unirradiated material, confirmed by measurement of its capture cross section as $1.67 \times 10^{-14} cm^{-2}$ in table 6.3. The main effect of irradiation with 5×10^{13} 1.8 MeV protons cm^{-2} is the introduction of the level found at 0.57 eV with a concentration of $4 \times 10^{14} cm^{-3}$. It is assumed that this level is the EL3 As_iV_{As} complex [76], consistent with the results of chapter 5. The capture cross-section for the EL3 defect is quoted as $2.9 \times 10^{-14} cm^{-2}$ in reference [76], and the measured value using equation 6.2 is $1.15 \times 10^{-15} cm^{-2}$ in table 6.3. Sources of error in the cross-section measurements arise from difficulty in accurately measuring T_m, and from uncertainty in values of E_t calculated from the gradient of the TSC slopes.

In table 6.2 the defect identified as the EL3 at 0.592 eV has an emission time constant τ_{emm} of 0.04s, giving an emission rate of 25 s^{-1}. While this emission rate is higher than that quoted for the EL2 level in reference [40] as

0.045 s^{-1}, it is low enough to confirm that this slow emptying time is responsible for the capacitance dependency on frequency observed after irradiation with 24 GeV protons in section 5.4.2.

Chapter 7

Noise Analysis

It is well known that currents flowing in semiconductor devices are affected by random fluctuations that can be described in the frequency domain in terms of noise spectral densities[54]. The measurement of current noise spectra is a non-destructive test that can give information about the quality of a device, as it allows analysis of phenomena that occur in the semiconductor, such as trapping-detrapping of carriers. The purpose of this chapter is to investigate whether analysis of current noise spectra can be extended to irradiated samples such that they can be used as an analytical tool to determine irradiation fluence and energy. This chapter details the main sources of noise found in semiconductor devices and the measurement techniques used in their analysis. Results are then presented of the analysis of the noise spectra from unirradiated devices and on devices irradiated with 1.8 MeV and 24 GeV protons.

7.1 Noise Theory

The magnitude of noise in the semiconductor devices under investigation relates to the random fluctuations of charge carrier transport and increases if there are more individual sources of randomness. The magnitude may also increase if a given source changes its condition so that the overall effect is that the system becomes less predictable. An electron trap will contribute most noise if it is at the Fermi level, where it has an equal probability of being occupied or empty, therefore its state is at its most uncertain[57].

A measure of current that exhibits noise can be expressed as:

$$i(t) = \langle i \rangle + \Delta i_n(t) \tag{7.1}$$

where $\Delta i_n(t)$ is the deviation in i(t) from its mean value $\langle i \rangle$ at a time t. The average value $\langle i \rangle$ is obtained for the current $i\,(t)$ if it is measured over a sufficiently long period of time. The mean squared noise current fluctuation intensity is given as $\overline{\Delta i_n^2}$, however the most commonly used form is the noise spectral density, given by:

$$S_i(f) = \frac{\overline{\Delta i_n^2}}{\Delta f} \tag{7.2}$$

where Δf is the bandwidth of the measurement. The spectral density is therefore defined as the noise per unit bandwidth. A similar definition can be given for voltage fluctuations:

$$S_v(f) = \frac{\overline{\Delta v_n^2}}{\Delta f} \tag{7.3}$$

Sources of noise are classified into two groups, extrinsic and intrinsic. Extrinsic noise sources are those from outside the system under test and may be connected, for example, to external magnetic fields from current carrying conductors (e.g. 50 Hz oscillations from mains supplies), or due to the layout or construction of any circuit used in the measurement procedure. While extrinsic noise sources are an important consideration in the design of the amplifier and associated electronics used in noise analysis, only intrinsic sources are relevant to this chapter. The four major classifications of intrinsic noise in semiconductors are now introduced.

7.1.1 Thermal Noise

Thermal noise in semiconductors[56] is caused by the random Brownian motion of the charge carriers. The current noise spectral density (S_i) per unit bandwidth can be described as a current source in parallel with a resistive element R, and voltage noise spectral density (S_v) can be described as a voltage source in series with R. This random charge carrier motion results in a uniform spectral density (white noise) given by[57]:

$$S_i = \frac{4k_BT}{R} \tag{7.4}$$

$$S_v = 4k_BTR \tag{7.5}$$

The thermal noise of known resistors is often used to calibrate a noise measurement experiment.

7.1.2 Shot Noise

This type of noise is the result of the discrete nature of the charge carriers in an electric current and the random emission of charge carriers over a potential barrier, and is independent of frequency (white spectrum) at low and intermediate frequencies[26]. For a reverse biased diode with current I equal to q$\langle n \rangle$, where n is the spontaneously fluctuating number of electrons that cross the barrier per second and q the electronic charge, the spectral density is given in reference [54] as:

$$S_i(f) = 2\alpha q^2 \langle n \rangle = 2\alpha q I \tag{7.6}$$

Based on the definition given in [54], the condition where $\alpha = 1$ for full shot noise is when the leakage current is purely thermionic. For this to be the case there must be a low probability of trapping in the space charge region to ensure that each current pulse displaces a charge equivalent to that of one electron in the external circuit. In most practical measurements this is not the case and α is often less than unity.

7.1.3 Generation-Recombination Noise

Generation-Recombination noise (g-r noise) is a fluctuation in the conductance caused by a fluctuation in the number of carriers between a band and trap at a particular energy level. For a semiconductor with a significant trap density the carrier fluctuation Δn is caused by continuous trapping and detrapping of carriers. The spectral density S_{GR}(f) for G-R noise from a single trap level is given by a Lorentzian[55]:

$$S_{GR} = \frac{(\Delta n)^2 4\tau_n}{(1 + (2\pi f \tau_n)^2)} \tag{7.7}$$

where Δn is the carrier density fluctuation. The corner frequency f_n of a Lorentzian spectrum is given by the inverse of τ_n, the relaxation time (also known as mean free time) of the electrons in the conduction band. If an energy level in the band gap is considered, its G-R noise appears only if the Fermi level is less than a few kT away from the level[59].

7.1.4 1/f Noise

The origin of low frequency, "flicker" noise with a spectral density proportional to 1/f is not completely understood. It is possible that there are several different mechanisms of 1/f noise and that different mechanisms occur in different systems, for example, a trend is observed of low 1/f noise in bipolar devices and high 1/f noise in Field Effect Transistors (FET's)[58]. It is observed that there is generally a decrease in this noise source as the quality of device fabrication improves, but devices fabricated using the same process can have very different levels of noise.

However, although there is no single fundamental noise source with a 1/f spectrum, it is widely accepted that the superposition of a number of G-R noise sources with differing relaxation time constants τ results in a spectrum proportional to $1/f^\gamma$, where γ often is equal to unity, but can vary between 0.5 and 2[57]. Lee suggested in reference[60] that the exponent γ, refered to as the noise index is related to the distribution of trap energies. The origin of

γ will be investigated further in 7.2.4. The origin of these different relaxation time constants can be explained by assuming different defect levels with a distribution of various trapping cross sections.

The distribution of time constants required for a mathematical description of 1/f noise can be obtained in terms of a distribution of thermal activation energies of traps, where a peak of energies a few kT wide is sufficient to produce the $1/f^{\gamma}$ spectrum[60]. For this to be valid the assumption must also be made that there is no transition between trap states. The bending of bands in the depletion region of a semiconductor diode can provide the wide range of time constants by exposing the trap levels in the band-gap to the Fermi level.

7.2 Analysis of Noise Spectra

The noise spectra of the GaAs pad diodes were investigated both before and after irradiation. Two different regions were investigated, the first in the frequency range of 10 Hz to 100 kHz to investigate the effects of irradiation on the white noise. The second, extending only up to 1 kHz, enabled a more detailed investigation of the 1/f noise.

A measurement of the output noise voltage S_{Vout} of a well characterised transimpedance amplifier (which converts current to voltage) can give complete information about the current noise spectrum, S_{Idev}, of a device under test provided the transfer function of the amplifier is known and the amplifier noise is negligible. Two different amplifiers were used in this investigation to measure the low frequency range and the high frequency range. The low noise amplifier used for measurements up to 100 kHz was built in-house by the author and therefore merits a detailed description.

7.2.1 The Low Noise Transimpedance Amplifier

A low-noise, wide-band transimpedance amplifier for measurement of the spectral noise densities of currents as described in this chapter was built by the author, modified from a design by De Geronimo, Bertuccio and Longoni as described in reference [53]. The amplifier is designed to operate in the frequency range of 10 Hz to 100 kHz, with an intrinsic noise as low as 3 fA/$\sqrt{Hz}$ at 1 kHz and 20 fA/$\sqrt{Hz}$ at 100 kHz at room temperature. The equivalent circuit and schematic are shown in figures 7.1 and 7.2 respectively.

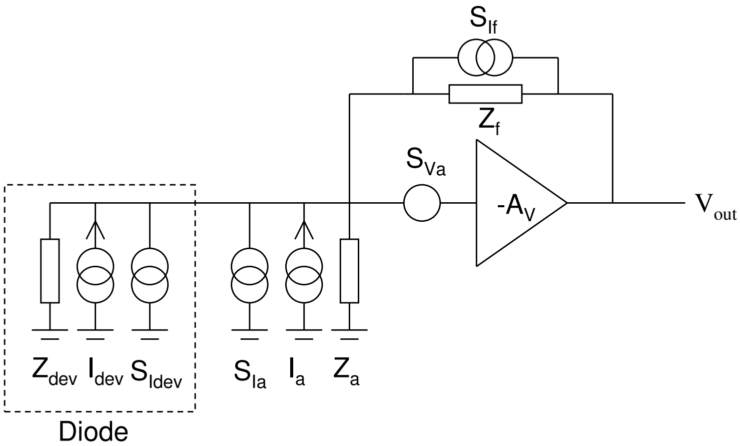

Figure 7.1: Equivalent circuit of low noise transimpedance amplifier used for noise investigations up to 100 kHz

A feedback transimpedance amplifier can be obtained by connecting an impedance Z_f between the output and inverting input of a high-gain voltage amplifier. The current noise spectral measurements of the Schottky diode detectors are obtained by connecting the Schottky contact of the device under test to the input of the amplifier. The device is reverse biased using batteries ranging from 1.5V to 45V between the ohmic contact and ground. The gate node of input JFET J1 of figure 7.2 and the Schottky contact of the diode can be trimmed to 0V to enable accurate measurement of the current through the feedback resistance. By assuming negligible gate leakage current in J1 then it is assumed that the current through Z_f is the reverse bias leakage current I_l of the diode. This can be evaluated by measuring the dc output voltage and the value of the feedback impedance Z_f. Because Z_f is a function of frequency then Z_f(f) must be well known for accurate measurement of I_l. The pcb was designed by the author such that its area was small and therefore the dimensions of any conducting loops that might act as antennae to inductively coupled noise was reduced[54]. To aid in this dimension reduction surface mounted passive components were used where possible.

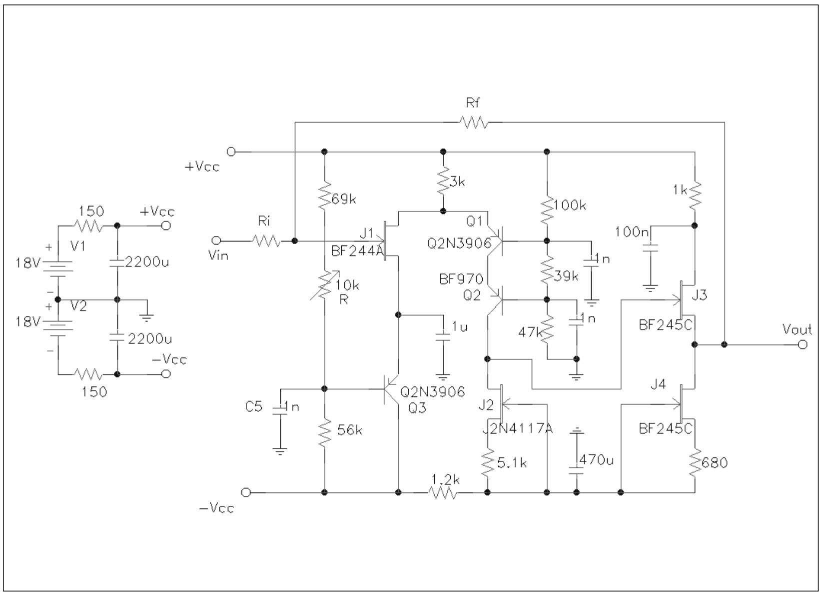

Figure 7.2: Schematic of low noise transimpedance amplifier

The component specifications were as described by Bertuccio et-al in reference [53] where a detailed circuit description is given, however certain component changes were made by the author on the grounds of availability. The choice of a JFET as the amplifier input was based on the requirement for low gate leakage current and therefore low input shot noise. The effects of any excess noise generated at the input stage will be most damaging to the characteristics of the amplifier as this input shot noise will be amplified throughout. The chosen JFET, the BF244A has an input leakage current below 20 pA and a transconductance g_m, defined as the change in current resulting from an applied small signal voltage across the gate-source[79], and is equal to 5 mS[77].

The main gain stage of the amplifier is made up of components J1 and bipolar transistors Q1 and Q2 in a double cascode configuration[80] with an active FET load J2. The purpose of this cascode configuration is to increase the output impedance of this stage[79]. The output stage, composed of J3 and J4 is an active loaded source follower that was chosen by Bertuccio et al because of its effect of maximising the open loop low frequency gain of the amplifier. The open-loop output resistance of the amplifier is about 150Ω.

The choice of the feedback resistor R_f was made as the result of a compromise between the following requirements:

- to give a minimum noise current contribution in all of the frequency ranges of interest, where noise current as a function of resistance is given by equation 7.4,
- to achieve the maximum transimpedance gain i.e. conversion from current to voltage,
- to be as stable as possible with respect to temperature variation or dc voltage across it, and
- to achieve maximum loop gain.

Based on these requirements, the value of feedback resistor R_f was chosen as 33 MΩ. The actual feedback impedance is frequency dependent and will from now on be defined as $Z_f(f)$.

7.2.2 Amplifier Characterisation

The spectral noise density of the output voltage S_{Vout} is given by:

$$S_{Vout} = [S_{Idev}(f) + S_{Iamp}(f)]\,|Z_f(f)|^2 \tag{7.8}$$

where S_{Iamp} is the amplifier equivalent input current noise spectrum. If the amplifier is characterised such that S_{Iamp} and $Z_f(f)$ are well known then complete information can be gained of S_{Idev}. The measurement of $Z_f(f)$ is made by injecting a sinusoidal signal current i_j of frequency f at the input of the amplifier through a well known injection impedance Z_j. If the measured voltage gain $G_j = v_{out}(f)/v_j(f)$ then:

$$|Z_f(f)| = |G_j||Z_j(f)| \tag{7.9}$$

Resistors have a stray capacitance (typically around 200 fF[53]) and for high value resistors the effect of this capacitance becomes important as the corner frequency of the resistor may be within the operating frequency range of the amplifier of 10 Hz to 100 kHz. The injection impedance Z_j is therefore chosen as a 1MΩ resistor which, with a stray capacitance of 200 fF has a corner frequency of 795 kHz, above the frequencies of interest. The measured value of Z_f(f) is given in figure 7.3.

The total equivalent amplifier input current noise S_{Iamp} is comprised of the sum of contributions from shot noise due to leakage current at the gate of the input JFET S_I, thermal noise contributions from the feedback impedance S_{If} and noise due to dielectric losses arising from capacitances or dielectric material close to the input of the amplifier[53]. S_{Iamp} is measured with the input of the amplifier floating and measuring the output voltage noise spectrum divided by the square of the modulus of the feedback impedance $|Z_f(f)|^2$. With a 33MΩ resistor as the feedback impedance, S_{Iamp} was measured as $5.3 \times 10^{-28} \pm 10\%$ A^2/Hz across the frequency of interest. This is similar to the theoretical thermal noise current of a 33 MΩ from equation 7.4 of $5 \times 10^{-28} \pm 10\%$ A^2/Hz, where the error in this case is due to the manufacturers tolerance on the resistor value.

7.2.3 White Noise Investigations

The measured levels of white noise under reverse bias of the AX1221-9 VPE GaAs device, as shown in figure 7.4 are compared with theoretical full shot noise predictions from 7.6, in table 7.1. The resulting, close to unity, values of α suggest that thermionic emission is the dominant process in the reverse

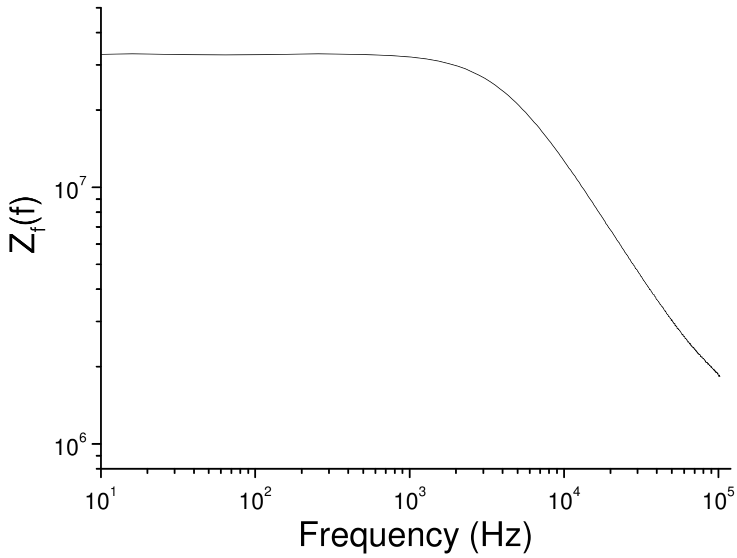

Figure 7.3: The measured feedback impedance Z_f as a function of frequency

bias leakage current, consistent with measurement of the ideality factor of 1.024 in section 4.2.1. The noise is white throughout the frequency range of interest due to the fast transit time of electrons across the high field region behind the Schottky contact. There is no evidence of a Lorentzian with characteristic corner frequency, suggesting that the concentrations of G-R centres with a corner frequency within the range of interest is negligible. An error in γ of $\pm 20\%$ is estimated due to the difficulty in measuring S_{imeas} with great accuracy due to the presence of externally induced noise fluctuations, and also uncertainty in measurement of leakage current I_l.

The levels of white noise shown in figure 7.4 differ from the levels of white noise in the SI-U LEC GaAs diode shown in figure 7.5 and table 7.2, where it is seen that at 10 kHz the value of α is between 0.51 and 0.63. If the leakage current is purely thermionic (measurements of the ideality factor n of this material as 1.04 in reference [12] suggest this is the case) then a value of $\alpha = 1$ is expected. A model to describe the values of α around 0.5 is proposed in reference [61]. If an electron is trapped and at a later time

$Voltage(V)$	$Current(A)$	$S_{imeas} A^2/Hz$	$S_{itheory} A^2/Hz$	α
45	8.05×10^{-9}	2.5×10^{-27}	2.57×10^{-27}	0.97
135	32×10^{-9}	9×10^{-27}	1.02×10^{-26}	0.87
220	215×10^{-9}	8×10^{-26}	6.88×10^{-26}	1.14

Table 7.1: Measured shot noise S_{imeas} and theoretical shot noise $S_{itheory}$ for unirradiated device AX1221-9 under reverse bias. Also given is the value of α

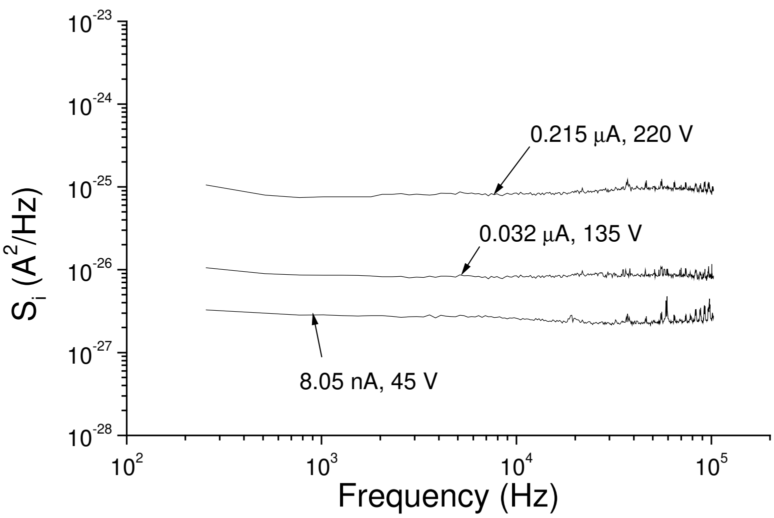

Figure 7.4: Reverse bias noise of unirradiated device AX1221-9

$Voltage(V)$	$Current(A)$	$S_{imeas} A^2/Hz$	$S_{itheory} A^2/Hz$	α
9	60.6×10^{-9}	1×10^{-26}	1.94×10^{-26}	0.51
18	95.45×10^{-9}	2×10^{-26}	3.05×10^{-26}	0.65
27	128×10^{-9}	2.4×10^{-26}	6.09×10^{-26}	0.58
35	149×10^{-9}	3×10^{-26}	4.77×10^{-26}	0.63

Table 7.2: Measured shot noise S_{imeas} and theoretical shot noise $S_{itheory}$ for LEC GaAs device G175-5 under reverse bias. Also given is the value of α

released then this electron will produce two pulses of charge whose sum is equal to q. If the electron is captured after producing a pulse equal to $\frac{1}{2}$q in the external circuit and subsequently released, on average the frequency of charge pulses produced by the emitted electrons is doubled while the charge is halved. The power spectral density is thus reduced by a factor of two.

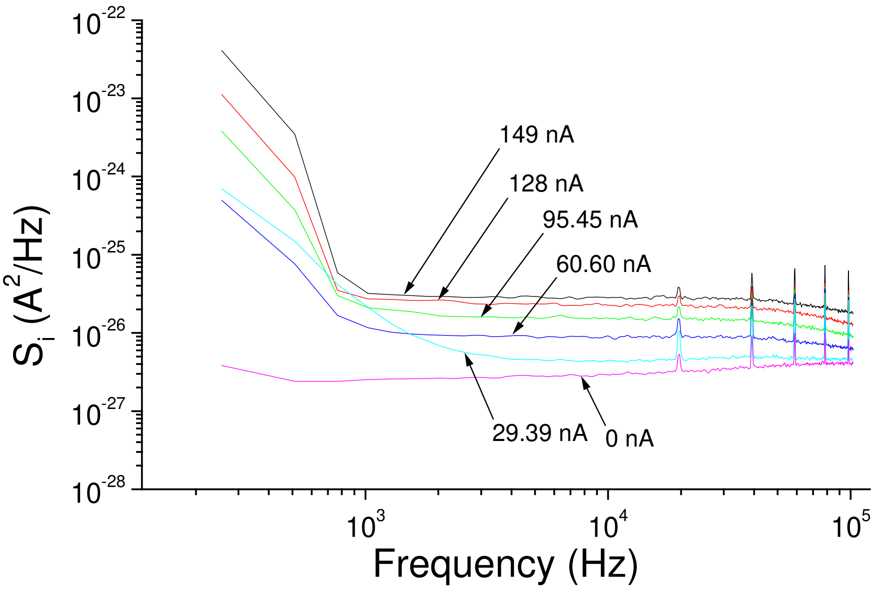

Figure 7.5: Noise spectra for unirradiated LEC GaAs diode G175-5 under reverse bias.

After proton irradiation the measured levels of white noise of the VPE GaAs diodes under application of reverse bias exhibit similar properties to those of the unirradiated LEC GaAs devices. The value of α from equation 7.6 is observed to decrease exponentially with increasing fluence, as shown in figure 7.6(a) for 24 GeV protons and figure 7.6(b) for 1.8 MeV protons. The initial fall in α is more extreme for 1.8 MeV proton irradiation, where it is observed that with a fluence of 1×10^{13} protons cm^{-2} α is equal to 0.6, compared to 0.8 for 24 GeV protons. For both energies a plateau is ultimately reached at a value of α around 0.3.

In section 5.1.2 it is discussed that several authors had reported that damage in GaAs is proportional to NIEL, where the damage due to 1.8 MeV proton irradiation would be an order of magnitude greater than that from 24 GeV proton irradiation. However, as also reported in chapter 5 this is not observed with all macroscopic characteristics. Changes in reverse bias leakage currents with 24 GeV proton irradiation are not proportional to NIEL because protons at this high energy incident on GaAs schottky diodes induce micro-inhomogeneities that act as trapping centres. The presence of these defects are confirmed by TSC measurements reported in section 6.1.2 which show that while 1.8 MeV proton irradiation induces several shallow defects with electron capture cross-sections in the range of 10^{-13} cm^2, 24 GeV proton irradiation induces a tight group of defects identified as the microinhomogeneity modified EL6 (with possibly some EL3 contribution) with characteristics given in table 6.2. The electron capture cross-sections of these related defects are lower than those induced by 1.8 MeV protons, but the greater number of these defects mean that their combined concentrations are greater, therefore their impact as trapping centres is significant. Several radio-nuclide defects were identified by γ spectroscopy, and while it was not possible to identify their energies in the band-gap, it is probable that these defects are acting as trapping centres which capture the electrons generated through shot noise mechanisms, releasing them back to the conduction band some time later. Because current is inversely proportional to charge carrier transit time then the measured noise current is reduced.

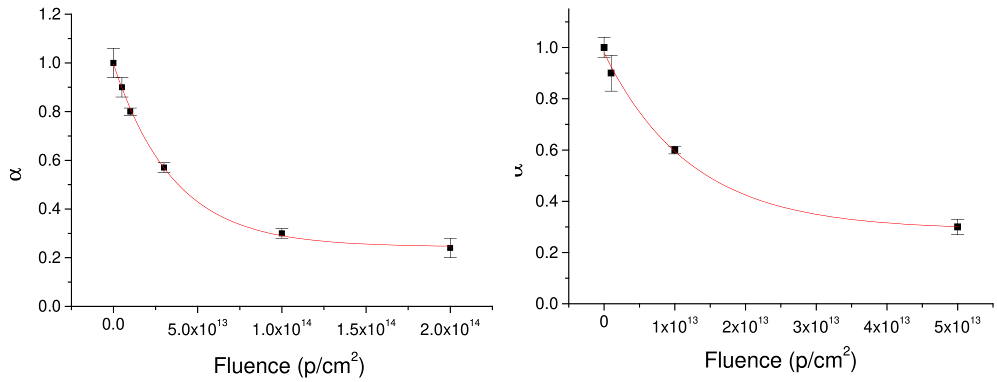

(a) 24 GeV proton irradiation (b) 1.8 MeV proton irradiation

Figure 7.6: Reducing α for shot noise as a function of fluence for proton irradiation of VPE diodes, where α equals $S_{imeas}/S_{itheory}$

7.2.4 Low Frequency Noise Specta

It is observed in figure 7.5 that the SI-U LEC GaAs device exhibits greater 1/f noise below 1 kHz compared to the VPE devices. The concentration of defects in the unirradiated SI-LEC GaAs material is greater than in the unirradiated VPE GaAs material, and based on this fact it is reasonable to assume that if a significant percentage of these defects are G-R centres, and if the theory of 1/f noise described in section 7.1.4 is true then the greater 1/f noise observed in SI-LEC material is valid. Measurement results are first presented, then a detailed investigation of 1/f noise relative to the defects in a material will be made in section 7.2.4.

Reverse Bias Measurements

The low frequency 1/f noise spectra of the GaAs devices were investigated using a discrete component, low noise transimpedance amplifier, designed and built by Ms Sandra Pralgauskaite and Dr Jonas Matukas at Vilnius University in Lithuania. The noise spectra for the unirradiated VPE GaAs diode AX1221-11 under reverse bias were measured between 4 Hz and 2 kHz. The results are shown in figure 7.7. It can be seen that under reverse bias the low frequency noise is directly proportional to 1/f. It should further be noted that when the reverse bias increases in the steps shown in figure 7.7 the magnitude of 1/f noise in the frequency range of interest increases disproportionally to the reverse bias and current. For example at 10 Hz, as the reverse bias increases from 138V to 163V then 182V, the noise spectral current density increases from 2.30 $\times 10^{-25}$ to 3.89 $\times 10^{-25}$ then to 5.86 $\times 10^{-25} A^2/Hz$. It should be noted that the noise corner frequency where 1/f noise and white noise meet gives no information on material characteristics. It is therefore not necessary to plot 1/f noise and white noise on the same graph.

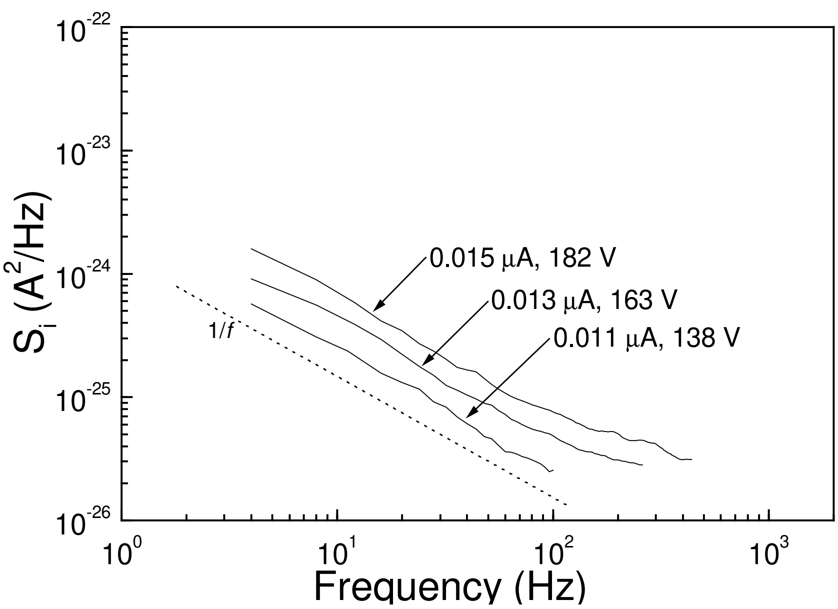

Figure 7.7: Reverse bias noise spectra for unirradiated device AX1221-11 between 4 Hz and 2 kHz

After irradiation with 24 GeV protons the low frequency noise characteristics are seen to change significantly from the unirradiated characteristics.

Device AX1221-ukn1 was exposed to a fluence of 3×10^{13} 24 GeV protons cm^{-2}. The noise characteristics shown in figure 7.8 show a reduction in the noise index γ from unity, resulting in a level of noise proportional to $1/f^{0.8}$.

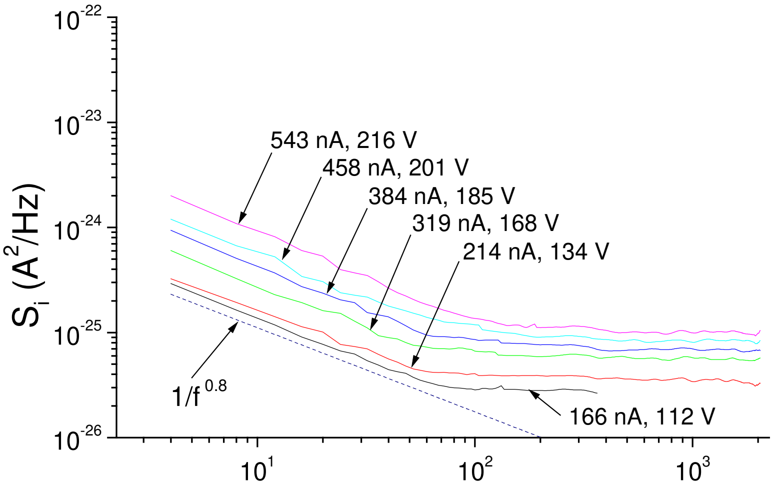

S_i (A^2/Hz)
10^{-22}
10^{-23}
10^{-24}
10^{-25}
10^{-26}
10^1
10^2
10^3
543 nA, 216 V
458 nA, 201 V
384 nA, 185 V
319 nA, 168 V
214 nA, 134 V
166 nA, 112 V
$1/f^{0.8}$

ERROR: syntaxerror
OFFENDING COMMAND: ----nostringval----

STACK: